Flow curve determination by torsion tests using inverse modelling

Relatori:

Ch.mo Prof. Stefania Bruschi

Prof. Dr.-Ing. Gerhard Hirt

Dr. Martin Franzke

Mario di Donato 1082593

A mio padre

Table of contents

1 Introduction

In the industrial practice with the help of the FEM simulation, the distribution of stress and strain during the deformation can be analyzed in any part of the workpiece. To obtain accurate simulations and good results, the knowledge of the elasto-plastic material properties, especially in metal forming, is very important. Therefore, the materials flow stress has to be determined in reliable basic experiments. Some tests like tensile tests, compression tests, etc. have been developed with the aim to characterize the materials flow stress.

However, the achievable strain is smaller than that in the metal forming process due to their limitations. The tensile test suffers from the necking and fracture that appear at strain less than 0.5. Friction has a great influence on compression tests and large strain introduce barreling. Since torsion test is not subjected to necking or barreling, it is suitable to measure the flow curve at large strain. The disadvantage of the torsion test is the non-uniform deformation, which makes the evaluation of the data more complicated. The analytical evaluation methods of the torsion test include simplifications trying to compensate the inhomogeneous non-uniform deformation and therefore the results are containing errors. In this way, the material behavior, obtained with these evaluation methods is an approximation that proves insufficient to simulate complex forming operations.

Therefore, the goal of this thesis is to investigate the inverse modelling for the evaluation of torsion test. Suitable flow models and modelling approaches are determined in a literature survey and utilized to determine the flow curves of a 18CrNiMo7-6 case hardening steel by torsion test.

In order to determine flow curves from torsion test by inverse modelling, a FEM model of the torsion test was developed.

Different flow models have been proposed and studied by several researchers. Ludwick's model gave the most widely used equation for describe the material behavior at cold deformation. Voce model is particular suitable to fit data to higher strains, and because of this it was chosen for the torsion test. Hansel-Spittel model is widely used for hot deformation, but it is very complex because many parameters are used.

In this thesis, all three flow model will be used in the inverse modelling to calculate flow curves from torsion test data; Ludwick and Voce's model for cold torsion test and Hanse-Spittel model for hot torsion.

The results for cold deformation shows that the Ludwick's model has a good agreement with the experimental data, but with some difference in some areas. A better result was achieved with the Voce model, that had show a very good agreement with the experimental data.

For hot deformation, instead, the Hansel-Spittel model provide an accurate result for determination of flow stress in the steady state but not in the onset of dynamic recrystallization.

All of these results are hardly influenced by the starting points for the evaluation.

2 State of the art

2.1 Flow stress

Workability is a complex property and describes the mechanical performance of the material. An explicit and simple definition of workability is: "*The ability to impart a particular shape to a piece of metal under the load capacity of the available tooling and equipment*" [1].

A full description of the workability of the material is performed by the ***flow curve***. These curves are influenced by two factors substantially:

- Those factors, which relate to the material, e.g. chemical composition, metallurgical structures ecc.
- Those factors, which are function of the forming process, e.g. temperature, strain rate, heat pre-treatment ecc.

For a metal forming operations, it is important to assess loads and forming energies that will be needed to accomplish the necessary deformation. The ***flow stress*** is directly connected to the instantaneous value of load, which is necessary to continue the yielding and flow of the material at any point during the process. The flow stress, σ, can be considered to be a function of temperature, T, strain, ε, and strain rate, $\dot{\varepsilon}$.

$$\sigma = f(\varepsilon, T, \dot{\varepsilon})$$ Eq 2.1

In hot forming of metals, for example, the influence of strain rate is significant while the influence of strain is insignificant; this is possibile when the temperature it's below the recrystallization's one. For cold forming, instead, the influence of strain rate is negligible and the effect of strain prevails. The dependency of flow curves upon temperature varies considerably for different material [2] [3].

2.1.1 Elastic and plastic behavior

When a solid material is subjected to an external load, it can recover its original dimensions when the load is removed; This effect is better know as **elastic behavior.** Related to this latter there is the **elastic limit,** this is the limit of application of the load, below which the material has an elastic behavior. If the elastic limit is exceeded, the body experience a permanent deformation when the load is removed. This permanent deformation is also known as **plastic deformation** [4].
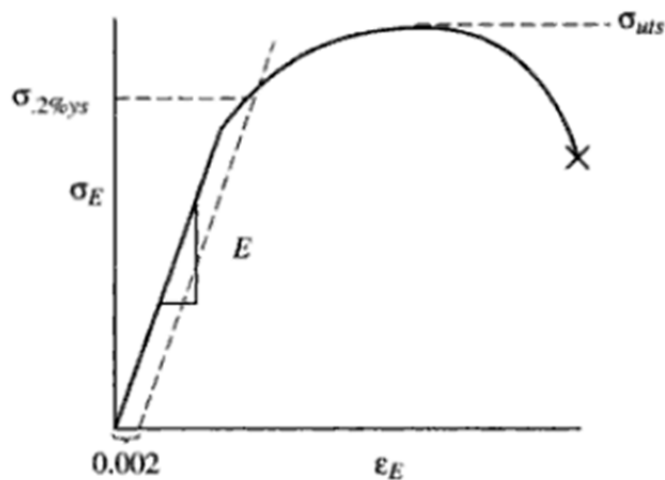
Figure 2.1: typical sytess-strain curve [5]

In Figure 2.1 there is shown a typical stress-strain curve, where the segment that start from 0.002, defines the elastic limit, which worth the Hooke's law; and E (Young's modulus) it's the slope of the curve. $\sigma_{0.2\%}$ define the yield stress, which is the stress where the remaining strain would be 0.2%. Exceeding the yield stress, the stress first increase with strain (strain hardening) , passes through a maximum UTS (ultimate tensile strength) and then decrease until the strain to fracture (the x in Figure 2.1).

In the plastic stage, the deformation it's made possible thanks to the microscopic dislocations; however, the crystal structure does not change during a plastic deformation. A conservation of crystal structure concurrent with an external change of shape is

possible only if complete blocks of a crystal are translated parallel to crystallographic planes by integer multiples of the atomic spacing in those planes (Figure 2.2) [6].
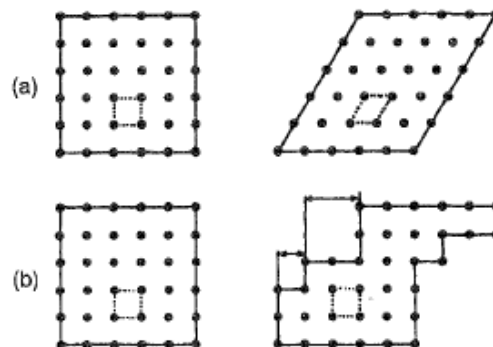
Figure 2.2: plastic deformation of crystals. (a) changing the crystal structture.
(b) without changing the crystal structure [6]

The plastic deformation of material results in ***strain hardening***, also known as work hardening. To explain the strain hardening mechanism, dislocation models are often used. In Figure 2.3 typical schematic hardening curve of single crystals under a single slip is presented. The hardening curve can be interpreted as follows. During the stage I, the dislocations can move easily, once the flow reaches the critical shear stress, and the flow stress increase with the strain. The stage II it is caused by the interaction of primary dislocations with the dislocations on the secondary slip system that generate a group of immobile dislocations. To maintain the level of imposed strain rate, for every immobile dislocation, another mobile dislocation has to be generated. Therefore, the dislocations density increases rapidly in this stage. The stage III is the longest of the hardening curve. In this stage, the hardening rate decreases due to the cross slip of screw dislocations. The decrease of hardening rate during the deformation process is a recovery process [6].
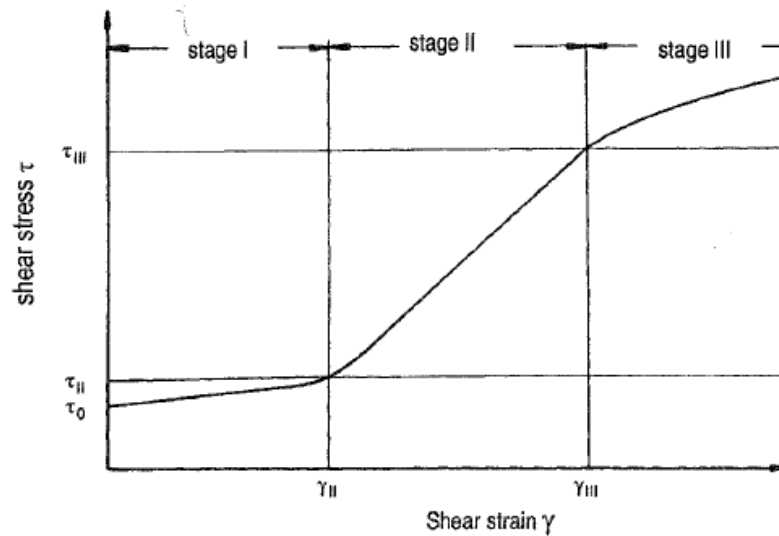
Figure 2.3: schematic hardening curve of fcc single crystal [6]

2.1.2 Metal forming processes

2.1.2.1 Cold working

In general it is possible to classify metal forming processes into two broad categories, according to the operating temperature: **cold working** and **hot working.** *"Cold working processes are conducted at the temperature which is lower than recrystallization temperature, generally at the ambient temperature"* [7].

Typical cold working processes are cold forging, cold rolling, bending ecc. There are some advantages and disadvantages, of course, of cold working. The advantages are beside others:

- No heating is required
- Better surface finish is obtained
- Improved strength properties

The disadvantages are beside others:

- Higher forces are required for deformation
- Less ductility is available
- Metal surfaces must be clean and scale-free
- Strain hardening occur
- May produce undesiderable residual stresses

After a plastic deformation at room temperature the strenght is generally increased while the ductility is decreased. Therefore work hardening is dominating in the cold working processes [4] [8] [9].

2.1.2.2 Hot working

Hot working, is a metal forming process that is carried out at a temperature range that is higher than the recrystallization temperature of the metal being formed. This ***recrystallization temperature*** is the temperature at which new <u>unstrained crystals from the original distorted grains are formed</u> after being plastically deformed [10] [11].

Generaly the hot working is conducted at temperatures such that the ratio T/T_m is greater than 0.6; where T is the process temperature and T_m is the melting temperature of the metal. Clearly, not all materials can be hot worked bringing them to the temperature such that $T/T_m > 0.6$, but each material has its own range of formability as a function of the melting temperature. The typical lower limit of the hot working it's defined by that temperature above which it occurs a lowering of the ductility [12] [13]. However in practice, this lower limit temperature depends on many factors such as deformation time, conduction between tool and metal, etc. ; for example most of thermal energy conducts to the cool tooling and a temperature gradient in the workpiece will appear. So this loss effect of the heat, due to conduction, need to be compensated, maybe with a preheating of the cool tooling before the hot working process [7].

The upper limit of hot working process, instead, is the melting temperature, as said previously. In general is 50°C below the melting temperature. Such as cold working also hot working has its advantages and disadvantages. The advantages of hot working processes are beside others [14]:

- The elevated temperatures promote diffusion that can remove chemical inhomogenities, pores can be welded, shut or reduced in size during deformation and the metallurgical structure can be altered to improve the final properties.
- Undesirable coarse or columnar grains may be eliminated and a fine, randomly oriented grain structure may be obtained.
- Metals with fine grain structures have superior strength, ductility and toughness.
- Impurities which are located around grain boundaries are often reoriented into a "crack-arrestor" configuration, perpendicular to crack propagation.
- Less force and lower power

The disadvantages are:

- The high temperatures may promote undesirable reaction between the metal and surroundings.
- Tolerances are poorer due to thermal contractions and possible non uniform cooling.
- Metallurgical structure may also be non-uniform
- High energy is needed

2.1.2.3 Temperature influence

The temperature influence on the flow behavior of metals is significant. In cold working process for example, work hardening dominates the deformation process, so *recovery* and *recrystallization* (RX) are not effective [15].

In hot working processes, in contrast to cold working processes, the recrystallization may significantly influence the forming process. Figure 2.4 shows typical flow curve under hot working condition.It can be seen for higher deformation levels, that the flow stress approaches a constant value. This behavior is due to recovery and recrystallization, which are thermally actived [16].
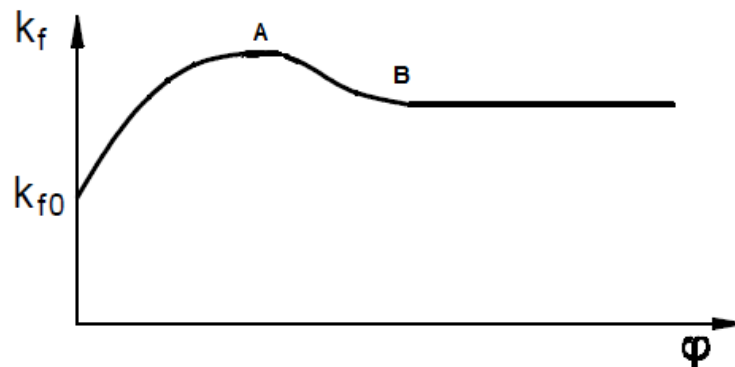
Figure 2.4: typical flow curve at hot working temperature [17]

2.1.2.4 Strain rate influence

Strain rate is also an important factor which influence the flow behavior. The typical effects of strain rate have it on the strenght of metals, are shown in Figure 2.5. Infact with

increasing of the strain rate, the strenght of the material (**strain-rate hardening**) increase [18].
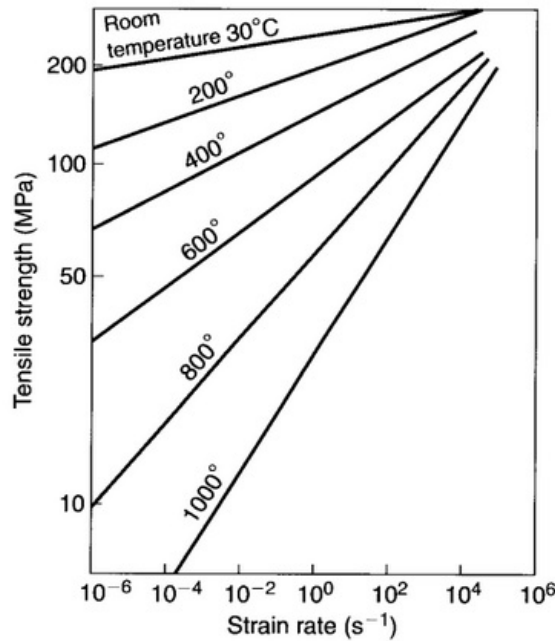
Figure 2.5: the effect of strain rate on the ultimate tensile strenght [18].

The slope of the curves in Figure 2.5 is called **strain-rate sensitivity exponent** *m;* this latter describe also the dependency of flow stress σ on the strain rate $\dot{\varepsilon}$, and to show this effect usually it is used the following mathematical expression [6, 19]:

$$m = \frac{d \ln \sigma}{d \ln \dot{\varepsilon}}$$
Eq 2.2

This relationship is given by the fact that stress and strain ratehas been described by this correlation:

$$\sigma = C\dot{\varepsilon}^m$$
Eq 2.3

Where C is the strength coefficient and is dependent of strain. From Figure 2.5 it can be seen that the sensitivity of strenght to strain rate increase with temperature, according to the Eq 2.3; in other words, *m* increases with increasing temperature, so the flow stress increases with the increasing of strain rate. Both recovery and recrystallization are promoted at low strain rate. In case of high strain rate, for example, the deformation is too fast, so mechanism like recrystallization does not develop completely [6] [20].

2.2 Material testing

As mentioned previously a complete description of the workability of a material is specified by its flow curve. From these curves it is possible calculate the load and forming energy that are also important in the process design of forming processes. At industrial level there are many tests that are capable of providing this kind of information, the most important ones are *tension, compression, bend* and *torsion tests*. ; The reason for these different tests is that the materials are subjected to different types of load which depend on the type of process that they undergo. So flow curves should be obtained by tests which reproduces the mode of load that will suffer the material in the practice [1] [21].

2.2.1 Tension test

"The tension test is the most common method for determining the mechanical properties of materials, such as strenght, ductility, toughness, elastic modulus and strain hardening capability" [22]. In this test, the specimen is mounted in the jaws of a tension-testing machine equipped with various accessories which applies uniaxial force and then is elongated untile fracture occurs. When the load is first applied, the specimen elongates in proportion to the load (elastic behavior), as show in Figure 2.6.
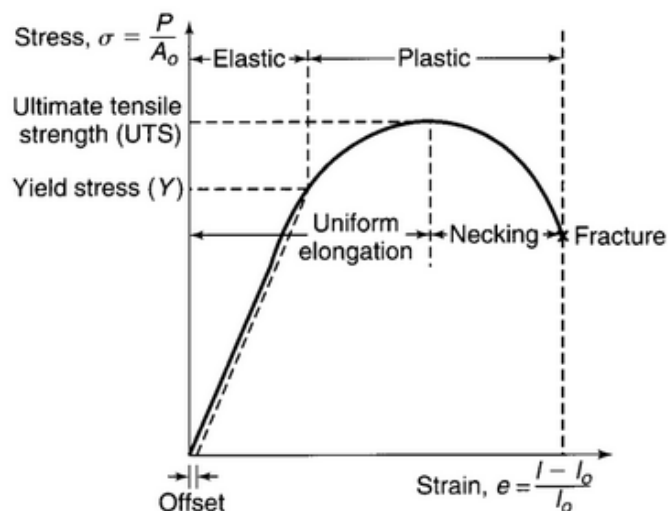

Figure 2.6: typical stress-strain curve obtained from tension test [23]

The engineering stress (nominal stress) is defined as the ratio of the applied load, F, to the original cross-sectional area, A_0, of the specimen:

$$\sigma = \frac{F}{A_0} \qquad \text{Eq 2.4}$$

and the engineering strain is:

$$e = \frac{(l - l_0)}{l_0} \qquad \text{Eq 2.5}$$

where l is the instantaneous length of the specimen and l_0 the initial length.

True stress is defined, instead, as the ratio of the load, F, to the actual (istantaneous, hence true) cross-sectional area, A, of the specimen:

$$\sigma = \frac{F}{A} \qquad \text{Eq 2.6}$$

For true strain, the elongation of the specimen is considered an increment of instantaneous length. Then, the true strain is:

$$\varepsilon = \ln\left(\frac{l}{l_0}\right) \qquad \text{Eq 2.7}$$

As the specimen begins to elongate under a continuously increasing load, its cross-sectional area decreases permanently and uniformly throughout its gage length. As the load is increased further, the engineering stress eventually reaches a maximum which is called ultimate tensile strenght (UTS) and then begins to decrease.

If the specimen is loaded beyond its ultimate tensile strenght, it begins to **neck** (decrease of cross-sectional area), as show Figure 2.6. The cross-sectional area of the specimen is no longer uniform along the gage length and is smaller in the necked region. Because of this, for most metals, the uniform strain that precedes necking rarely exceeds a true strain of 0.5. The tension test is convenient to perform and not influenced by friction, but the necking make the control of strain rate difficult and leads to uncertainties of stres and strain calculation [24]. Hence, the utility of the tension test is limited in workability testing [25] [26].

2.2.2 Compression test

The compression test is the most commonly used method for measure the flow curve of bulk material. In this test, a cylinder specimen is subjected to a compressive load, betweem two parallel dies with a constant strain rate.

Obviously the height and the diameter of the specimen change during the experiment, and these changes are calculated. So when a cylinder specimen with a diameter D_0 and initial height h_0 is compressed to height h and spread out to diameter D according to the law of constancy of volume:

$$\pi \frac{D_0^2}{4} h_0 = \pi \frac{D^2}{4} h \rightarrow D_0^2 h_0 = D^2 h \qquad \text{Eq 2.8}$$

The flow stress, σ is:

$$\sigma = \frac{F}{A} = \frac{4F}{\pi D^2} = \frac{4Fh}{\pi D_0^2 h_0} \qquad \text{Eq 2.9}$$

and

$$\varepsilon = \ln\left(\frac{h_0}{h}\right) \qquad \text{Eq 2.10}$$

where ε is the true compressive strain. These equations are used to obtain the flow curve. The main advantage of the compression test is that no necking occurs, in contrast with the tension test, so relatively large strain can be achieved.

The disadvantage in this test is the friction between the specimen and the dies, that cause an effect called *barreling*. The equations described above are valid if there is a condition of uniaxiality, with friction neglected. The barreling estabilishes a triaxial state of stress tensor, because of interaction of the friction forces.

This happens since the expansion of cross section in the center of specimen is greater than at the surface, see Figure 2.7. The less deformed zone at the contact surface lead to the accumulation of stress and loss of uniaxial deformation.

This effect can be eliminated by using a rastegaev specimen with grooving end to retain lubrificant [27] [28]; or use some good lubrificant such as teflon sheet, glass etc. for reduce the friction [24].
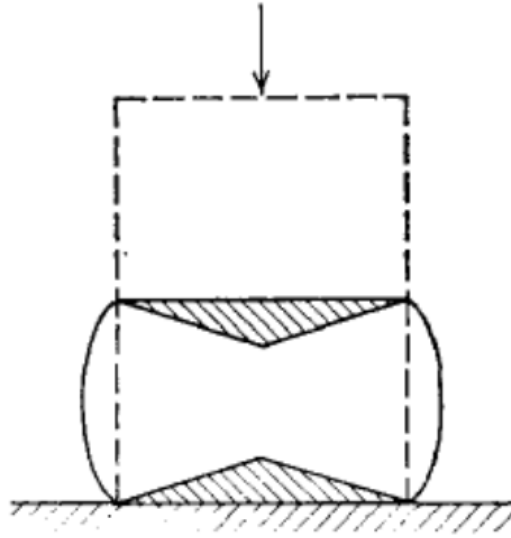
Figure 2.7: barreled specimen with less deformed zone [4]

2.2.3 Bending test

The bending test is useful for assessing the workability of thick sheet and plate. Generally, this test is most applicable to cold working operation. The specimen is placed on two supporting pins with a set distance and a loading pin is lowered from above at a constant rate until specimen failure. As a result these tests, are referred to as ***three-point*** and ***four-point bending***, respectively, see Figure 2.8. The longitudinal stresses in the specimen are tensile at their lower surface and compressive at their upper surfaces [29].
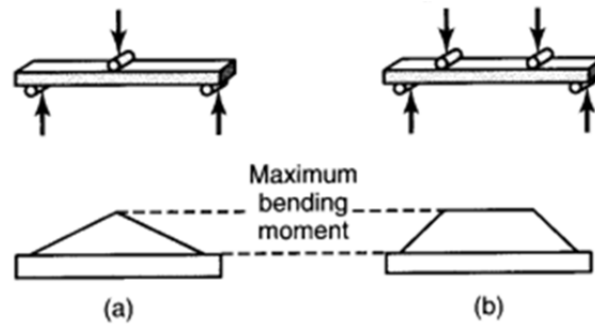
Figure 2.8 (a) three points bending. (b) four points bending [18]

The principal stress and strains developed during bending are defined in Figure 2.9. For pure plastic bending, in which elastic deformation can be ignored, the maximum tensile fiber strain is:

$$\varepsilon_0 = \ln \sqrt{\frac{R_0}{R_i}}$$

Eq 2.11

Where R_0 is the radius of curvature on the outer (tensile) surface, and R_i is the radius of curvature on the inner (compressive) surface [24] [29].
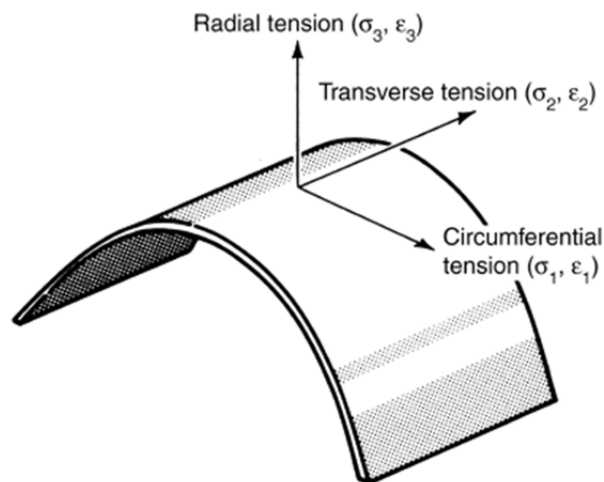
Figure 2.9: schematic of the bend region defining direction of principal stresses and strains [24]

The main advantage of these tests is the ease of the specimen preparation and testing. However, this method has also some disadvantages: the results of the testing method are sensitive to specimen and loading geometry and strain rate.

2.2.4 Torsion test

The torsion test has been used for about 50 years as a means of hot workability assessment in metals and alloys [30] [31]. For this method the specimen is mounted between the two heads of a testing machine and twisted, as Figure 2.10 shows.
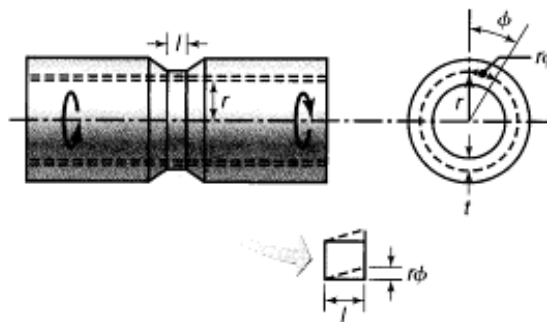
Figure 2.10: typical torsion-test specimen [21]

The main advantage of the torsion test is the fact that is possible reach very large strain and investigare the plastic behavior without friction or necking. Furthermore the specimen does not present significant changes in shape during deformation as long as the gage section is restrained to a fixed length [32] [33]. The disadvantage of the torsion test is the fact that is characterized by non-uniform distribution of deformation over the length and cross-section of specimen, infact the stress and strain are 0 at the center and maximum at the surface of the specimen. Hence the deformation in the torsion is not an accurate simulation of metalworking processes, because of excessive material reorientation at large strain [34].

The output of the torsion test is represented by torque versus twist angle, that must be converted into the stress and strain (determination of flow curve). For this purpose there are several methods, such as Nadai's graphical method, Field and Backofen method etc. The problem of these methods is characterized by the fact that, for the conversion they use analytical equations that reproduce homogeneous deformation; this is in contrast with the nature of the torsion test that is an inhomogeneous process. Therefore the aim of this thesis is to investigate the data analysis using the ***inverse modelling***, which provides the most convincible and reliable result.

2.2.4.1 Specimen design

As mentioned previously the torsion test has been used for many years, but there are no standards for sample design. The typical geometry of the specimen is of two types: *solid* and *tubular specimen*, as is show in Figure 2.11. Solid bar specimens are easiest to be manufactured and tested [35]; are favored for high-strain because tubular specimen have a tendency to buckle in this regime. Tubular specimen, instead, are particularly suitable for analysis stress and strain of work hardening at low strains. These latters are made with a thin-wall in the manner of that the shear-strain and shear-strain-rate gradients are eliminated in radial direction and the variation of temperature across the section [1].

The main components of design are gage section, fillet radius, shoulder length and grip design. The geometry of gage section is very important because determines the deformation level and deformation rate, and these are studied for calculate the flow stress and strain. For solid bar specimens, a possible diameter is 6.5 mm and length varies from 6.5 to 50 mm. For tubular specimens, possible dimensions are 12.5 mm outer diameter, 11 mm inner diameter and 2.5 mm gauge length [1].

(a)   (b)
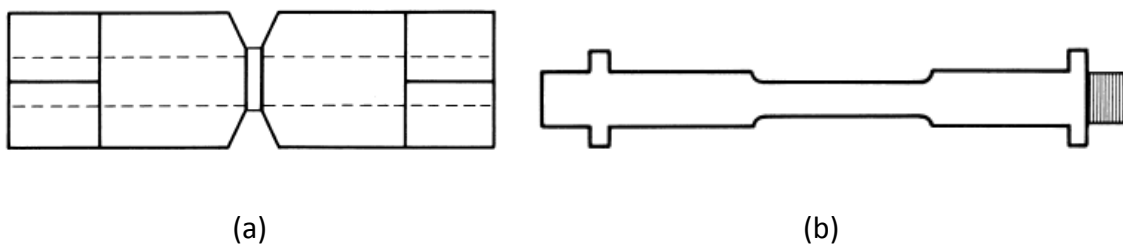
Figure 2.11: (a) Tubular specimen (b) Solid bar specimen [1]

2.2.4.2 Test device

Being that the torsion test is not widely used as compression and tension test, there were few available commercially torsion test machines. Individual researcher, designed the apparatus for specific experiments, and most of these machines are designed to provide a range of constant twist rate only [36] [37]. In general the torsion machines have: test frame, drive system, twist and torque monitoring device and a furnace [1]. The two major types of test frame are horizontal and vertical frame. The test machine used for the experimental part of this thesis is a electrohydraulic machine with vertical frame, as show Figure 2.12.

In the torsion test the specimen is twisted around its axis without bending, therefore the test frame should have high rigidity and an accurate alignment. The drive system is the set of a twist head, a weight head and a motor. The twist and torque sensor (monitor system) record the twist of specimen and torque of the motor.
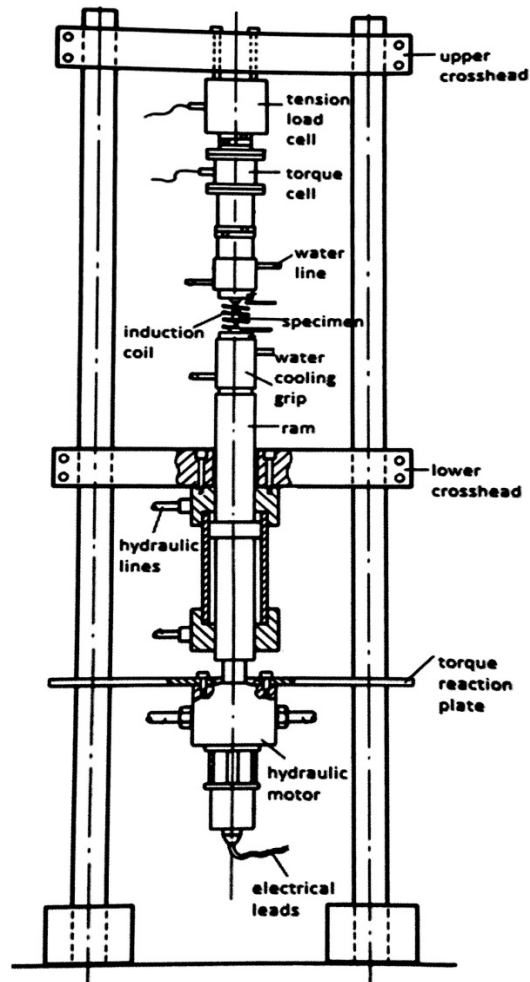
Figure 2.12: electrohydraulic torsion test machine with vertical frame [38].

For investigate the workability at elevated temperatures using torsion tests, a heating system is necessary. The two most common methods of heating are furnace and induction. For facilitate specimen quenching induction or radiant heaters are more suitable. [39] [40].

2.2.4.3 Evaluation methods

In order to analyze and therefore predict the constitutive equation that represents the flow behavior of material, the raw data must be converted into flow curves.

There are different methods for converting this raw data (torque-twist) to the shear stress-shear strain curve. In any case a cylinder solid bar is considered with length L and the radius R. The torque M is applied at one end of this bar which introduces the shear stress τ and shear strain Υ.
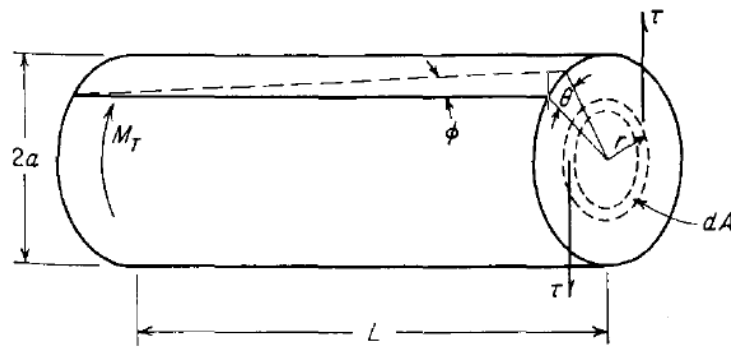
Figure 2.13: solid bar specimen [4]

In according to the Hooke's law, the relationship between shear stress and shear strain can be expressed as:

$$\tau = G\Upsilon \qquad \text{Eq 2.12}$$

Where the shear strain is:

$$\Upsilon = \frac{r\theta}{L} \qquad \text{Eq 2.13}$$

Herein, θ is the twisted angle (in radians), r is the radial position and L the length of gauge [41] [42].

When the specimen is twisted, the component of torque, dM in area dA is given by:

$$dM = \tau r dA \qquad \text{Eq 2.14}$$

Instead the total torque applied to the specimen is:

$$M = \int_m dm = \int_A \tau r dA = 2\pi \int_0^R \tau r^2 \, dr \qquad \text{Eq 2.15}$$

The resistance to torsion is represented by the polar moment (I) of area *(A)*, and can be expressed as:

$$I = \int_A r^2 dA \qquad \text{Eq 2.16}$$

Combining Eq 2.15 and Eq 2.16, the shear stress is:

$$\tau = \frac{Mr}{I} \qquad \text{Eq 2.17}$$

For a solid bar specimen, being that the polar moment is $I = \pi r^4/2$, the maximum shear stress is:

$$\tau_{max} = \frac{2M}{\pi R^3} \qquad \text{Eq 2.18}$$

The maximum shear stress for a tubular specimen, instead, is:

$$\tau_{max} = \frac{2M}{\pi(a_1^3 - a_2^3)} \qquad \text{Eq 2.19}$$

Where a_1 is the outsied radius of tube and a_2 the inside radius.

In the tubular specimen, the shear stress gradient can be neglected since the wall is very thin. The yield strength can be obtained by using the tubular specimen. The effective stress, σ, and effective strain ε are converted by means of the von Mises yielding criterion [24].

$$\sigma = \sqrt{3}\tau \qquad \text{Eq 2.20}$$

$$\varepsilon = \frac{\Upsilon}{\sqrt{3}} \qquad \text{Eq 2.21}$$

2.2.4.4 Nadai's graphical technique

In 1950, Nadai was the first to formally extend the elastic analysis of a torsional bar to include the case of fully plastic flow [43]. He argues that the distortion produced in a solid bar by relative twist with small angle can be expressed as simple shear strain that is proportional to the distance, r, of an element from the bar axis. Hence, according to Eq 2.15, the torque is:

$$M = \int_m dm = \int_A \tau r dA = 2\pi \int_0^R \tau r^2 \, dr \qquad \text{Eq 2.22}$$

The shear strain is defined in Eq 2.13 and being $d\Upsilon = \theta dr$, substituting the variables of integration in Eq 2.18:

$$M = \frac{2\pi}{\theta^3} \int_0^{\Upsilon_R} \tau \Upsilon^2 d\Upsilon \qquad \text{Eq 2.23}$$

Where $\Upsilon_R = R\theta$ is the shear strain of the specimen. The Nadai's approach assumes that the shear stress of specimen depends only on the local value of the shear strain, namely [1]:

$$\tau = f(\Upsilon) \qquad \text{Eq 2.24}$$

Since the value of the integral in Eq 2.23 depends on the upper limit, combining Eq 2.24 with Eq 2.23 and differentiation with respect to θ, is possible to obtain:

$$\tau_{max} = \frac{1}{2\pi R^3} \left(3M + \theta \frac{dM}{d\theta}\right) \qquad \text{Eq 2.25}$$

This expression is the basis of the graphical technique for obtaining shear stresses from torque-twist records; $dM/d\theta$ is the slope of the torque-twist per unit length curve, and can be obtained with this graphical method, as Figure 2.14 show. In the point B, a tangent line is made; $DC = \theta/L$ is the twist angle per unit length, BA the torque at this point; clearly $\frac{dM}{d\left(\frac{\theta}{L}\right)} = BC/DC$, then $BC = \theta \frac{dM}{d\theta}$, so the Eq 2.25 become:

$$\tau_{max} = \frac{1}{2\pi R^3} (3BA + BC) \qquad \text{Eq 2.26}$$
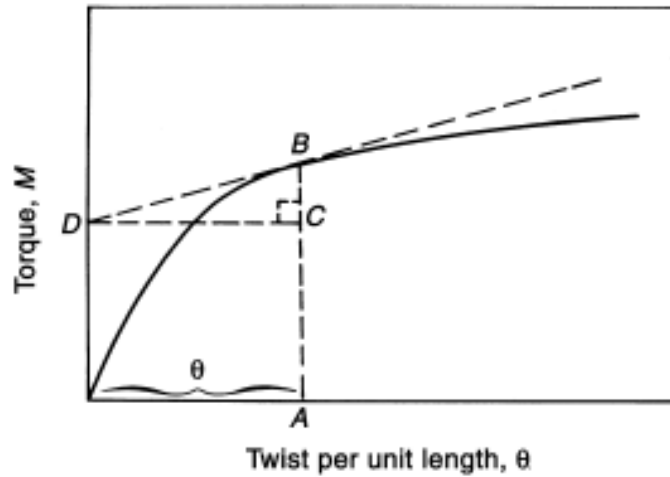
Figure 2.14: graphical determination of shear stress [1]

2.2.4.5 Field and Backofen's technique

The Nadai's method although it is easy to use, suffers from two limitations. First, the Eq 2.24 takes no account of the strain-rate sensitivity of the shear stress, so the Eq 2.25 cannot be applied at high temperature, where the strain rate sensitivity is significant. Second, the stress is considered only dependent on the strain. Therefore, Fields and Backofen developed their method which takes into account the influence of strain and strain rate change over the radius [44].

According to Eq 2.13 the strain rate can be written as:

$$\dot{Y} = r\frac{\dot{\theta}}{L}$$
Eq 2.27

Here, $\dot{Y}$ is strain rate and $\dot{\theta}$ is the angular speed.

According to Eq 2.23 for a tubular specimen wih the outside surface radius a_2 and inside radius a_1, the torque is:

$$M = \frac{2\pi}{\theta^3}\int_{Y_1}^{Y_2}\tau Y^2 dY$$
Eq 2.28

Now in order to make the derivation process easier, a solid specimen is considered to consist of two part, a solid core with radius r within a tube of outer radius a and inner radius r.

This specimen now is twisted to an amount of θ_a at the rate $\dot{\theta}_a$, the total torque is:

$$M_a = \frac{2\pi}{\theta_a^3}\left(\int_0^{\Upsilon_r} \tau \Upsilon^2 d\Upsilon + \int_{\Upsilon_r}^{\Upsilon_a} \tau \Upsilon^2 d\Upsilon\right)$$

Eq 2.29

A second specimen, also with a radius a, is twisted, but by a smaller amount of θ_b and at a lower twisted rate $\dot{\theta}_b$. These value of strain and strain rate are selected so that at the specimen surface the strain is $\Upsilon_b = a\theta_b = r\theta_a = \Upsilon_r$ that is the strain at the suface of the core in the first specimen, and the strain rate is $\dot{\Upsilon}_b = a\dot{\theta}_b = r\dot{\theta}_a = \dot{\Upsilon}_r$. Then the torque M_b is:

$$M_b = \frac{2\pi}{\theta_b^3}\int_0^{\Upsilon_r} \tau \Upsilon^2 d\Upsilon$$

Eq 2.30

The integral quantity in Eq 2.30 is identical to that appearing in Eq 2.29; both integrations are performed over the same range of strain and strain rate, so the Eq 2.29 can be rewritten:

$$M_a = \frac{\theta_b^3}{\theta_a^3}M_b + \frac{2\pi}{\theta_a^3}\int_{\Upsilon_r}^{\Upsilon_a} \tau \Upsilon^2 d\Upsilon$$

Eq 2.31

The difference in torque between the two specimens (M_a-M_b) is:

$$M_a - M_b = \left(\frac{\theta_b^3 - \theta_a^3}{\theta_a^3}\right)M_b + \frac{2\pi}{\theta_a^3}\int_{\Upsilon_r}^{\Upsilon_a} \tau \Upsilon^2 d\Upsilon$$

Eq 2.32

Now for the first specimen, considering the interval of integration $M_b \rightarrow M_a$, dM is equal to $M_a - M_b$ and $(\theta_b^3 - \theta_a^3)/\theta_a^3 = -3d\theta/\theta$. Introducing these changes in Eq 2.32 leads to:

$$\tau = \frac{1}{2\pi r^3}\left(3M + \theta\frac{dM}{d\theta}\right)$$

Eq 2.33

This Equation it is not restricted to rate insensitive materials if $dM/d\theta$ is obtained from a torque-twist curve which satisfies the condition under which the derivation was made. The condition, restated, was that $a\theta_b = R\theta_a$ and $a\dot{\theta}_b = R\dot{\theta}_a$, it can also be described as:

$$\frac{\theta_a}{\dot{\theta}_a} = \frac{\theta_b}{\dot{\theta}_b}$$

Eq 2.34

If shear stress values are to be obtained from a single torque-twist record, the twist rate must vary in proportion to the amount of twist:

$$\dot{\theta} = \theta \left(\frac{\dot{\theta}_a}{\theta_a} \right)$$

The shear stress calculated by Eq 2.32 would be associated with a different strain rate for each value of strain. So this method requires the assumption that shear stess depends only upon shear strain and the instantaneous value of strain rate.

Considering a constant temperature from torsion test at various constant rate of twist, the change in torque due to the twisting is:

$$\frac{dM}{d\theta} = (\frac{dM}{d\theta})_{\dot{\theta}} + (\frac{dM}{d\dot{\theta}}) \frac{d\dot{\theta}}{d\theta}$$

Eq 2.36

According to Eq 2.33 is possible to write:

$$\frac{d\dot{\theta}}{d\theta} = \frac{\dot{\theta}_1}{\theta_1} = \frac{\dot{\theta}}{\theta}$$

Eq 2.37

Substuting in Eq 2.36:

$$\frac{dM_e}{d\theta} = (\frac{dM}{d\theta})_{\dot{\theta}} + (\frac{dM}{d\dot{\theta}}) \frac{d\dot{\theta}}{d\theta}$$

Eq 2.38

Since $d \ln x = dx/x$:

$$\frac{dM_e}{d\theta} = \frac{M}{\theta} (\frac{\partial \ln M}{\partial \ln \theta})_{\dot{\theta}} + \frac{M}{\theta} (\frac{\partial \ln M}{\partial \ln \dot{\theta}})_{\theta} \frac{\dot{\theta}}{\theta}$$

Eq 2.39

and finally, Eq 2.38 can be espressed:

$$\frac{dM_e}{d\theta} = \frac{M}{\theta} (m + n)$$

Eq 2.40

Where n and m are, respectively, the slopes of the plots of M versus θ at constant $\dot{\theta}$, and of M versus $\dot{\theta}$ at constant θ, on logarithmic coordinates. The last step is a substitution of Eq 2.40 into Eq 2.33, and in this way is possible to obtain the expression for converting torque-twist into shear stress and shear strain:

$$\tau = \frac{M}{2\pi r^3} (3 + m + n)$$

Eq 2.41

For determine the value of *n*, torsion tests have to be conduct at different strain rates [44].

2.2.4.6 Khoddam's technique

The Field and Backofen's technique has been widely used in existing literature, but in those cases where the effects of work hardeing and rate sensitivity are taken into an average sense. These average parameters are not adequate for representation of phenomena occurring during real hot forming processes, especially when multiple regimes of hardening or rate hardening and competing effects of hardening and softening mechanisms do exist; so this is a drawback [45].

In the Field and Backofen's method, for determine hardening characteristics, a linear relationship between log *M* and log *θ* is assumed to avoid a large number of experiments and to reduce the existence of noise in measured data. This makes it possible to calculate strain hardening and strain rate hardening indices, from a linear regression of the experiment data. Whatever, this assumption is not valid for those deformation processes where multiple regimes of hardening and softening are involved [45].

The basic principle of the Khoddam's method is to estimate the instantaneous strain rate *m* and strain parameter *n*. For this goal, the experiment data need to be represented by an appropriate and universal model. The rational model that represent a wide rage of torque-twist behavior, introduced and explained by some authors is:

$$M(\theta) = \frac{\sum_{i=1}^{q+1} b_i \theta^{q+1-i}}{\theta^s + \sum_{j=1}^{s} b_{q+j} \theta^{s-j}}$$

Eq 2.42

in which *q*, and *s* are highest orders of the polynomial terms in the numerator and denominator of the rational model, respectively, and b_i's are the parameters of the model [46].

For estimate instantaneous rate sensitivity, at least three sets of experiment data at constant twist rate $\dot{\theta}_1, \dot{\theta}_2$ and $\dot{\theta}_3$ are needed. Figure 18 show three torque-twist models M_A, M_B and M_C for three different strain rate $\dot{\theta}_1, \dot{\theta}_2$ and $\dot{\theta}_3$ respectively
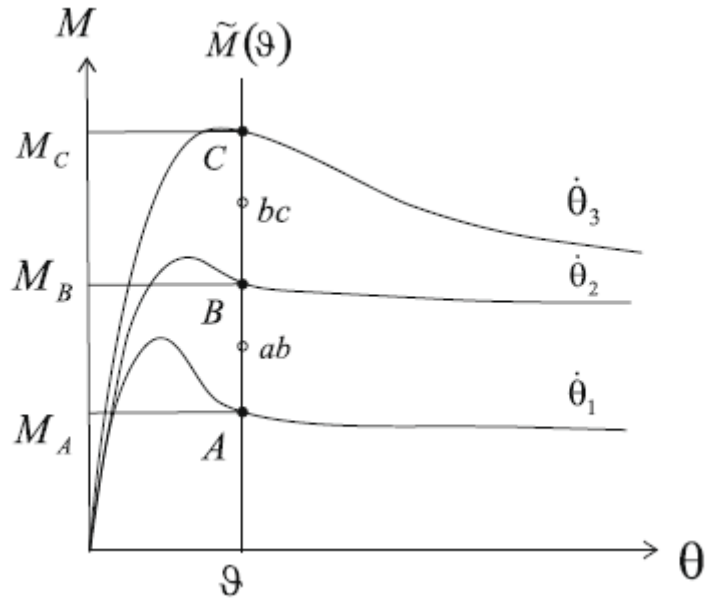
Figure 2.15: torque-twist data at different strain rate [45]

In Figure 2.15 four types of nodes are shown: boundary node with highest twist rate (node C), boundary node with lowest twist rate (node A), internal node (node B) and two auxiliary nodes (node ab and node bc). The strain rate hardening for the ith node can be described as:

$$m_i = \frac{\partial \ln M}{\partial \ln \dot\theta} = \frac{\dot\theta_i \partial M}{M_i \partial \dot\theta} \qquad \text{Eq 2.43}$$

The strain rate hardening index m can be easily estimated for boundary nodes using:

$$m_A = \frac{(M_A - M_B)\dot\theta_1}{(2M_A - M_B)\dot\theta_1 - M_A \dot\theta_2} \qquad \text{Eq 2.44}$$

$$m_B = 0.5\dot\theta_2 \left(\frac{M_A - M_B}{M_A\dot\theta_1 - M_B\dot\theta_2} + \frac{M_B - M_C}{2M_B\dot\theta_2 - M_C\dot\theta_2 - M_B\dot\theta_3} \right) \qquad \text{Eq 2.45}$$

$$m_C = \frac{(M_C - M_B)\dot\theta_3}{M_c(\dot\theta_3 - \dot\theta_2)} \qquad \text{Eq 2.46}$$

The strain hardening index, *n* can be obtained for the model by partial derivation of Eq 2.42 using the definition of the index:

$$n = \frac{\theta}{M} \frac{\partial M}{\partial \theta}$$

<div align="right">Eq 2.47</div>

Once calculated these instantaneous parameters is possible put them into the Eq 2.40 for more accurate flow curve [45].

The three conversion methods described above, have however, some limitations. Because, as mentioned previously, these methods base their principle of operation on assumptions which have a certain uncertainty. This means that there isn't a perfect match between the flow curve of the material, obtained from one conversion method, and the flow curve that derived from another one of these conversion methods, so it is very complex to find the model most suitable to describe the flow behavior of material. Assuming, for example, the stress-strain curve obtained from compression test like reference, it has been shown by recent studies that there are differences between this latter and the stress-strain curves obtained with the FB method or Khoddam's method, as shows in Figure 2.16.
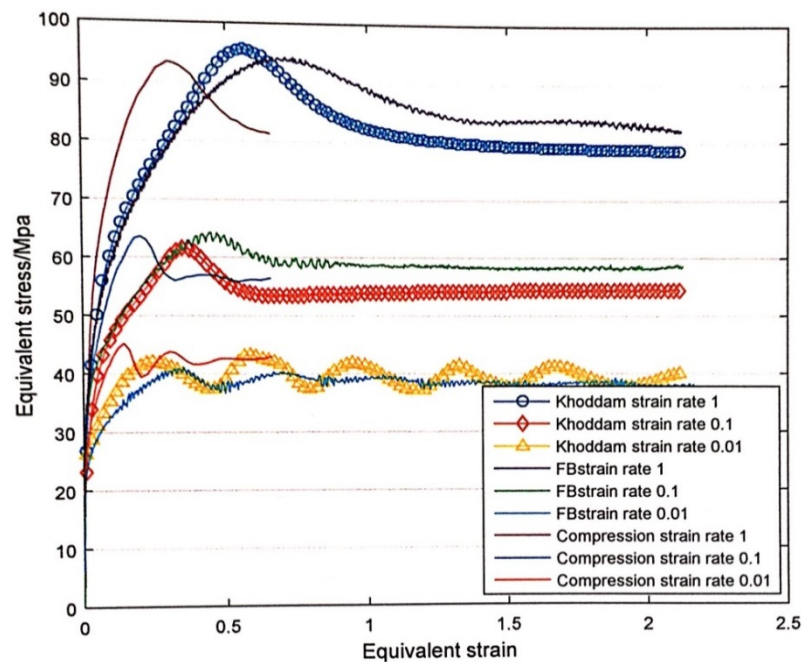

Figure 2.16: comparison with flow curves from torsion test and compression test [47].

The value of peak stress from compression tests and torsion test are similar, but the peak strain of compression test is much smaller than that of torsion test. So these methods do

not give a complete and accurate description of the material behavior; another possibility to determine the materials flow curve is the ***inverse modelling***.

2.3 Inverse modelling

The knowledge of the elasto-plastic material properties, especially in metal forming, is very important. Some tests like tensile tests, compression tests, bending tests etc. have been developed with the aim to characterize the deformation behavior of materials [48].

For data analysis, these traditional tests use analytical equations and these latters requires some assumptions and are mostly limitted to homogeneous deformations. Then the deformation fields from these tests are not perfectly in agreement with heterogeneous deformation fields, that are more complex, and occuring in the real metal forming operations.

In this way, the material behavior, obtained with this standard test is an approximation that proves insufficient to simulate complex forming operations. A different way for data analysis is ***inverse modelling***, which can also cope with inhomogeneous deformations [48].

The definition of inverse theory is: "[...] *the (mathematical) process of predicting (or estimating) the numerical values (and associated statistics) of a set of model parameters of an assumed model based on a set of data or observations*" [49].

Schematically it is the set of three factors:

Model: the model is the (mathematical) relationship between model parameters and the data. It may be linear or nonlinear, etc. In the case of metal forming the model is a mathematical representation of flow behavior of material (FE-Model).

Model Parameters: the model parameters are the numerical quantities, or unknowns, that one is attempting to estimate. The choice of model parameters is usually problem dependent, and quite often arbitrary. In the case of metal forming, could be the material data

Data: the data are the observations or measurements one makes in an attempt to constrain the solution of some problem of interest (i.e. Force vs. displacement or Torque vs. angle) [50].

The inverse methods offers a powerful tool for the identification of the elasto-plastic material parameter and consequently the deformation behavior.

2.3.1 General procedure

The main aim of inverse modelling is to identify a set of unknown parameters in a numerical model. For this goal, a set of iterations are executed for minimize a *cost function* which express the discrepancy between the experimental data and the numerical's one, by comparing displacement fileds, strain fields, etc. By running some simulations the numerical strain fields are computed with a FE model. The unknown material parameters, which are estimated at the beginning, are iterated in such a way that the computed strain fields match the measured fields as closely as possible. Figure 2.17 shows a flow-chart of the inverse method [48].
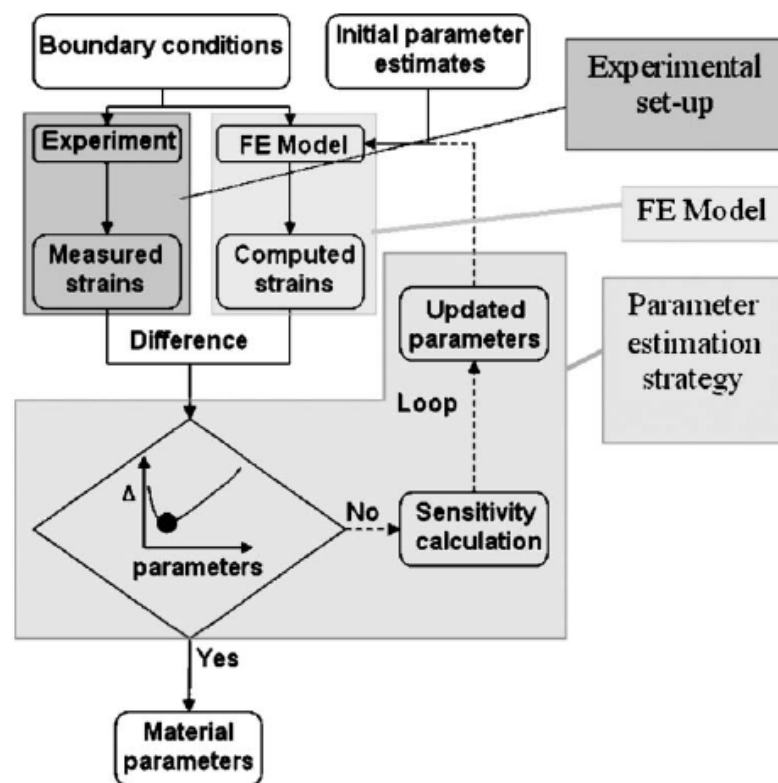

Figure 2.17: flow-chart of inverse method for material parameters identification [48]

The success of the inverse modelling is due to the careful choice of the mathematical model (material model), which are able to describe, or better simulate the deformation of materials in the operations of metal forming. So these material models "*usually*

describing the flow stress as a function of the deformation conditions"
[51].

The accuracy of the choice of material model depends on mathematical structure of the model itself and the material parameters used in the model, that are guessed, based on experiments.. Hence for the choice of the model, it must ensure that the mathematical structure of this latter take into account the physical phenomena that occur in the material, which depend on the kind of material, the conditions of forming and the history of deformation [51].

One of advantages of the inverse methods is the fact that are able to deal with heterogeneous deformation field, i.e. that are present in the torsion sample. Heterogeneous strain fields provide much more information respect uniform stress and strain fields, that are the results of the standard tests such as tensile and compression tests. Hence, heterogeneous fields allow the identification of more complex material models with more model parameters [48].

The limitation of the inverse methos is the computational effort, both with respect to computing power and time, and the complexity of the software involved. Furthermore, an assessment of the reliability of the results is sometimes not as straightforward as for classical material testing. Estimates of parameter accuracy and the range of validity, for example, are readily obtained for most direct measurement methods, but not easily for inverse modelling [52].

As previously mentioned, the determination of parameters of material model is perfomed by a series of iterations that minimizes a cost function; this function expresses the discrepancy between experimentally measured data and the numericallz computed data. An example of cost function can be the mean square error [53]:

$$MSE = \sum \left[\frac{1}{p} \sum_{i=1}^{N} \left(\frac{\varepsilon_i^{exp} - \varepsilon_i^{num}}{\varepsilon_i^{exp}} \right)^2 \right]$$

Eq 2.48

where N is the number of different experimental configurations considered and *p* is the number of points in each configuration. The operation of minimization of the cost function requires the use of particular ***optimization algorithms***.

2.3.2 Optimization algorithms

The most widely used search method for solving the optimization problem, is the ***Nelder-Mead simplex algorithm.*** This algorithm is used to find the minimum or maximum of a given objective function:

$$\min f(x) \qquad\qquad \text{Eq 2.49}$$

This method uses the concept of a simplex, which is the generalization of the notion of a triangle or tetrahedron to arbitrary dimension [54]. A simplex is a *k*-dimensional polytope which is the convex hull of its *k+1* vertices. For example, a 2-simplex is a triangle, a 3-simplex is a tetrahedron ans so on. The method approximates a local optimum of a problem with *n* variables when the objective function varies smoothly. It begins with a set of *n + 1* point that are considered as the vertices of a working simplex *S*, then performs a sequence of transformations of the working simplex *S*, aimed at decreasing the function values at its vertices. At each step, the trasformation is determined by computing one or more test points, with their function values, and by comparison of these function values with those at the vertices. At this test point, the method extrapolates the behavior of the objective function, in order to find a new test point and to replace the old one. So the approach replace the worst point with a point reflected through the centroid of the remaining *n* points [55] [56].

This process is terminated when the working simplex *S* becomes sufficiently small in some sense [55] [56], as shows in Figure 2.18.
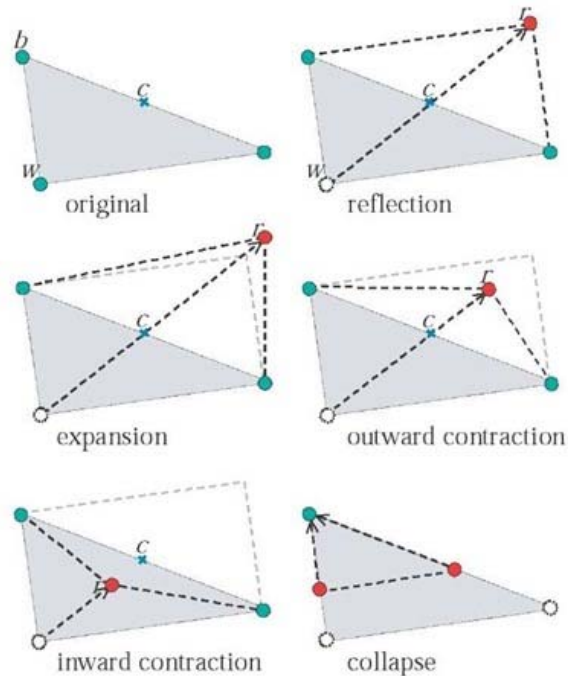

Figure 2.18: reduction of working Simplex [57]

The advantages of this method are that gives significant improvement in the first few iterations and quickly produce quite satisfactory results. Also, required only one or two function evaluations per iteration and this is very important in applications where each function evaluation is very expensive. So the main advantage is:

- In many numerical test, the method succeeds to obtaining a good reduction in the function value using a relatively small number of function evaluation

On the other hand, the lack of convergence theory is often converted in practice as a breakdown of the algorithm, even for smooth fucntions.

The main disadvantage is:

- The method can take an enormous amount of iterations, despite nowhere near to a minimum. This results in premature termination of iterations

Another algorithm widely used in mathematics and computing, is the **_Levenberg-Marquardt algorithm (LMA)_**. The LMA is used in many software applications for solving generic curving-fitting problem, so it is particularly suitable to identifty the parameters of the material models, in order to create a fit with the flow curves of the material itself. However the LMA finds only a local minimum, which is not necessarly the global minimum, see Figure 2.19
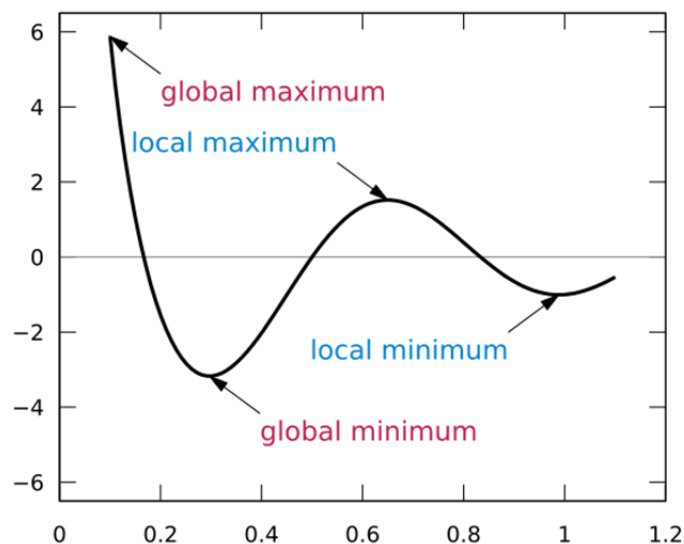

Figure 2.19: difference between local and global minimum [58]

This algorithm is an iterative technique that locates the minimum of a multivariate function that is expressed as the sum of squares of non-linear real-valued functions [58] [59]. It has become a standard technique for non-linear least-squares problems, that have the form [60]:

$$f(x) = \frac{1}{2}\sum_{i=1}^{m} f_i^2(x) = \frac{1}{2}\|F(x)\|^2 \qquad \text{Eq 2.50}$$

The function f is assumed as a functional relation which maps a *parameter vector* $p \in R^m$ to an estimated *measurement vector* $\hat{x} = f(p)$, $\hat{x} \in R^n$. An initial parameter estimate p_0 (i.e. the parameters of material model have to be guessed at the beginning) and

a measured vector x are provided and it is desidered to find the vector p^+ that satisfy the functional relation f. In each interation step of algorithm, the parameter vector p, is replaced by a new estimate, $p + \delta_p$. To determine δ, the function f are approximated by a Taylor series [61]:

$$f\left(p + \delta_p\right) \approx f(p) + J\delta_p \qquad \text{Eq 2.51}$$

where J is the jacobian matrix:

$$J_i = \frac{\partial f(p)}{\partial p} \qquad \text{Eq 2.52}$$

This method initiate at the starting point p_0, and produces a series of vectors $p_1, p_2, \dots$, that converge towards a local minimizer p^+ for f. Hence, at each step, it is required to find the δ_p that minimizes the quantity:

$$\left\| x - f(p + \delta_p) \right\| \approx \left\| x - f(p) - J\delta_p \right\| = \left\| \epsilon - J\delta_p \right\| \qquad \text{Eq 2.53}$$

where ϵ is the error (for i.e. discrepancy between experimental data and numerical data). The minimum is attained when $J\delta_p - \epsilon$ is orthogonal to the column space of J. This leads to $J^T\left(J\delta_p - \epsilon\right) = 0$, which is the solution of the so-called *normal equation* [61]:

$$J^T J \delta_p = J^T \epsilon \qquad \text{Eq 2.54}$$

The matrix $J^T J$ is the approximate Hessian. Levenberg's contribution is to replace the Eq 2.54 by a "*damped version*" [61]:

$$N\delta_p = J^T \epsilon \qquad \text{Eq 2.55}$$

where the off-diagonal elements of N are identical to the corresponding elements of $J^T J$ and the diagonal elements are given by:

$$N_{ii} = \mu + [J^T J]_{ii}$$

herein, μ is the *damping term*. If the parameter vector $p + \delta_p$ with δ_p computed from Eq 2.56, leads to a reduction in the error ϵ, the process repeats with a decreased damping term. Otherwise the dampimg term is increased, and the process iterates until a value of δ_p that decreases error is found.

The advantage of this method is the fact that needs much less iterations to find a converged solution that the simplex algorithm, so it is very fast. On the other hand if the value of damping term, is large, inverting $\mu + [J^T J]_{ii}$ is not used at all. Marquardt scale each component of the gradient so that there is a larger movement in the direction where the gradient is smaller. This avoids slow convergence in the direction of small gradient [62].

2.4 Material models

The material models, or constitutive equation, are the mathematical representation of the flow behavior of materials and are used as input to FE code for calculating the material's response under determinated loading conditions. Then, the success of the numerical simulation to accurately reproduce the flow behaviour, depends on how accurately the constitutive equation represent the deformation behavior of the material [63]. The models can be classified into three categories: ***empirical analytical, physically-based*** and ***empirical non-analytical models***.

Empirical non-analytical models, usually use a neural network-based approach, but they are not widely used because of their complexity.

2.4.1 Empirical analytical

Empirical analytical models deploy phenomenological derived expressions to model the flow stress as a function of macroscopic process parameters. The material constants within such formulations do not have a physical meaning and are usually determined by regression analysis.

2.4.1.1 Ludwick´s/Hollomon's model

This model use an empirical analytical approach, and as in most models that follow this approach, the various components that account for the strain, strain hardening etc. are multiplied with each other. The Ludwick's model is:

$$\sigma = \sigma_0 + k\varepsilon^n \qquad \text{Eq 2.57}$$

herein σ is the stress, σ_0 is the initial yield stress, ε is the strain, k is the strain hardening and n is the strain hardening exponent.

A reduced form of Ludwick's equation, that is commonly used, is called the **Hollomon equation**:

$$\sigma = k\varepsilon^n \qquad \text{Eq 2.58}$$

The Ludwick's model is widely used in those case where the deformation behavior of the material is dominated by strain hardening, therefore it is particulary suitable for describe the behavior of material at low temperature (cold working) [64]. The Hollomon's model is less suitable that the Ludwick's one, because it assumed the initial yield stress equal to zero, therefore it does not provide a very accurate reproduction of the flow behavior.

2.4.1.2 Johnson-Cook model

This empirical model has been successfully used for a variety of materials and for different ranges of temperature and strain rate. The Johnson-Cook (J-C) model and is particularly suitable to predict the mechanical behavior of materials at high temperature and high strain rate. The model has five material parameters which are determinated by experiment. The accuracy of these parameter is most important for the reliability of the numerical results [65]. The J-C model expresses the flow stress as:

$$\sigma = (A + B\varepsilon^n)(1 + C \ln \frac{\dot{\varepsilon}}{\dot{\varepsilon}_0})\left[1 - \frac{T - T_{ref}}{T_m - T_{ref}}\right]^m \qquad \text{Eq 2.59}$$

Where σ is the flow stress, ε is the plastic strain, $\dot{\varepsilon}$ is the strain rate (s), $\dot{\varepsilon}_0$ is the reference plastic strain rate (s-1), T (°C) is the workpiece temperature, T_m is the melting temperature of the workpiece material and T_{ref} is the reference temperature (for

example minimum temperature of test) . The material yield strength is defined as coefficient A (MPa) and the hardening modulus is defined as coefficient B (Mpa). C and *m* represent the coefficient of strain rate hardening and thermal softening exponent, respectively. The parameter *n*, instead, is the hardening exponent [63].

The J-C model considers isotropic hardening, strain rate hardening and thermal softening, but as three independent phenomena whence these can be isolated from each other. Thus, the total effect of strain hardening, strain rate hardening and thermal softening on flow stress can be calculated by multiplying these three terms.

At the reference temperature the J-C's equation will reduce to:

$$\sigma = A + B\varepsilon^n \qquad \qquad \text{Eq 2.60}$$

2.4.2 Physically-based

The physically-based models are functions of internal variables, which reflect the initial physical structure of the material as well as its evolution.

2.4.2.1 Mechanical Threshold Stress model

Nowdays with the advent of powerful computational machines, it is possible to simulate processes such as high-speed machining, explosive forming, impact of vehicles etc. In these processes the level of strain rate is much higher (10^2 s^{-1} to 10^9 s^{-1}) and the temperatures involved are greater than $0.6T_m$. So an important component in the numerical modeling of plastic deformations under these condition is a model that describes the evolution of the flow stress under a large range of strain rates and temperatures [66]. The model suitable for this purpose it the Mechanical Threshold Stress. The MTS model is based on two fondamental assumptions:

- Thermally actived dislocation motion are dominant and viscous drag effects on dislocation motion were small
- High temperature diffusion effects are absent. This assumption limit the range of applicability of the model to the temperatures less than around $0.6T_m$ [66].

The Mechanical Threshold Stress (MTS) model has the follow form:

$$\sigma_y(\varepsilon_p, \dot{\varepsilon}, T) = \sigma_a + (S_i \sigma_i + S_e \sigma_e) \frac{\mu(p, T)}{\mu_0} \qquad \text{Eq 2.61}$$

Herein σ_a is the athermal component, σ_i is the intrinsic component of the flow stress due to barriers to thermally activated dislocation motion, σ_e is the strain hardening component of the flow stress, (S_i, S_e) are strain-rate and temperature dependent scaling factors, and μ_0 is the shear modulus at 0 K and ambient pressure [67].

This model provides more accurate representation for the deformation behavior of the material over a wide range of temperatures and strain rates. However, this together with other physically-based models, are not always preferred by the industries, because they often require more data from precisely controlled experiments. More importantly, these models involve large number of material constants and properties than empirical models which may not be readily available in open literature.

2.4.2.2 Hansel-Spittel model

One of the most frequently used constitutive equation, for the bulk metal forming simulations, is the Hansel-Spittel model:

$$\sigma = A e^{m_1 T} \varepsilon^{m_2} \dot{\varepsilon}^{m_3} e^{\frac{m_4}{\varepsilon}} (1+\varepsilon)^{m_5 T} e^{m_7 \varepsilon} \dot{\varepsilon}^{m_8 T} T^{m_9} \qquad \text{Eq 2.62}$$

The Hansel-Spittel law has many rheological parameters very complex to identify for a given material: $\sigma, \varepsilon, \dot{\varepsilon}$ are respectively stress, strain and strain rate and T is the temperature given in Celsius, m_1 and m_9 define the material's sensitiviy to temperature, m_5 term coupling temperature and strain, m_8 term coupling temperature and strain rate, m_2, m_4 and m_7 define the material's sensitivity to strain, m_3 depends on the material's sensitivity to the strain rate.

This model is widely used for hot deformation, but it is very complex because have too parameters, therefore it requires considerable computational resources, and this corresponds to an increase of the time required to reach the convergence. To overcome this problem, there is a simplified version of the model:

$$\sigma = A e^{m_1 T} \varepsilon^{m_2} \dot{\varepsilon}^{m_3} e^{m_4 \varepsilon} \qquad \text{Eq 2.63}$$

In this case there are 5 coefficient A, m_1, m_2, m_3, m_4 to determine [68]. The term that take into account the material's sensitivity to temperature (m_1), the material's sensitivity to strain (m_2, m_4) and the material's sensitivity to the strain rate (m_3), are decoupled so the term which take into account coupling phenomena are absent. This is order to semplify the calculation of the material's coefficient.

2.4.3 Semi empirical

For practical applications empirical analytical models, due to their seimplicity, are often favored over physically-based models. It is also common to use a combination of both approaches, called *semi empirical models*.

2.4.3.1 Voce model

This is model is quite similar to the Hollomon's one:

$$\sigma = \sigma_s - (\sigma_s - \sigma_0)e^{\left(-\frac{\varepsilon - \varepsilon_I}{\varepsilon_c}\right)}$$

Eq 2.64

Herein, σ_s is the saturation stress, σ_0 and ε_I are the true stress and the true plastic strain at the onset of plastic deformation, respectively, and ε_c is a constant. For initial plastic strain $\varepsilon_I = 0$ the Eq 2.64 reduces to:

$$\sigma = \sigma_s - (\sigma_s - \sigma_0)e^{(-n\varepsilon)}$$

Eq 2.65

with three constant σ_s, σ_0 and n. This model assumes the flow curve as a transient of the flow stress from an initial value to the saturation one corresponding to equilibrium structure. The constant n in Eq 2.65 determines the rate at which the stress goes from its initial value to the saturation value [69].

This is model is suitable for simulation of metal forming at ambient temperature and at a relatively low rate of deformation, where the effect of the temperature rise caused by plastic work on flow stress can be neglected; in particularly it's suitable to fit data to higher strains.

3 Material

This chapter provides a brief overview of the investigated material and conducted experiments.

3.1 Description of the material

In this thesis, the flow behavior of the case hardening steel 18CrNiMo7-6 is investigated by torsion tests. Case hardening steel have low carbon content and a good formability at elevated temperature. The steels with low carbon content have poor to no hardenability of its own, so the case hardening process involves infusing additional carbon into the case, by carburization. Afterwards the parts are quenched and tempered. This process has the aim not only to confer to metal a high surface hardness due to the carbon-rich layer, but also to confer high resistance to wear and a good toughness. Case hardening steels are used to manufacture parts that are subject to high pressures and high strains, for example gears [70].

The investigated steel is described in Euronorm EN 10084 and its chemical composition is shown in Table 1.

Element	C	Si	Mn	P	S	Cr	Ni	Mo	Cu
Composition (wt%)	0.12-0.18	0.15-0.40	0.40-0.60	0.000-0.035	0.000-0.035	1.50-1.80	1.40-1.70	0.25-0.35	0.00-0.30

Table 1: chemical composition of 18CrNiMo7-6 [71]

3.2 Torsion test

3.2.1 Description of specimen and machine

In this thesis the flow behavior of the material it was measured at relative large strains, therefore, the solid bar specimen is chosen. The used specimen has a gauge length of 10 mm and a gauge diameter of 6 mm, as can be seen in Figure 3.1
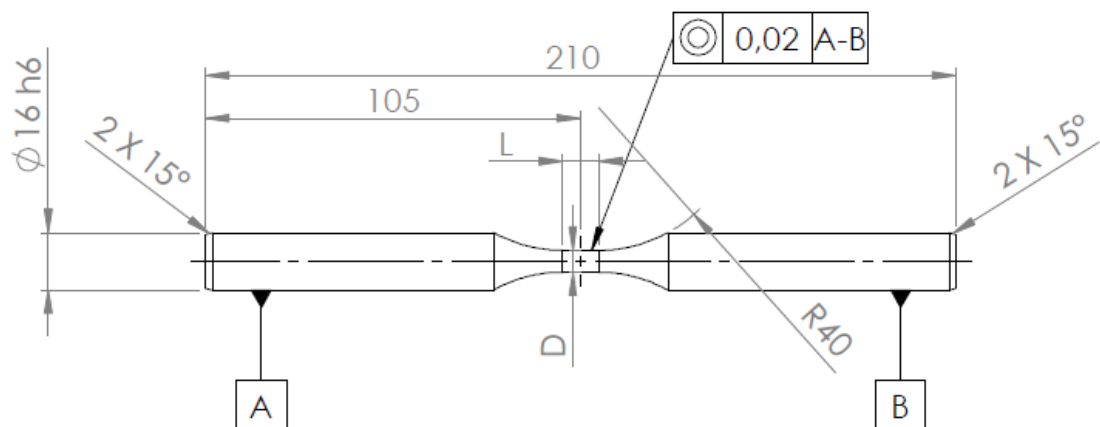

Figure 3.1: design of solid bar specimen

The torsion test machine used for the experiments is the STD812 machine produced by TA instrument. The STD812 is a servo hydraulic test machine and can perform torsion, tension and compression.
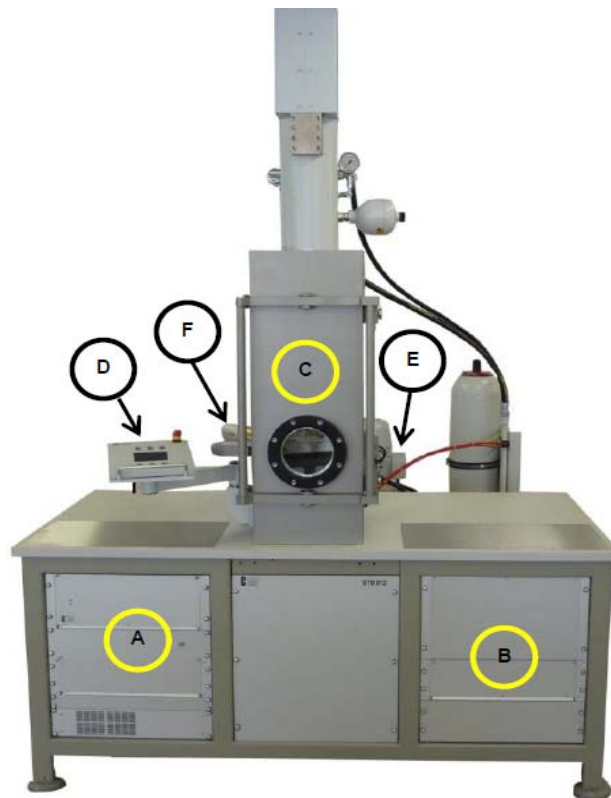
Figure 3.2: the torsion test machine STD812 [72]

This machine consists of six components substantially, as shown in Figure 3.2:

- A. Measurement data recording and control unit
- B. High-frequency generator, cooling water and gas supply
- C. Vertical measuring chamber
- D. Operating console with display
- E. Hydraulic unit
- F. Pyrometer

The measurement data recording and control unit is where the computer is connected with test machine. The operating console has a display for the monitoring of the experiments. The cooling system is connected to the measuring chamber, and argon gas was used as cooling medium.

In the Figure 3.3 it is shown the structure of measuring chamber. For perform the experiment, the specimen shall be fixed to the bottom and top clamping. The bottom clamping can rotate and torque is applied to specimen. The top clamping can be fixed in axial direction or movable. Experiments at room temperature are conducted with a quasistatic process and under atmosphere cirumstance. The strain rate for these experiments was $0.01\ s^{-1}$.

Experiments at hot working condition were conducted under vacuum circumstance. For hot torsion test, specimens are heated by inductive heating by coils. In order to control temperature during the experiment, two thermocouples are welded on the surface of the specimen. One thermocouples is fixed at the center of the gauge section and the other one thermocouples is fixed at the edge of gauge section. The investigated strain rates for hot working conditions are 0.01, 0.1 and 1 s^{-1}. The heating rate was set as 2 K/s with five minutes for temperature homogenisation

After the experiment, the main output is the raw torque-angle data, and these measurement data can be converted into stress-strain curves using an inverse modelling approach.
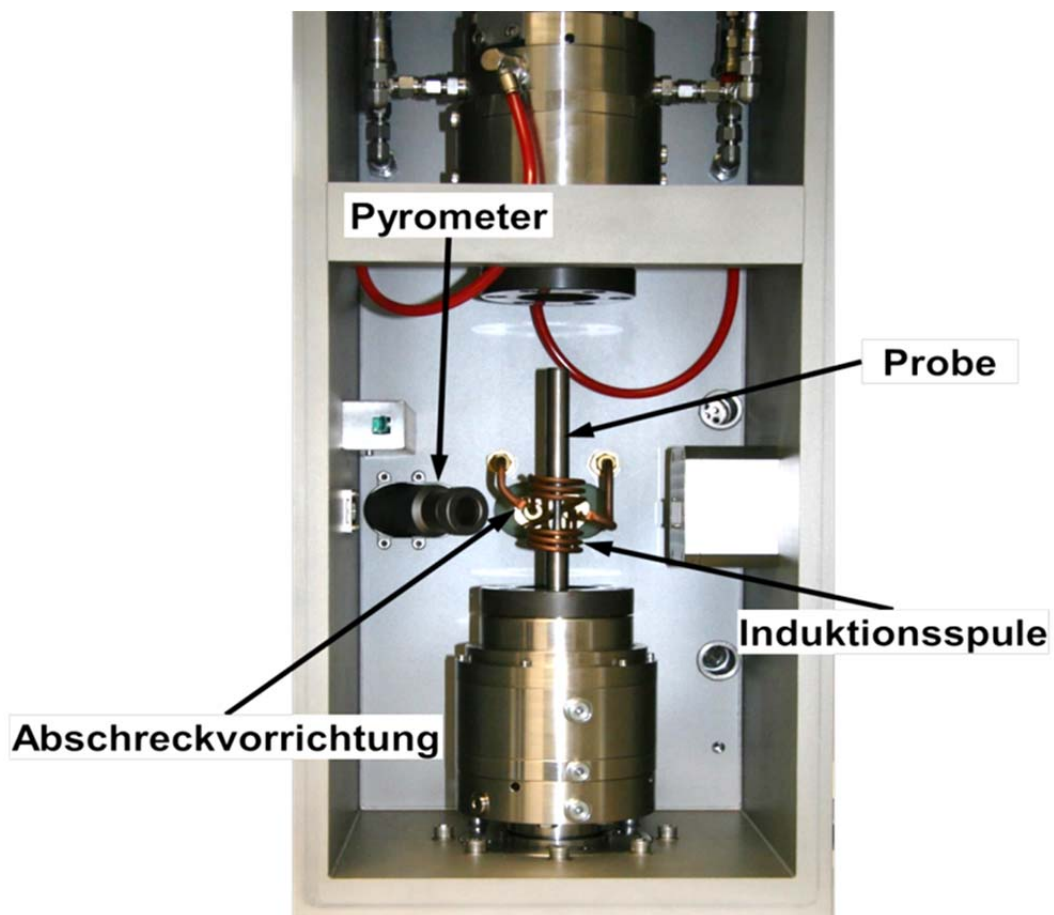

Figure 3.3: structure and components of measuring chamber in STD812 [72]

4 Finite element modelling (FEM)

To obtain accurate simulations and good results, the knowledge of the elasto-plastic material properties, especially in metal forming, is very important. Some tests like tensile tests, compression tests, torsion tests etc. have been developed with the aim to characterize the deformation behavior of materials [48].

In this thesis the FE modelling is used for inverse determination of flow curves out of torsion tests. For this purpose an elastic-plastic FE model is used which considers elastic and plastic deformation. With this method it is possible to analyse stress, strain distribution and variation of geometry during the deformation. So it is suitable for these deformation processes where the elastic deformation cannot be neglected [73].

The inverse evaluation of torsion test was conducted by comparing the measured torque in experiments and calculated by the FE-model. To minimize the difference between modelled and measured torque, parameters of the flow curve model has been optimized using Matlab-code. To simplify the inverse problem, simulation was done first for cold deformation and then for high temperature. The commercial FEM software used for the simulation of the torsion test is ABAQUS.

4.1 *Design of the FEM model*

The geometry of the FEM model represents half of the specimen geometry using a symmetry plane perpendicular to the axial direction. Figure 4.1 shows the design of the FEM model. Regarding the gauge section, the most important part for the calculation of strain and stress, more refined mesh was designed in this zone. The mesh type was hexahedron (cubic).

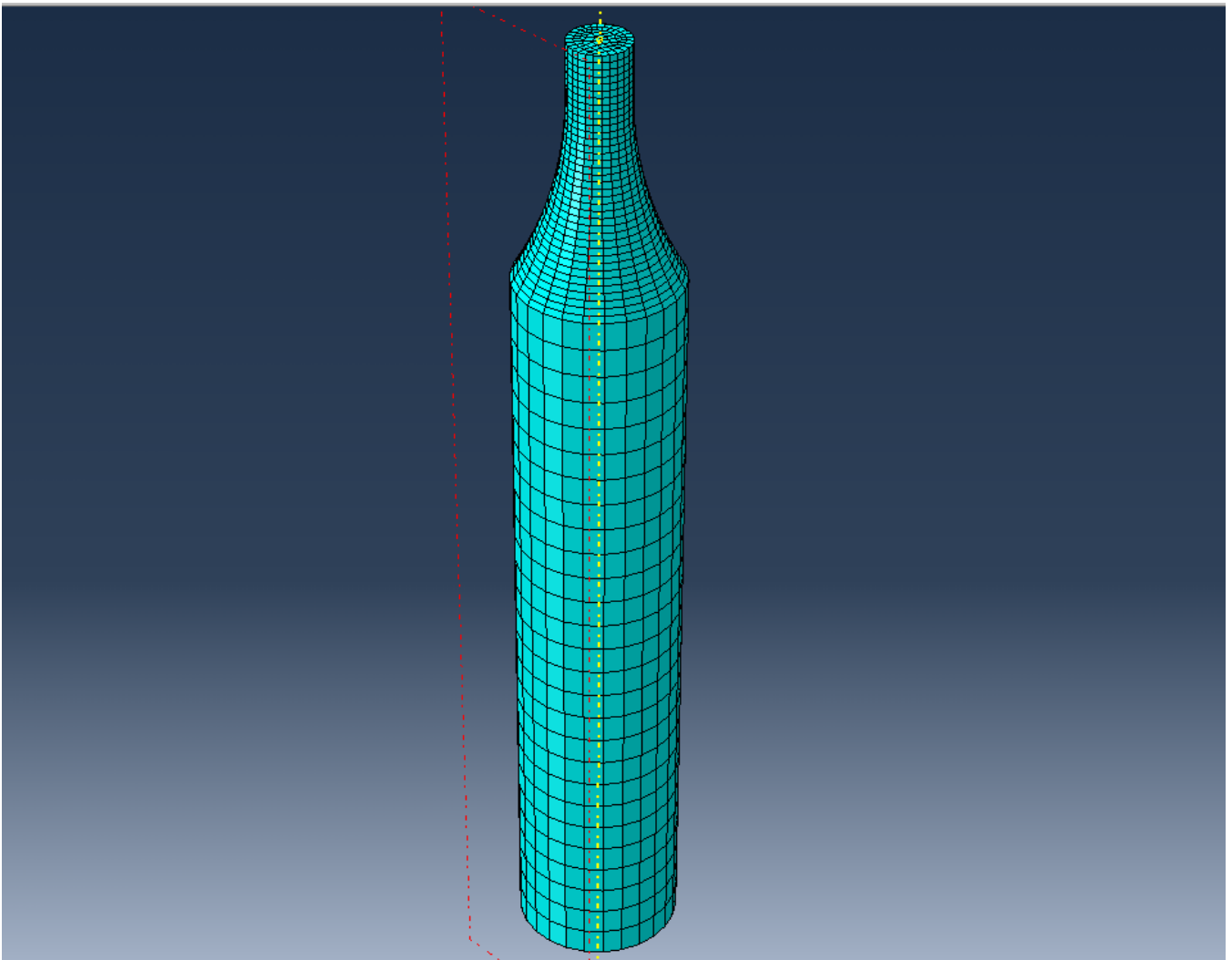**Figure 4.1:** FEM model of the torsion test

In the FEM model the convergence is the main purpose. The simulations are always a compromise of the calculation time and accuracy. In order to find the right compromise between calculation time and accuracy, the investigation and optimization of the FEM model was conducted. This includes the influence of boundary condition and the influence of the mesh size.

4.1.1 Boundary conditions

Within the FEM model the nodes of the ends of the specimen can be set as fixed or movable in axial direction according to the different boundary condition; but as show in Figure 4.2 from recent studies, there is no influence on the simulation result. Because of this, in the FEM model one end of the specimen was fixed and the moment was applied to nodes at the other end. The movement of specimen was defined as rotation to simulate the real experiment condition.
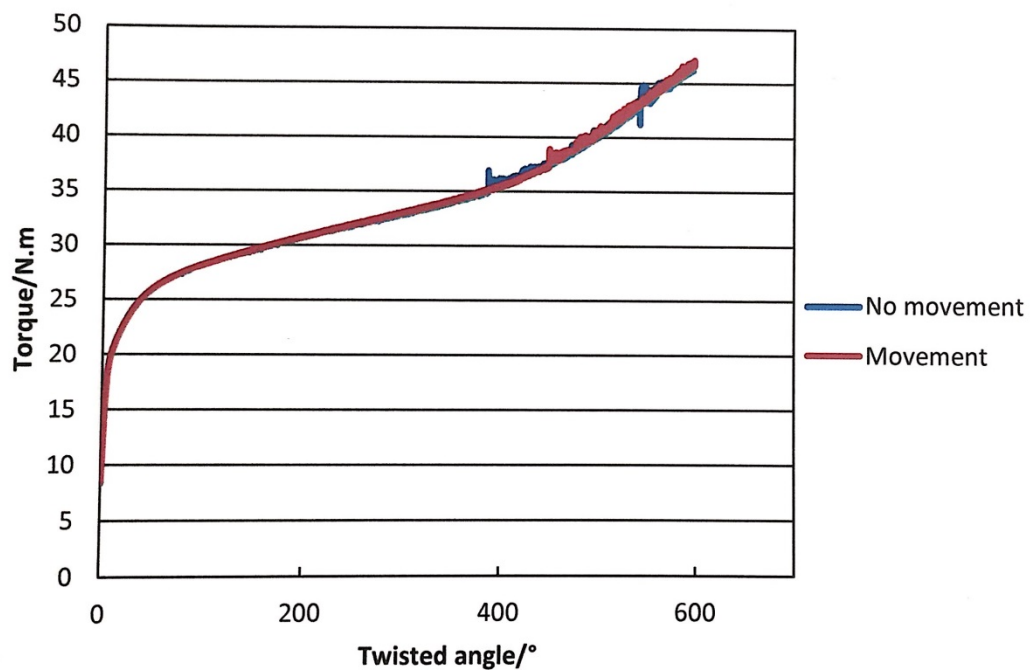

Figure 4.2: torque-twisted angle curves with different boundary condtion [47]

4.1.2 Load

As previously mentioned the rotational movement was applied to one end of the specimen. In the real experiments specimen was rotated 720°, what corresponds to 360° in the ABAQUS model. This effect may be explained in this way: using only half the geometry with symmetry and imposing a rotation of 720° to one end of the specimen, automatically it must impose another rotation of 720°, but in opposite direction, in the other end of the specimen. This results in a total rotation of 1440° along the gauge length of 10 mm, see Figure 4.3. Thus imposing a rotation of 360° in ABAQUS and multiplying by two, the target movement is obtained.
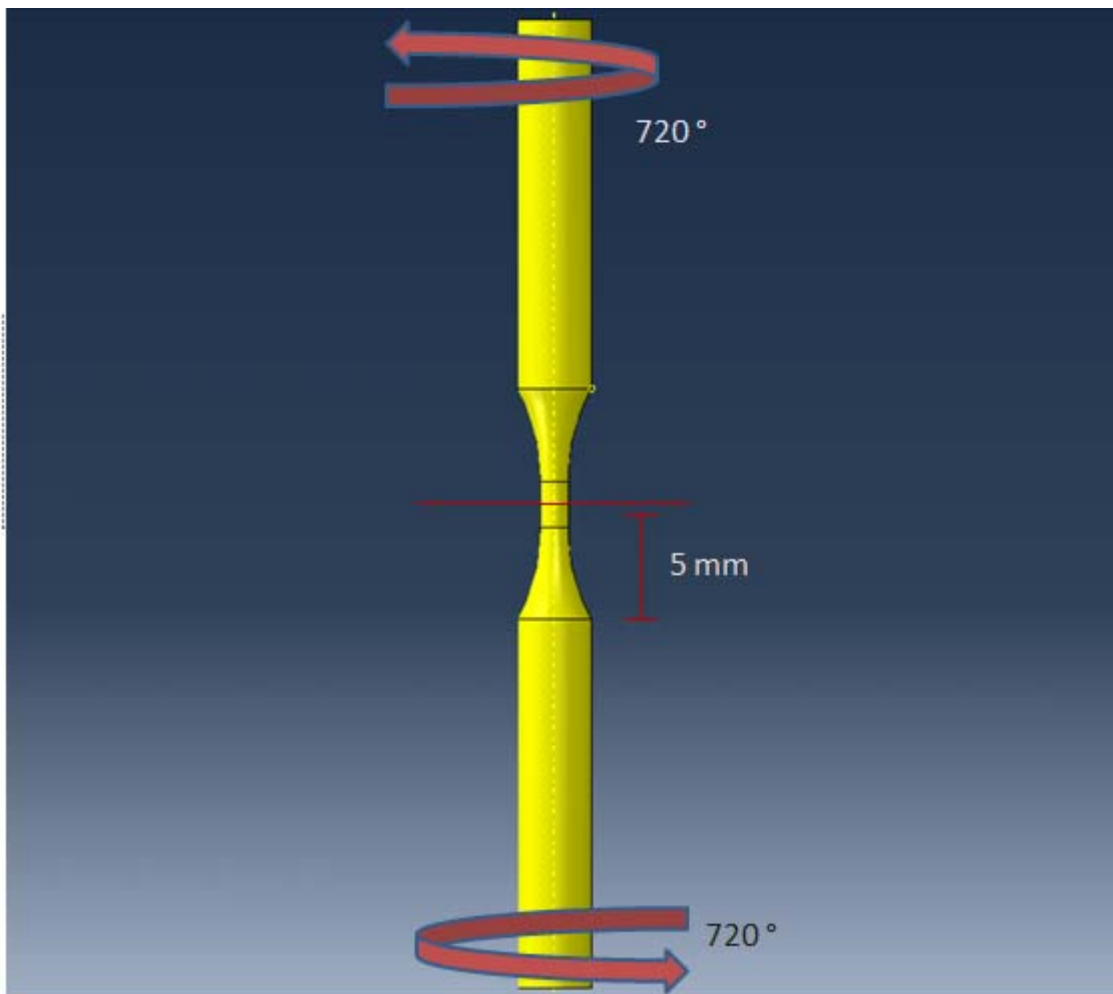

Figure 4.3: schematic diagram of the load

4.1.3   Mesh

In a simulation there are some user defined parameters. One of the most important is the mesh density which has a great influence on accuracy and calculation time. The discretization should be stable and convergent [4]. In general the accuracy increase with increasing number of elements, but the calculation time costs much more. To find a suitable mesh density which leads to sufficient precise results in acceptable calculation time, simulations with different element edge size were done.
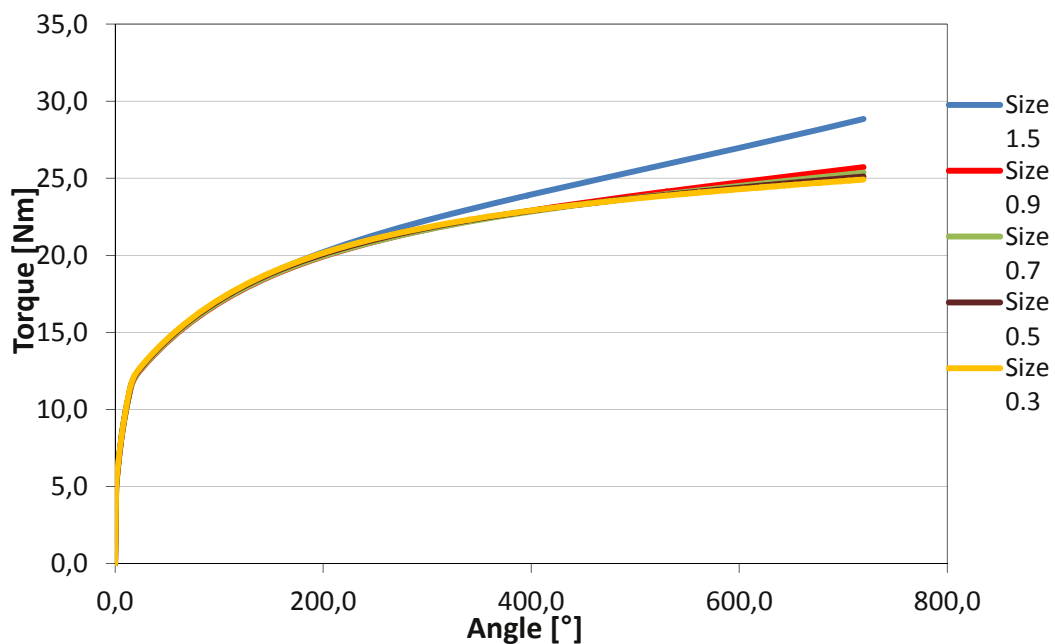
Figure 4.4: torque-angle curves with different mesh size

Figure 4.4 shows the different torque-angle curves obtained by simulation in ABAQUS. The mesh size used in FEM model varies from 1.5 mm to 0.3 mm. The curves of 0.9, 0.7, 0.5 and 0.3 mm overlap perfectly, but the curve of 1.5 mm is higher than other. This indicates that the mesh with the edge of 1.5 mm is not fine enough for this model. For a reliable and stable result in the simulation, the size of the element edges should be not less than 0.9 mm. In this model a size of 0.7 mm was selected, because that is the right compromise between accuracy, calculation time of simulation and also of the mesh distortion.

In fact another factor, which influences the success of the simulations in ABAQUS, is the excessive distortion of the mesh. Figure 4.5 show the excessive distortion of the elements during the simulation. This effect can cause an early stop of the simulation, or the final result may be completely wrong. To fix this problem some kind of pre deformed mesh mechanism for the simulation was developed.

ODB: Torsion_two_rotations.odb   Abaqus/Standard 6.14-3   Tue Dec 09 10:44:59 CET 2015

Step: Step-1
Increment   503: Step Time =   1.0000E-03
Primary Var: PE, Max. Principal
Deformed Var: U   Deformation Scale Factor: +1.000e+00
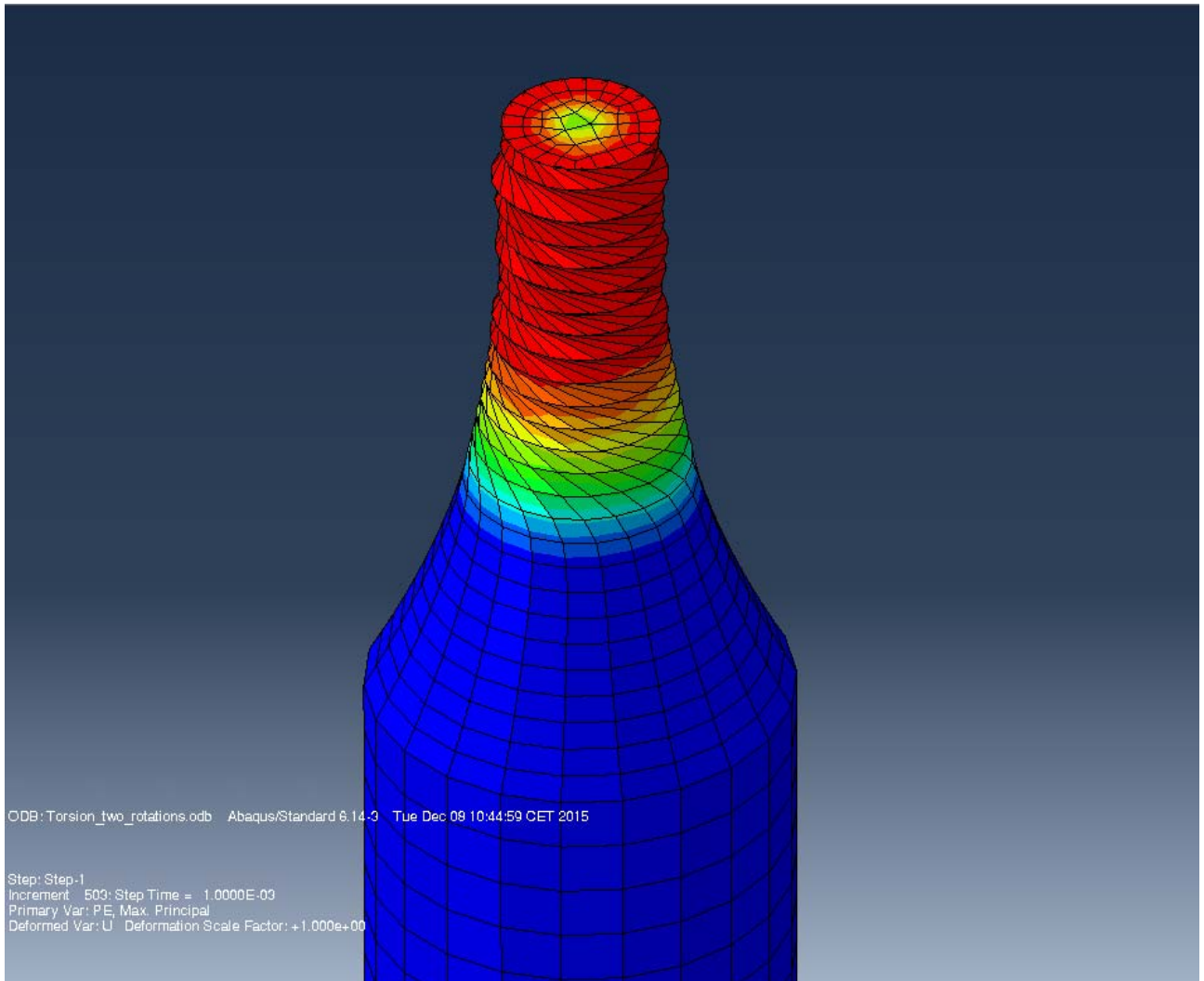
Figure 4.5: excessive distortion in the gauge length of the FEM model

4.1.3.1 The problem of pre-deformation

In many nonlinear simulations the material in the structure or process undergoes very large deformations. These deformations distort the finite element mesh, often to the point where the mesh is unable to provide accurate results or the analysis terminates for numerical reasons. So in such simulations it is necessary to use some re-meshing tools for minimize the distortion of the mesh.

ABAQUS provides a very general adaptive meshing capability for highly nonlinear problems ranging from quasi-static to thigh-rate dynamic.

The main characteristics of the adaptive meshing are [75]:

- A smoother mesh is generated at regular intervals to reduce element distortion and to maintain good element aspect ratios
- The same mesh topology is maintained (the number of elements and nodes and their connectivity do not change).

Unfortunately this tool is very cost-effective, because improving mesh quality increases the computational time, therefore it was not used in this FE model. It was thought another, more simple method to be able to compensate the excessive distortion of mesh.

It was decided to use an algorithm that was able to give a sort of pre-deformation to the mesh (the mesh is pre-rotated at the beginning), and after which, set the rotation in the opposite direction in order to compensate the excessive distortion. This algorithm, which provide the pre-deformation, was developed in MATLAB. The way how it can work can be explained as follows.

The first thing to do is to import the node coordinates of the elements, as a vector in MATLAB. After that it must be indicated the desired angle for the pre-deformation, but obviously not all the elements, that are in the gauge length, must be rotated with a constant angle. The elements that are in the lower end of the gauge length should be rotated by a small angle, then this latter is increasing for upper elements, until reaching the desired angle. So the rotational gradient is a function of the gauge length and the desired angle:

$$y = mx + q$$

Eq 4.1

Where y is the gauge length, m is the rotational grandient and x is the angle. It is assumed that the intercept q is equal to zero. Therefore the rotational gradient is:

$$rotational\ gradient = \frac{angle}{gauge\ length}$$

Eq 4.2

As can be seen from the Eq 4.2, the smaller the gauge length, then getting closer to the upper end of this latter, the greater the rotational gradient.

The torsion in the simulation is carried out along the y-axis, so consequently the elements should be pre-deformed along this axis. For this purpose is introduced the rotational

matrix for a counterclockwise rotation around y-axis in MATLAB. The rotational matrix can be used to rotate a coordinate basis into new one and in this case, the vector is left alone but its components in the new basis will be different from those in the original basis. The rotational matrix is:

$$R_y(\beta) = \begin{bmatrix} cos\beta & 0 & sin\beta \\ 0 & 1 & 0 \\ -sin\beta & 0 & cos\beta \end{bmatrix}$$

<div align="right">Eq 4.3</div>

After the creation of this matrix, simply multiply the vector containing the node coordinates with the matrix itself, it is possible to obtain the new node coordinates. The results of the simulation after the pre-deformation, it is show in Figure 4.6. Where in the top part of the picture, the first and final step of the simulation before the pre-deformation are shown, in the bottom part of the picture, instead, the steps of simulation after the pre-deformation are shown.
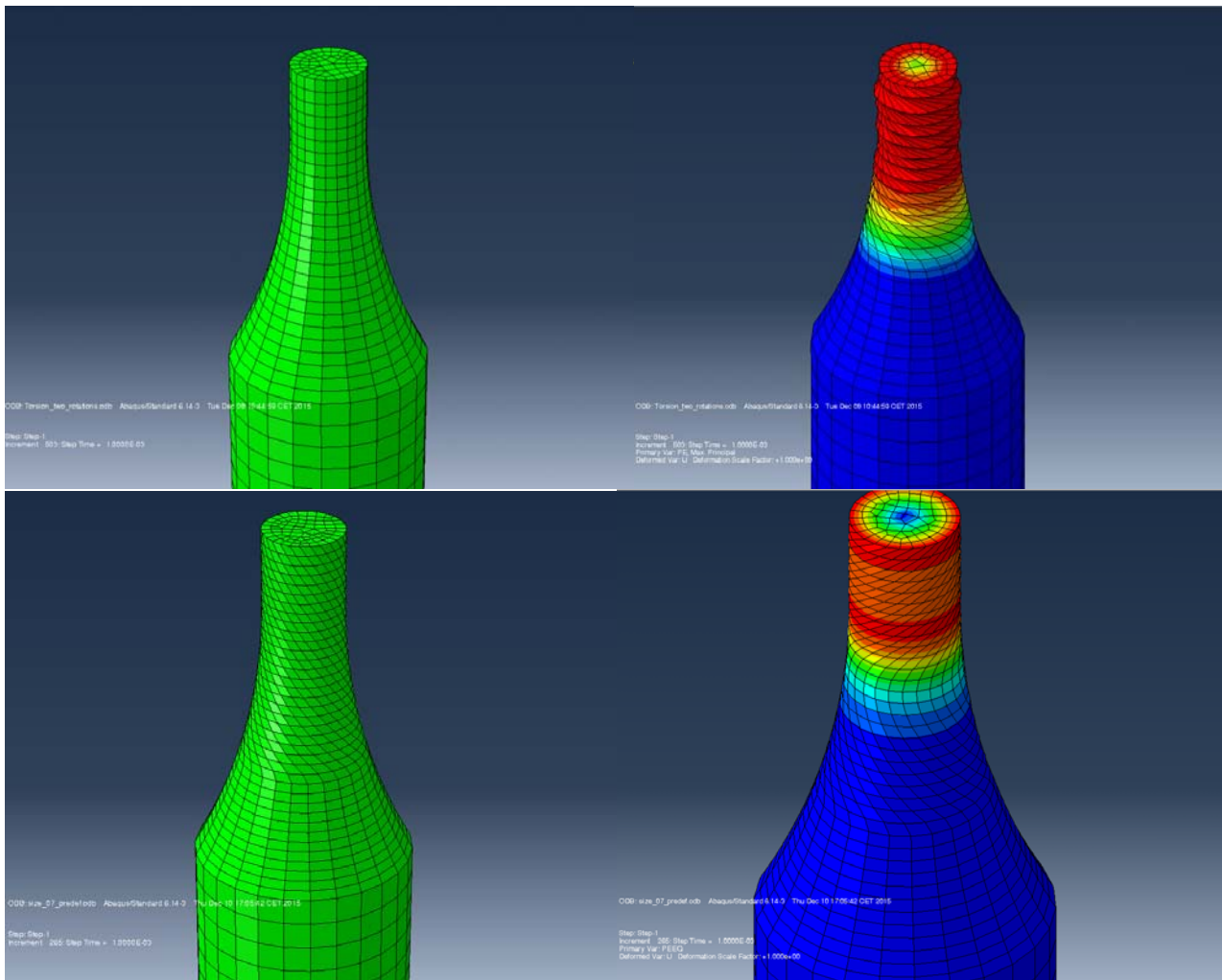

Figure 4.6: simulations before and after the pre-deformation

4.2 *Simulation*

Before run the simulation it was necessary to set some information about the behavior of the material in ABAQUS. In particular:

- Young's modulus and Poisson's ratio for the elastic behavior
- Flow curve (yield stress and plastic strain) from the experiment for the plastic behavior

The value of the Young's modulus is equal to 210 GPa, typical of steel. The Poisson's ratio varies between 0.0 and 0.5 in general. Most steels exhibit values of about 0.3. Therefore in the case of the 18CrNiMo7-6 hardening steel the value is 0.3, in according to the DIN EN 10084 [71].

The flow curve implemented in ABAQUS for the simulation of cold deformation, derives from the torsion machine used in the experiment, which is the red one in Figure 4.7 .
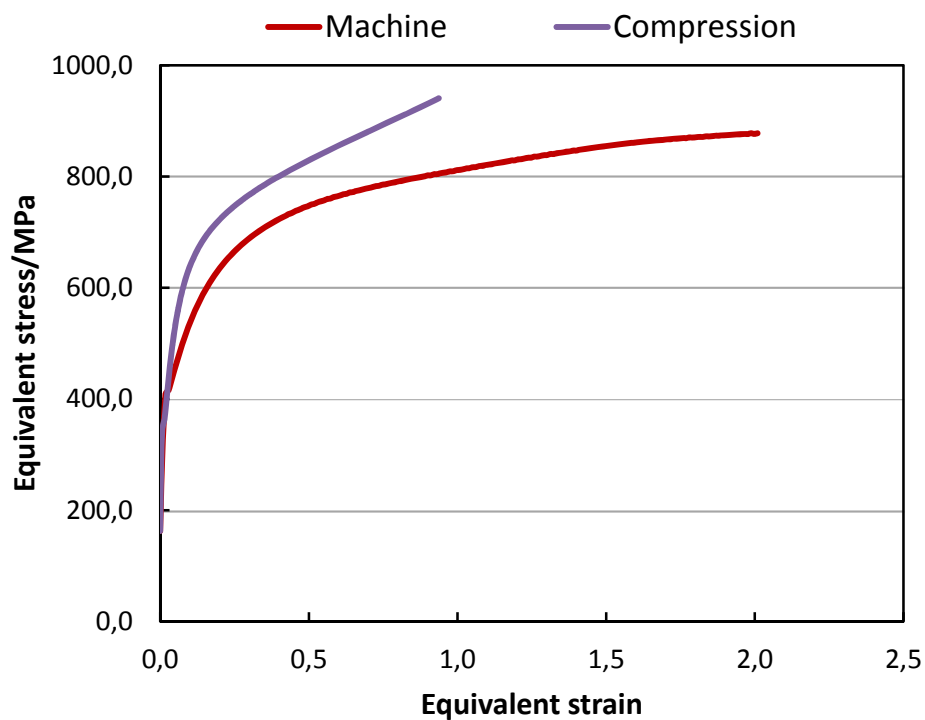

Figure 4.7: flow curve of torsion test machine from the experiment

In ABAQUS it is possible to obtain more than one output, the main output, for this case ,are:

- Reaction moment (torque)
- Rotations displacement (twisted angle)

The most important output data are the torque versus twisted angle curve, see Figure 4.8. This curve is subsequent to the simulation, compared with the experimentally measured torque versus twist angle curve. The optimization to reduce the discrepancy between the torque-twisted angle curve are described in chapter 5.
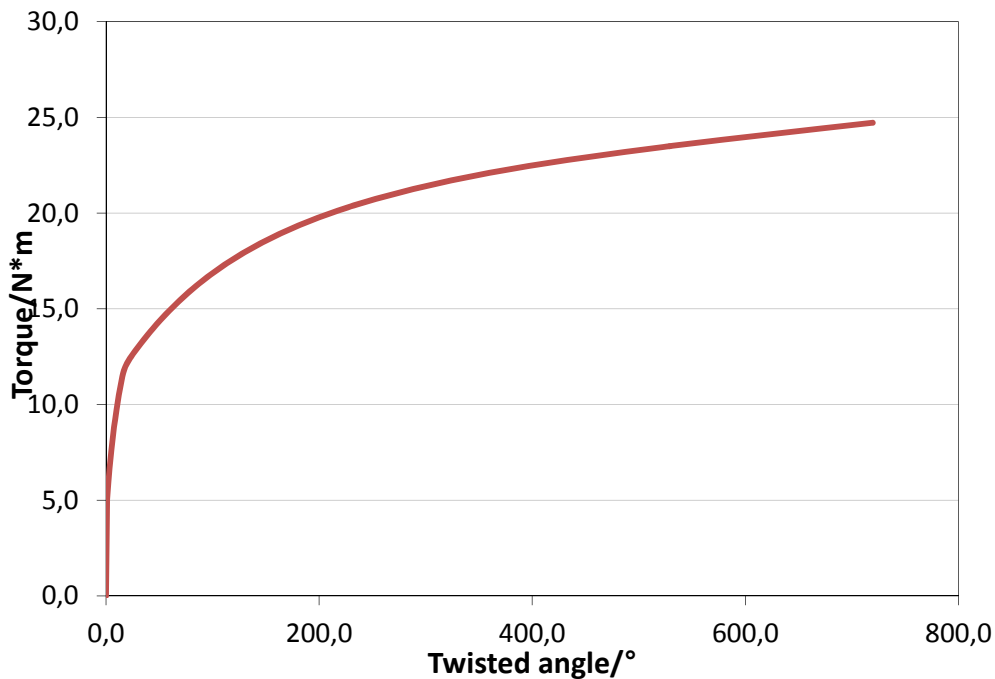
Figure 4.8: torque vs angle curve from ABAQUS

4.3 *Simulation of hot deformation*

By using hot working physical simulation, it can quickly generate the data necessary to improve or optimize a production hot working schedule [76]. One of the main factor which has a great influence in the accuracy of the hot working simulation, is the time period per step.

The deformation temperature is constant and it is set at 900 °C, therefore it is negligible for the purposes of the simulation. For the strain rate, instead, there were three different values:

- $0.01 \, s^{-1}$
- $0.1 \, s^{-1}$
- $1 \, s^{-1}$

For each of these values, it was necessary, run three simulation with three different model and for each of these latters set the time period equal to the time required to carry the torsion in the real experimental tests.

In the material section in ABAQUS was made the assumption that the elastic behavior is the same of the cold deformation, in order to simplify the simulation, but for the plastic behavior the experimental flow curves that correspond to the three different strain rate, have been implemented, as shown in Figure 4.9. Therefore it was necessary to perform three different simulation, but the main output of ABAQUS in the hot deformation is the same of cold deformation.
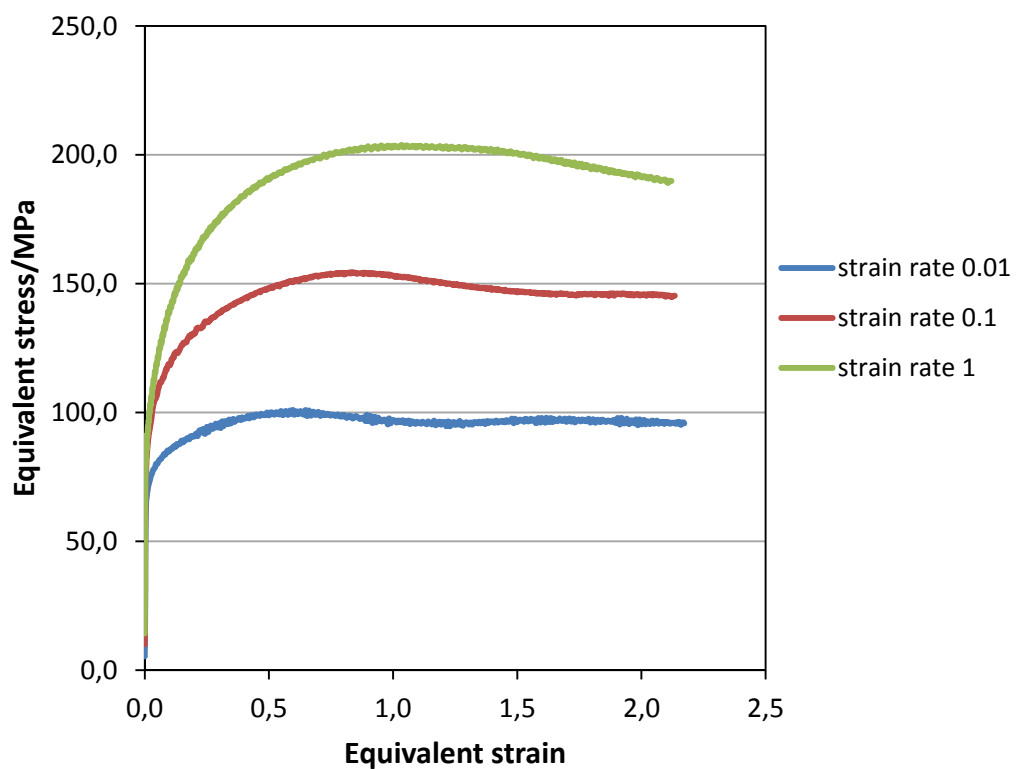

Figure 4.9: flow curves for different strain rate at 900°C

4.4 *Flow models for cold deformation*

The flow models used to describe the flow behavior, at room temperature, of the material investigated was: Ludwick's model and Voce model, which have the form:

$$\sigma = \sigma_0 + k\varepsilon^n \text{ (Ludwick)} \qquad \text{Eq 4.4}$$

$$\sigma = \sigma_s - (\sigma_s - \sigma_0)^{(-n\varepsilon)} \text{ (Voce)} \qquad\qquad \text{Eq 4.5}$$

In both models, there are three parameters to identify with the inverse modelling. In the Ludwick's model σ_0, k, and n, while in the Voce model σ_0, n, and σ_s. In the Ludwick's model, σ_0 is the initial yield stress, k is the strain hardening and n is the strain hardening exponent. In the Voce model σ_s is the saturation stress, σ_0 is the true stress and n is the strain hardening exponent.

These models have been discussed briefly in the paragraph 2.4.1.1 and 2.4.3.1. Both models are accurate into reproduce the flow materials behavior under cold deformation, and in particular the Voce model is suitable to fit data to higher strains.

4.5 *Flow model for hot deformation*

The flow model used to describe the flow behavior, at hight temperature instead, was the Hansel-Spittel model, which have the form:

$$\sigma = Ae^{m_1 T}\varepsilon^{m_2}\dot{\varepsilon}^{m_3}e^{\frac{m_4}{\varepsilon}}(1+\varepsilon)^{m_5 T}e^{m_7 \varepsilon}\dot{\varepsilon}^{m_8 T}T^{m_9} \qquad\qquad \text{Eq 4.6}$$

This model is complex because there are too many parameters to find with the inverse modelling, this corresponds to an increase of the time required to reach the convergence in the simulations. To overcome this problem, a simplified version of the model was used

$$\sigma = Ae^{m_1 T}\varepsilon^{m_2}\dot{\varepsilon}^{m_3}e^{m_4 \varepsilon} \qquad\qquad \text{Eq 4.7}$$

In this case there are five parameters to find with the inverse modelling: A, m_1, m_2, m_3, and m_4. This model has been discussed in the paragraph 2.4.2.2.

5 Inverse problem

The materials behavior can be obtained with the standard tests presents in the industrial practice, like tension test, compression test, bending test etc. For example the compression test is the most widely used, but one of the biggest disadvantage of this test, is that can be reached strain levels relatively low if compared to other tests, and is of about 0.8. Sometimes in the industrial processes there is the need to achieve higher strain levels, and it is possible to get them through the torsion test. Due to the inhomogeneous deformation in the torsion test, the analytical function used in this test, lead to no sufficient result, so it must be used another approach for optimize the flow models that describe the material behavior.

The unknown material parameters of the flow models are determined by means of a so-called ***inverse methods***, by iteratively minimizing the discrepancy between experimentally measured and numerically computed quantities. For implement this minimization operation, it must be use an optimization algorithm implemented in MATLAB were coupled with ABAQUS . In this thesis it was used the Levenberg-Marquadt algorithm.

5.1 *Matlab script*

A MATLAB script was developed and used in combination with ABAQUS for the inverse modelling. The first thing to do in the script is to implement the hypothesized flow model suitable to describe the material behavior. The initial parameters of the flow stress model are determined using the analytic evaluation of the torsion test.

The material parameters of flow model are determined in an iterative way by minimizing a cost function $C(\bar{p})$ which expresses the discrepancy between experimental measured torque and numerical computed torque. The cost function is the least squares expression [48]:

$$C(\bar{p}) = \left(\sum_{i=1}^{m} ((M^{exp})_i - (M^{num}(\bar{p}))_i)^2 \right)$$

Eq 5.1

where m is the number of measure, $(M^{exp})_i$ is the experimental measured torque, $(M^{num})_i$ is the numerical computed torque and $\bar{p}$ are the unknown parameters.

The necessary condition for a cost function to attain its minimum, can be expressed by stating that the partial derivatives of this cost function with respect to the unknown material parameters have to be zero:

$$\frac{\partial C(\bar{p})}{\partial p_i} = 0$$

<div align="right">Eq 5.2</div>

The goal, in fact, is to find the minimum value of the difference between the experimental measured torque and computed torque , by changing the material parameters of the flow model, see flow chart in Figure 5.1. To find this minimum value it was possible use the function non-linear least squares, which is called in MATLAB, $x = lsqnonlin(fun, x0)$. This function is used to fit a set of m observations with a model that is non-linear in n unkown parameters ($m>n$). The basis of the method is to approximate the model by a linear one and to refine the parameters by successive iterations [77]

In other words what it does the optimization algorithm is to start from the initial parameters of one flow model, and though simulations in ABAQUS, obtains the computed torque. Naturally there are differeces between the experimental and computed torque, so that MATLAB calculates this difference by performing a subtraction between the experimental and computed torque at certain angle values, and then raising it to the square.

If the quadratic error is not at its minimum value, the algorithm changes the parameters of the flow model and run a new simulation to calculate the torque again. This iterative process goes on until the flow model parameters that correspond to a minimum difference value are found.
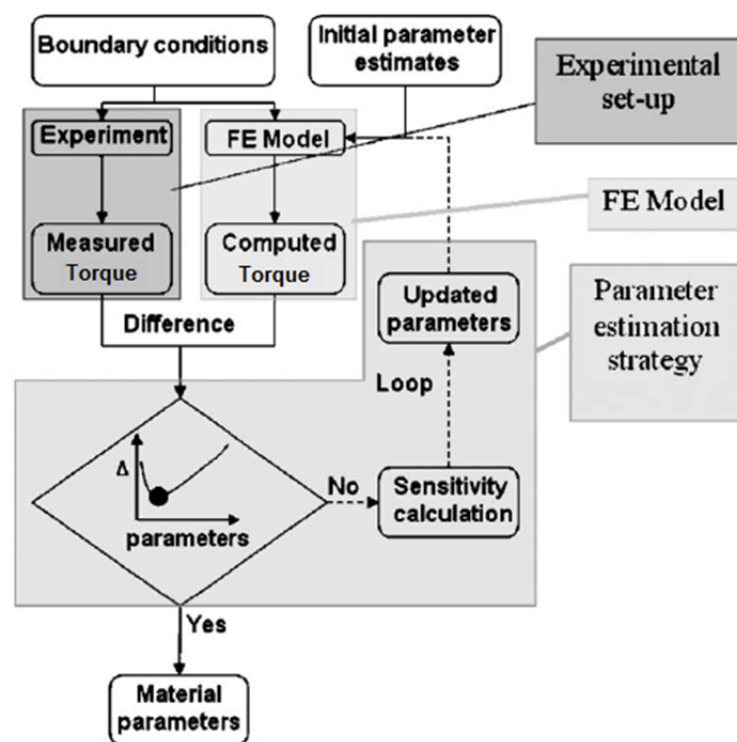

Figure 5.1: flow chart of the inverse method for material parameters identification [48]

Since the real cost function is locally approximated, the Levenberg-Marquardt algorithm determines the minimum of the local approximation and that is why it is an iterative procedure [48]. The Figure 5.2 show how the iteration procedure works. Where $C(\bar{p})$ is the real cost function, $C^*(\bar{p})$ is the local approximation of the real cost function, $\bar{p}^k$ are the initial estimated material parameters, $(\bar{p}^*)_{opt}$ are the material parameters that corresponds to the local minimum value of the square error and $(\bar{p})_{opt}$ are the material parameters that corresponds to the global minimum value of the square error. In order to obtain this value, it is possible change the initial material parameters from which to start the iteration of the algorithm.
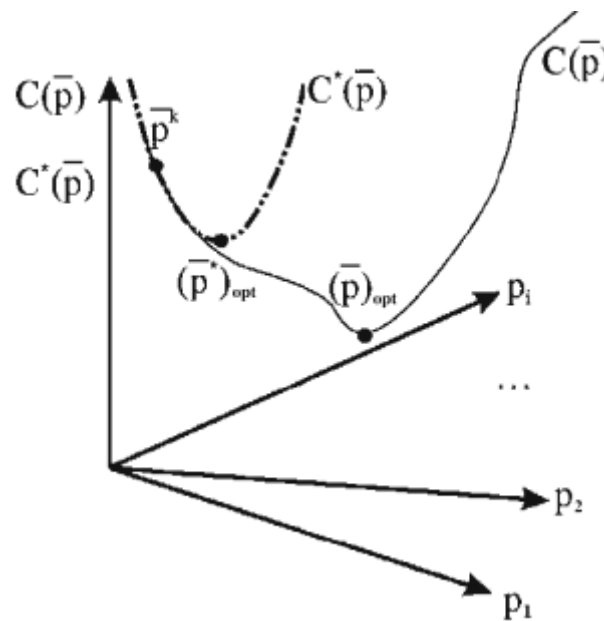

Figure 5.2: iteration procedure to find the minimum value [48]

5.1.1 Optimization

For the cold deformation the various optimization steps are described below.

Once the chosen flow model is implemented in the MATLAB script, the optimization can start. First of all MATLAB takes as the starting point of the iterations, the initial values of the material parameters (estimated).

The algorithm calculates the flow stress, using the definition of the chosen flow model. In this way the initial flow curve (the red one in Figure 4.7), is modified. Then MATLAB implements the new flow curve, with the new values of flow stress and plastic strain, in the FE model automatically.

After this MATLAB starts the simulation in ABAQUS, and at the end of this latter, makes a comparison between the simulation torque and experimental torque, calculating the

square difference. As previously mentioned MATLAB reduces this difference to a minimum value, by changing the material parameters.

Based on the number of the material parameters to be changed within the flow model, MATLAB carries these changes on the value that is indicated in an option of the lsqnonlin function, which is called "**DiffMinChange**". The DiffMinChange is the minimum change in variables for finite-difference gradients. In Figure 5.3 the optimization procedure of Ludwick's model for cold deformation is shown.

σ_0	K	n	Error
98,49	708,3	0,1769	7255,9323
98,4903	708,3	0,1769	7255,9238
98,49	708,3003	0,1769	7255,9276
98,49	708,3	0,1769003	7255,9416
200,60322	765,05925	0,0657743	5853,5555
200,60352	765,05925	0,0657743	5853,567
200,60322	765,05955	0,0657743	5853,5655
200,60322	765,05925	0,0657746	5853,5471
134,1023	707,06266	0,1140628	4009,3146
134,1026	707,06266	0,1140628	4009,3087
134,1023	707,06296	0,1140628	4009,3105
134,1023	707,06266	0,1140631	4009,3208
212,95462	762,03384	0,0310257	7951,0922
212,95455	762,03379	0,0310258	7951,0392
212,95383	762,0333	0,0310266	7950,9629
212,94671	762,02833	0,0310341	7949,7182
212,87556	761,97873	0,031109	7938,1544
212,17102	761,48757	0,0318509	7826,8865
205,76188	757,01949	0,0386002	6877,4498
173,45492	734,49699	0,0726217	3873,0376
173,45522	734,49699	0,0726217	3873,044
173,45492	734,49729	0,0726217	3873,0433
173,45492	734,49699	0,072622	3873,0298
140,19636	704,97049	0,1129108	3898,1946
166,22977	728,08259	0,0813742	3568,052
166,23007	728,08259	0,0813742	3568,0529
166,22977	728,08289	0,0813742	3568,0522

Figure 5.3: iteration step in MATLAB.

The detailed description of the optimization procedure is stated below.

The first three value in Figure 5.3 are the material parameters of Ludwick's model, σ_0, k, and n, the last value is the square error. At the beginning, starting from the initially estimated parameters, the algorithm runs the first simulation and calculates the square error. Obviously the first error value is not the minimum, therefore the algorithm runs a second simulation by changing the first parameters, σ_0. This change depends on the value

specified in the DiffMinChange option, so if this value is for example 3e^{-04}, MATLAB runs this second simulation by varying only σ_0 of 3e^{-04}. After this, it is runned another simulation by varying only k of 3e^{-04}, and another simulation by varying only n of 3e^{-04}.

Hence at the beginning the algorithm runs many simulation based on the parameters to be changed, changing them one per time. In the case of Ludwick's model for example there were three material parameters, so the algorithm has runned three simulation by changing one parameters per time and calcultes the square error.

After these variations, as it can be seen from Figure 5.3, the algorithm makes a large variation of all material parameters at the same time. On the basis of these new parameters, the algorithm starts again by changing one parameter per time. This iterative process goes on until the minimum value of the square error is found.

In other words looking at the Figure 5.2, the algorithm moves along the curve by performing these small changes of 3e^{-04} and if the point in which it is located in that moment is not a minimum, carries a largest change in order to find a minimum.

In Figure 5.4 the trend of the square error in function of the number of simulation runs is shown. It can see how it decreases with the increase of the number of simulations performed.
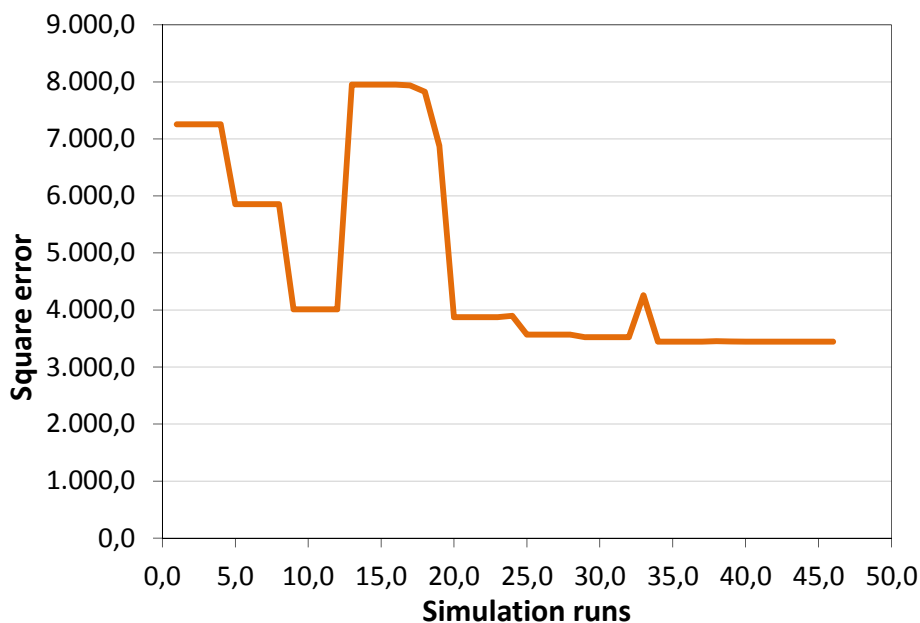

Figure 5.4: square error vs simulation runs curve for the first optimization of the Ludwick's model

This optimization procedure to find the material parameters is exactly the same for all the flow models both for cold deformation and hot deformation. The only difference in the hot deformation lies in the flow curves to be modified, in fact are the curves in Figure 4.9.

Since there are three different flow curves, with three different levels of strain rate, it was necessary to perform three optimization, one for each flow curve. Obviously the flow model used to describe the material behavior under hot working conditions, is the same for each flow curve, and it is the Hansel-Spittel model.

However, the working principle is exactly the same of the cold deformation optimization, just described.

5.1.2 Influence of starting point

When the algorithm ends the optimization and finds a local minimum value ($\bar{p}^*_{opt}$ in Figure 5.2), it is possible to set a new starting point, in order to obtain a better result and find a global minimum ($\bar{p}_{opt}$ in Figure 5.2). So these starting points have a big influence on the accuracy of the final result.

In particular in the Ludwick's model the strain hardening exponent, n, has caused many problems in the simulations, when it was adjusted by the algorithm.

Being n much smaller than the other two material parameters, its initial value was in fact 0.1769, when it was changed of $3e^{-04}$, resulted a variation of 0.17% compared to the initial value. This precentage increases much more, when the algorithm has made the largest change to all three parameters simultaneously. So n was adjusted to much, compared to the other parameters. This caused problem in the simulation, and it has finished early. In Figure 5.5 the effect of the change of n on the flow curve obtained by the Ludwick's model, is shown.
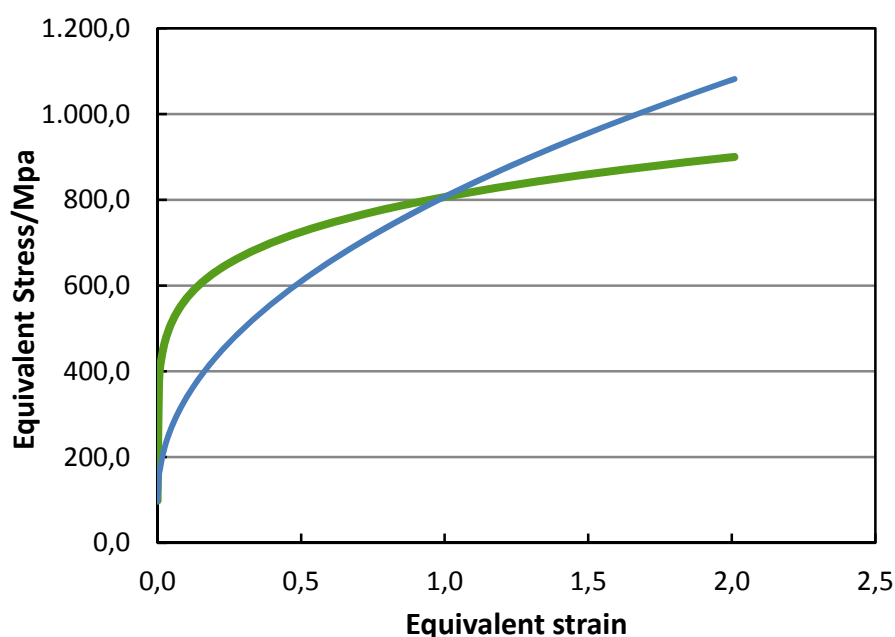

Figure 5.5: flow curves obtained with different value of n in the Ludwick's model

In Figure 5.5 the green flow curve is that obtained with the initial parameters of Ludwick's model, the blue one instead, is the flow curve obtained after the excessive adjustement of n. As it can be seen, the increase of n causes a flattening of the flow curve, assuming a similar appearance to that of straight line. This effect has caused a sudden stopping of the simulation in ABAQUS.

To fix this problem it was thought to scale n, multiplying it by 1000 (176.9), after this it is changed of $3e^{-04}$, and subsequently was divided again by 1000 before the implementation of the flow curve in the FE model. In this way the percentage of variation is 0.00017%, so with this scale factor the simulation and the optimization process have been successfully completed. In the case of hot deformation, there were no particular problems with the starting points.

6 Results and discussion

In this chapter, the result from the simulations and optimization of torsion test will be discussed. The results of investigation at room temperature with different flow model for the optimization are presented and analyzed. Subsequently, the results of investigation at high temperature with the Hensel-Spittel model for the optimization are discussed. The differences between the flow models, for the description of the material flow behavior, are discussed with the comparison between torque-twisted angle curves from the experiments and modeled ones.

6.1 *Investigation at room temperature*

As mentioned in the paragraph 4.2 for the simulation in ABAQUS it was necessary to implement a flow curve, deriving from the experiments, in order to reproduce the plastic behavior of the material. Initially for the simulation at room temperature, the flow curve obtained from the compression test has been implemented. The stress-strain curve obtained from this test is shown in Figure 6.1.
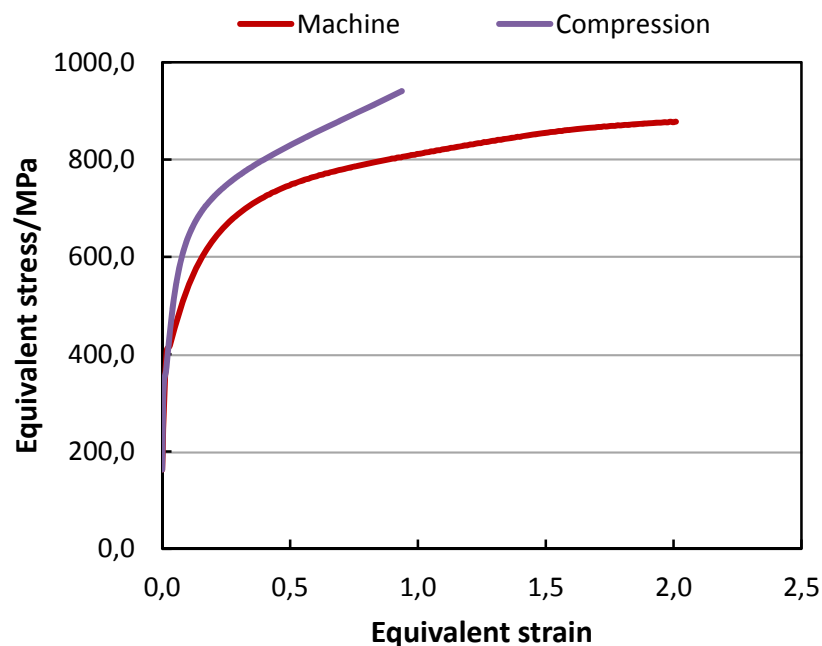

Figure 6.1: flow curve from the compression test and torsion test machine

The Figure 6.2 shows the comparison between torque-twisted angle curve measured from the torsion experiment at room temperature and torque-twisted angle curves from the simulations with the implementation of compression test curve and torsion test curve (machine evaluation method).
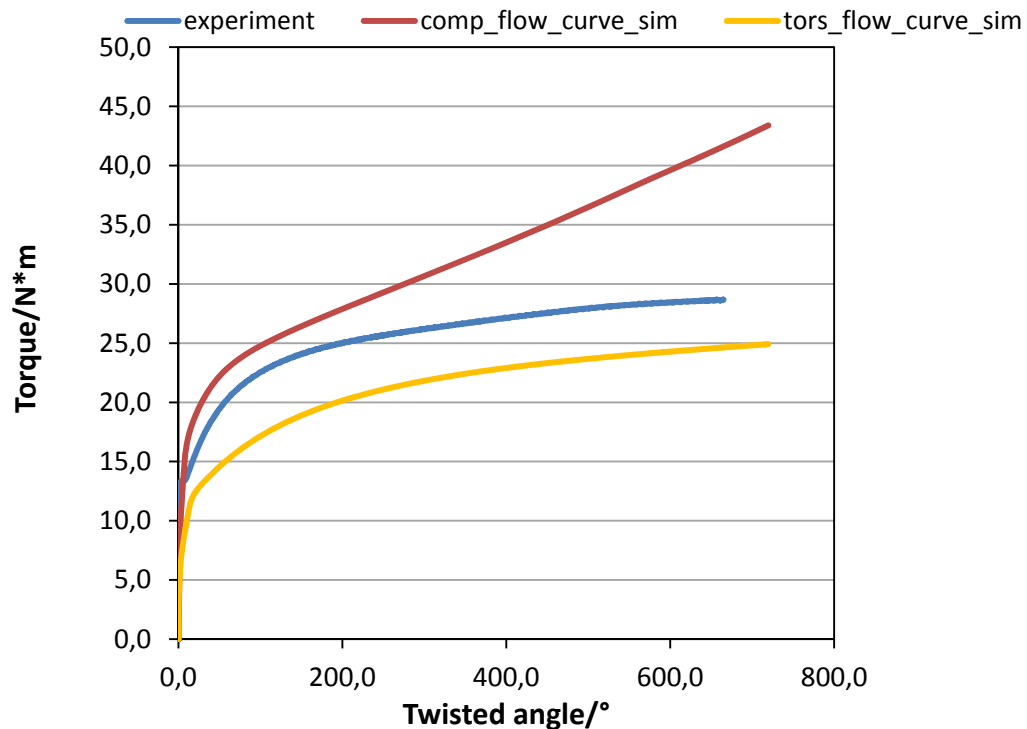

Figure 6.2: comparison between torque-twisted angle from experiment and different simulations

Since the experiment was conducted at room temperature, the work hardening dominated the deformation process. Apparently, the effective stress determined through compression test in Figure 6.1 is higher than torsion test. This may be caused by the fact that the material is hard to flow at room temperature, so the friction in the compression test influences more on the flow stress, despite the attempt of reducing by using lubricant. For this reason in Figure 6.2 the simulation curve deriving from the implementation of the compression test flow curve, reaches very high values of torque, moving away a lot from the experimental curve. The simulation torque-twisted angle curve deriving, instead, from the implementation of the torsion test machine flow curve, is much closer to the experimental one.

Therefore, for the simulation at room temperature the flow curve from torsion test machine has been used.

6.1.1 Evaluation of Ludwick's model

At first, it was necessary to calculate the initial material parameters (starting point) for the Ludwick´s model (see paragraph 2.4.1.1 for the description) from which to start the algorithm. For this purpose, the function "***cftool***" in MATLAB was used.

This simple function is able to create a fit, based on a specific equation, of any curve. Therefore, what has been done is to plot the experimental flow curve, and subsequent enter the Ludwick equation to fit the curve itself, see Figure 6.3. Following the "cftool" calculates the equation parameters to create the right fit. The determined parameters , are stated in Table 6.1

Starting points	First optimization
σ_0	98.49
k	708.30
n	0.1769

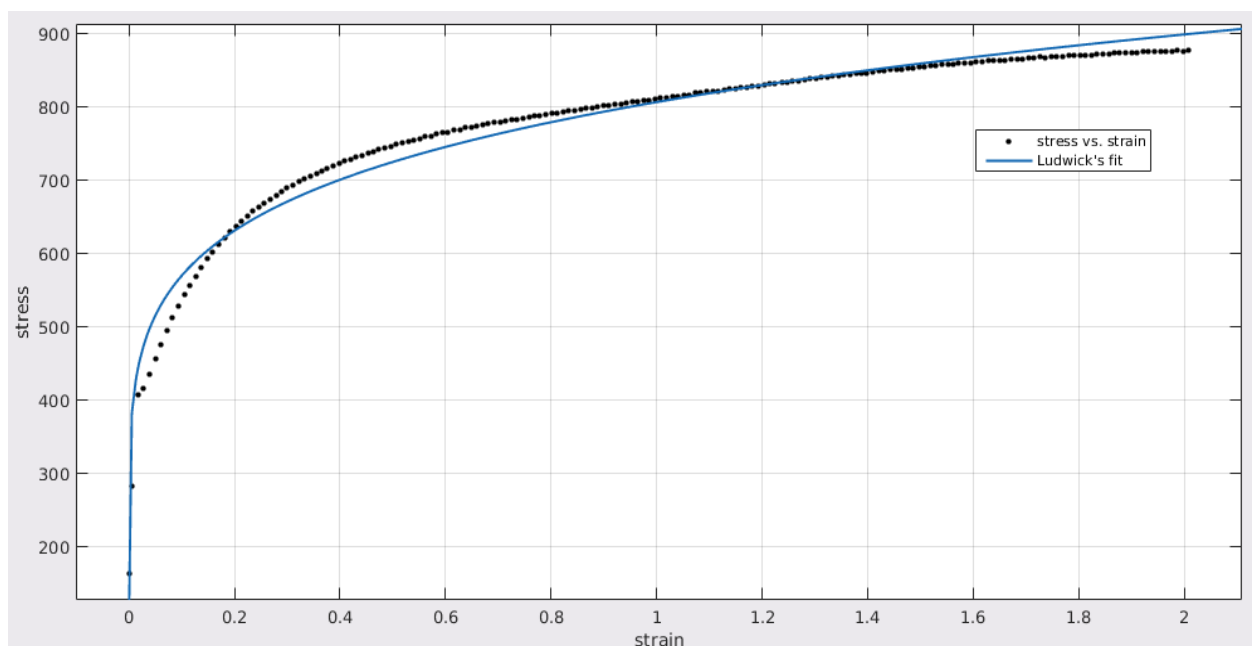**Table 6.1:** starting points for the first optimization of the Ludwick's model

Figure 6.3: curve fitting tool in MATLAB

These parameters are used as starting point. For the evaluation of goodnes of fit, this tool has used the coefficient of determination R_c . This coefficient varies between 0 and 1, and it shows how well the flow model fits the experiment data: if the coefficient of determination is 1, this means all the points of model fit the experiment data. If this coefficient is 0, this means no points of model fit the experiment data. The coefficient of determination is:

$$R_c = \sqrt{1 - \frac{\sum_i (M_i - f_i)^2}{\sum_i (M_i - \bar{M})^2}}$$

Eq 6.1

Where, M_i is the value of torque at certain point i, f_i is the value of modeled torque and $\bar{M}$ is the average value of torque [1]. The coefficient of determination in this case was 0.973, which is quite close to 1, so the Ludwick's model seemed to be suitable to represent the flow curve from torsion test machine.

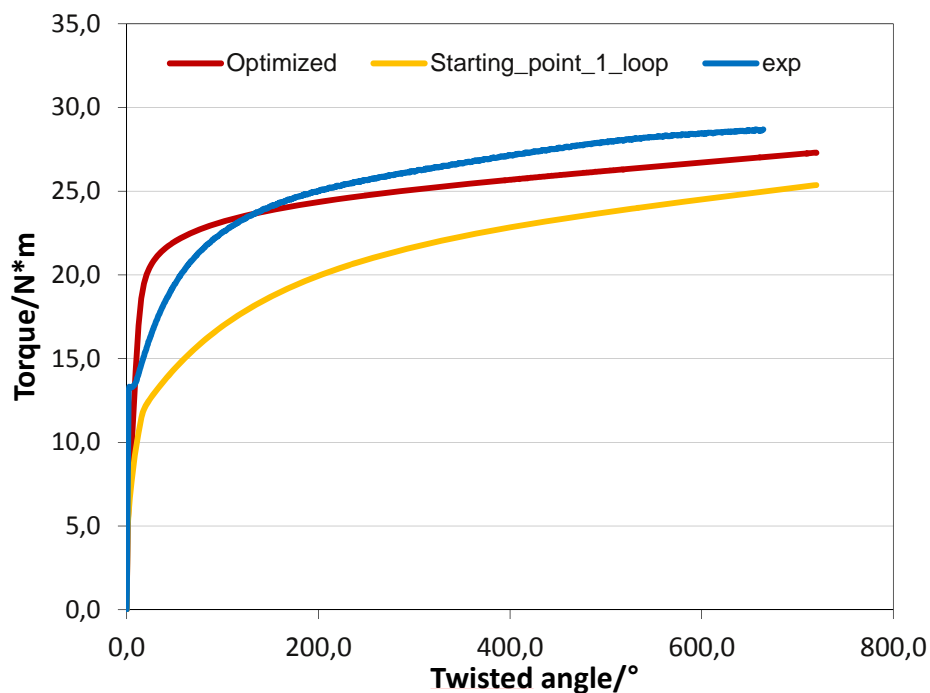The way that the algorithm works is explained in detail in the paragraph 5.1.1.

Figure 6.4: first optimization of the Ludwick's model

The results of the optimization of Ludwick's model are shown in Figure 6.4. The blue curve is the torque-twisted angle curve from the experiment at room temperature, the red one is the torque-twisted angle from the simulation of the optimized Ludwick's model

and the yellow one is the starting point. In Figure 6.5 the comparison between the flow curve obtained with the first optimization of Ludwick's model and the initial flow curve is shown.
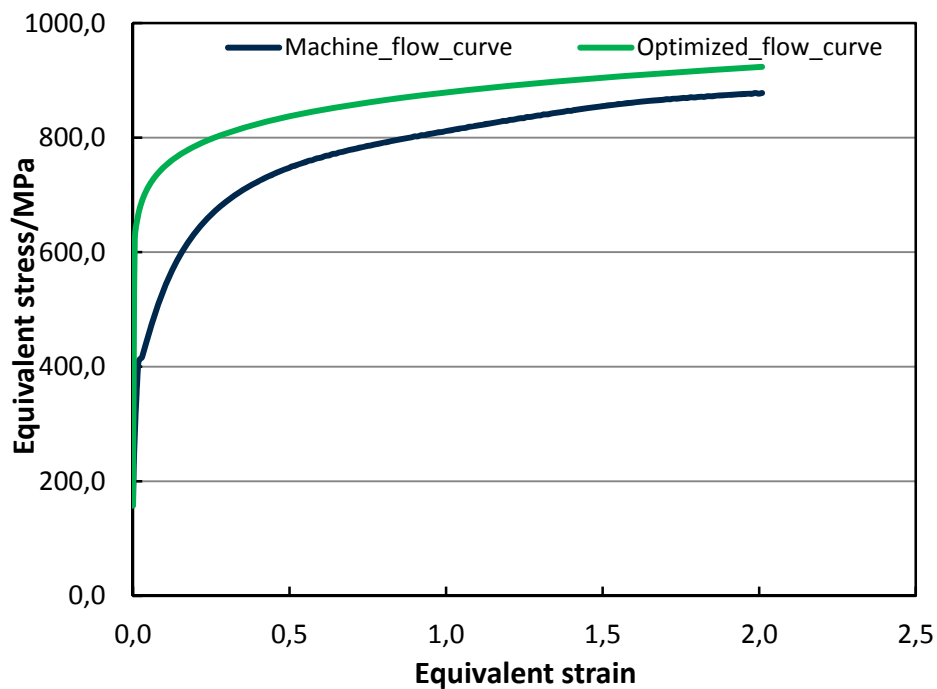

Figure 6.5: optimized flow curve from the first optmization of Ludwick's model

The result of this first optimization was not very accurate, in fact there was a large discrepancy between the experimental data and modeled ones, especially at small and very large angles.

A very simple way to achieve a better result, is to change the starting points (see paragraph 5.1.2). Looking at the flow curve obtained with the first optimization, it was possible to see what happens by changing the material parameters. With these change, it was seen what is the effect which they have on the flow curve, so as to reduce the difference between the torque-twisted angle curves. The result of the optimization with the new starting points is shown in the Figure 6.6 and Figure 6.7. For example, it was found that n, when increased, has the effect of flattening the flow curve, making it similar to a straight line. Therefore in order to reduce the discrepancy at small angle values in the dark curve, the strain hardening exponent n was incremented. The effect of σ_0, instead, is to increase the value of the flow stress in the final part of the flow curve. Therefore in order to reduce the discrepancy at large angle values, the initial yield stress σ_0 was incremented. The information regarding the starting points of the second optimization, are stated in Table 6.2

Starting points	Second optimization
σ_0	157.27
k	721.58
n	0.2570

Table 6.2: starting points for the first optimization of the Ludwick's model
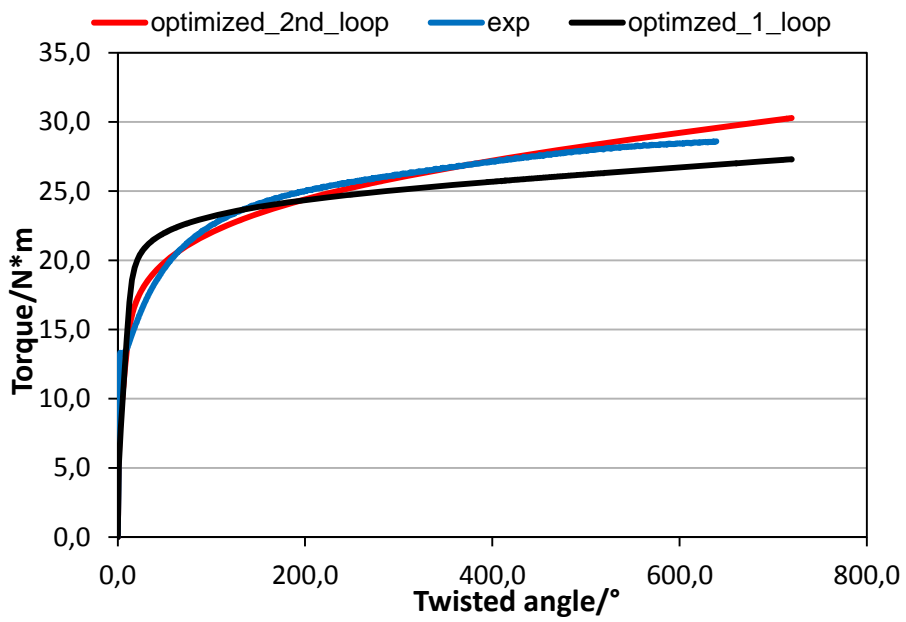

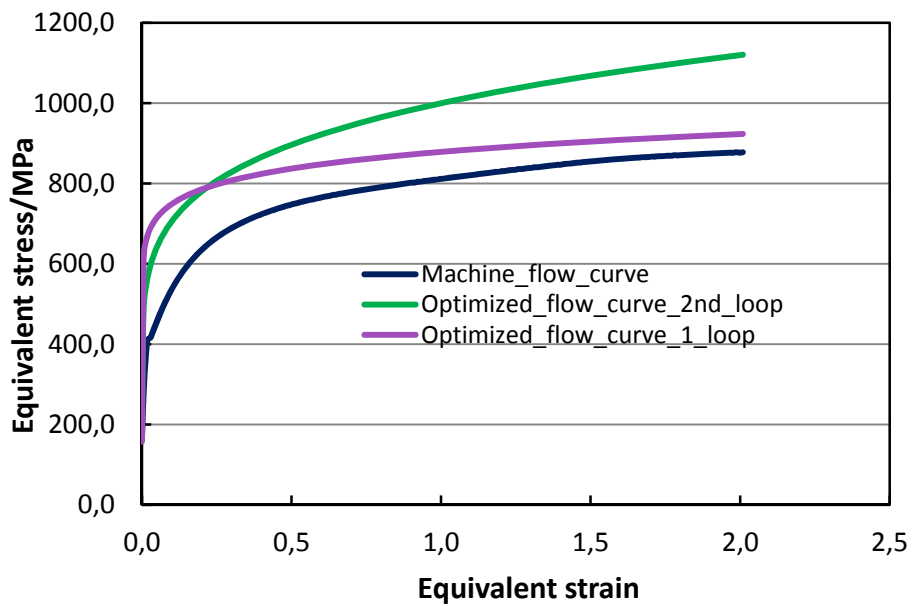**Figure 6.6:** second optimizaton of the Ludwick's model

Figure 6.7: optimized flow curve from the second optmization of Ludwick's model

The detailed information regarding the value of the material parameters after the optimizations of the Ludwick's model and the error are added in the follow table

Optimized parameters	First optimization	Second optimization
σ_0	157.27	227.68
k	721.58	772.47
n	0.0865	0.2087
$Error$	3444.56	79.94

Table 6.3: informations about material parameters of the Ludwick's model

As it can see from Table 6.3, that the error in the second optimization is much less than the first one, and this is also confirmed by the fact that the optimized curve in Figure 6.6, is much closer to the experimental one, so the difference between the experimental torque and modeled torque is much less.

Although this is a very good result, the trend of the optimized torque-twisted angle curve in Figure 6.6, does not follow perfectly the trend of the experimental curve, with marked differences in some areas. This means that maybe there are better modells to describe the flow behavior, at room temperature, of the investigated material.

6.1.2 Evaluation of Voce model

For the evaluation of the Voce model, the working principle is the same as for the Ludwick's model.

Regarding the calculation of the starting points, the coefficient of determination R_c was 0.951, that is less than in the case of Ludwick's model, but close to 1 so it is a good result.

The results of the optimization of the Voce model are shown in Figure 6.8. Also in this case, the blue curve is the torque-twisted angle curve from the experiment, the red curve is the torque-twisted angle from the simulation of the first optimization of Voce model and the yellow one is the starting point. In Figure 6.9 the optimized flow curve is shown
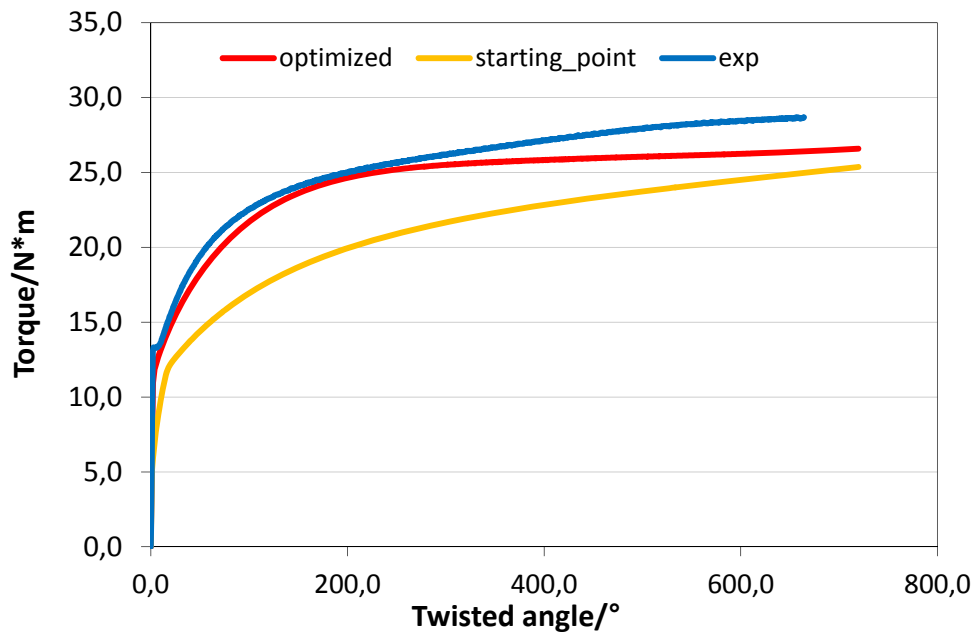
Figure 6.8: first optimization of the Voce model
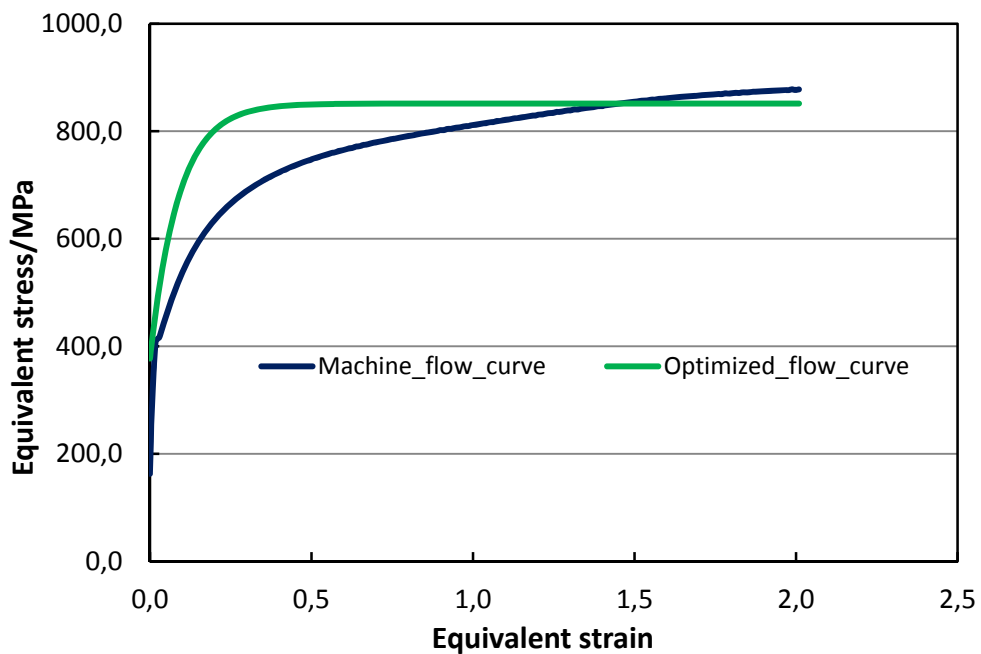
Figure 6.9: optimized flow curve from the first optimization of Voce model

As it can see, that the flow model reproduce the behavior of the material very well, in fact the simulation torque-twisted angle curve has a very loyal trend to the experimental one, especially in the initial part. From twisted angles of app. 300, due to achievement of the saturation by the flow stress, characteristic of the Voce model, the curves have a considerable discrepancy.

To reduce this discrepancy, thus obtaining a more accurate result, the starting points have been changed, in particular σ_s in order to increase the saturation point and thus get closer to experimental curve. The results of the optimization with the new starting points are shown in the Figure 6.10 and Figure 6.11. The information regarding the starting points of the optimizations, are shown in the Table 6.4.

Starting points	First optimization	Second optimization
σ_s	851	900
σ_0	376.50	376.50
n	3.23	3.50

Table 6.4: starting points of the optimization of the Voce model

The detailed informations regarding the value of the material parameters after the optimizations of the Voce model, instead, and the error are added in the follow table

Optimized parameters	First optimization	Second optimization
σ_s	851.50	902.87
σ_0	377.32	378.98
n	11.309	10.42
Error	355.20	63.67

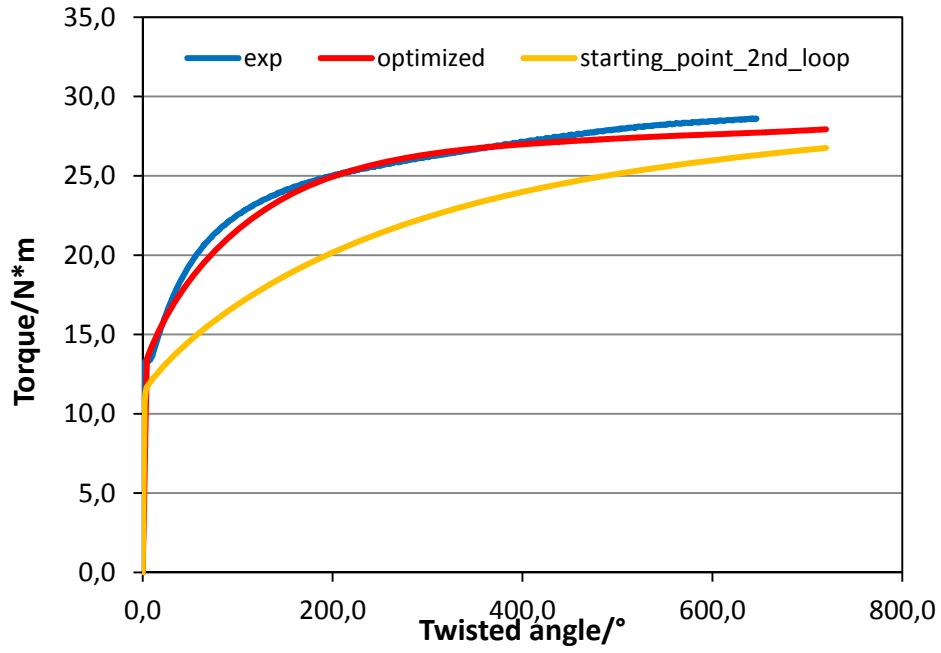**Table 6.5:** information about material parameters of the Voce model

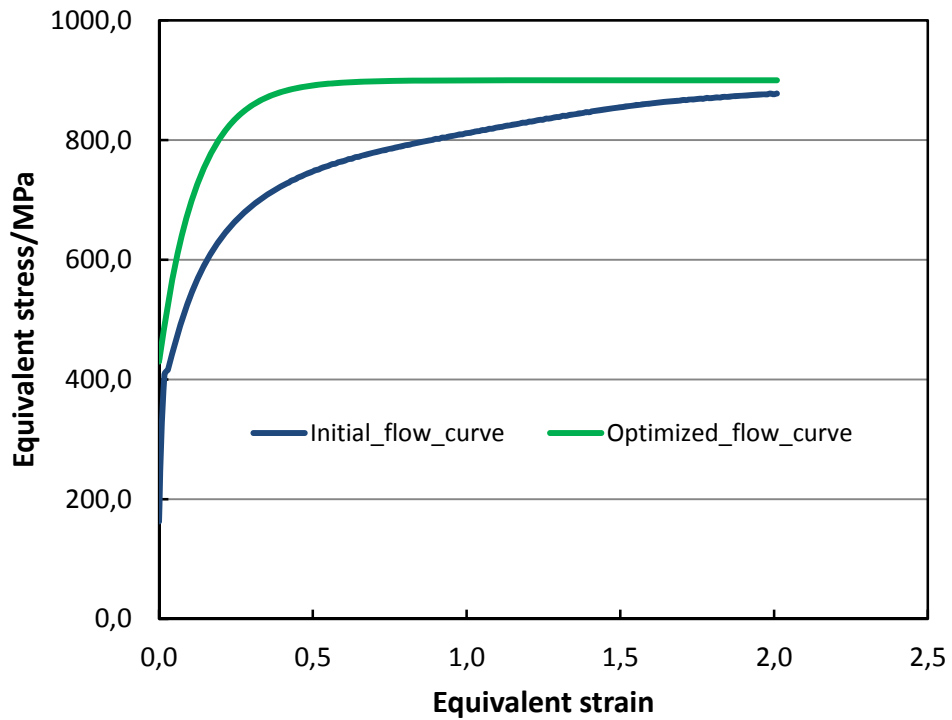**Figure 6.10:** second optimization of the Voce model

Figure 6.11: optmized flow curve from the second optimization of Voce model

In the Table 6.5 is shown the value of error in the two optimizations. The second shows a much lower error not only than the first, but also than the second optimization of the Ludwick's model, which however had a low value of error.

In fact, as it can see from Figure 6.10 that the optimized torque-twisted angle curve follows in an excellent way the trend of the experimental one, with very little difference. Therefore, the Voce model seems to be the most suitable one to describe the flow behavior of the 18CrNiMo7-6 hardening steel, when it subjected to a cold deformation

6.2 *Investigation at high temperature*

For the simulation at high temperature in ABAQUS, experiment data at 900 °C with different strain rate $0.01 \ s^{-1}$, $0.1 \ s^{-1}$ and $1 \ s^{-1}$ are used in order to reproduce the plastic behavior of the material at this temperature.
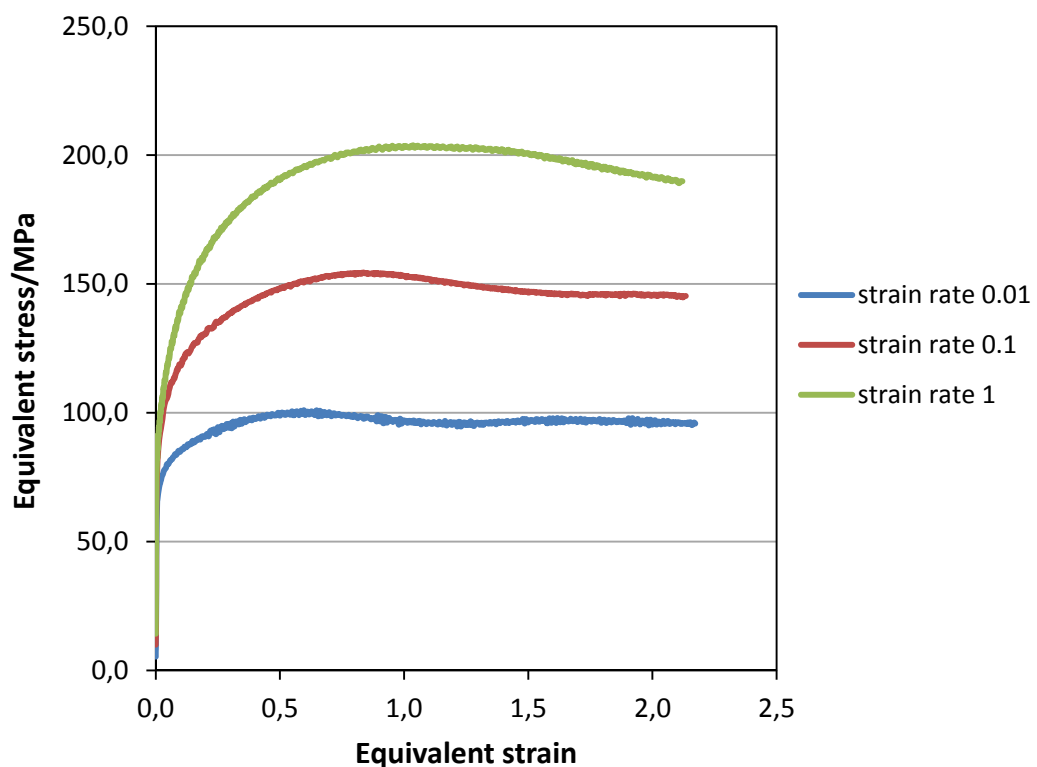

Figure 6.12: flow curves for different strain rate at 900°C

As we can see from Figure 6.12, the stress increases with increasing strain rate. In general, the flow curve of a material under hot working condition presents an apparent peak of the stress. The stress decreases rapidly after this peak. This is due to the occurrence of dynamic recrystallization.

Therefore, the flow curve at high temperature presents a very complex trends because of the just described physical phenomena, which occur. This caused an increment of the time required to reach the convergence in the simulation.

6.2.1 Evaluation of Hansel-Spittel model

The optimization procedure of the hot deformation is the same of the cold deformation. The only difference lies in the fact, that the flow curves at different strain rate to implement in ABAQUS for the simulations had much background noise, see Figure 6.13
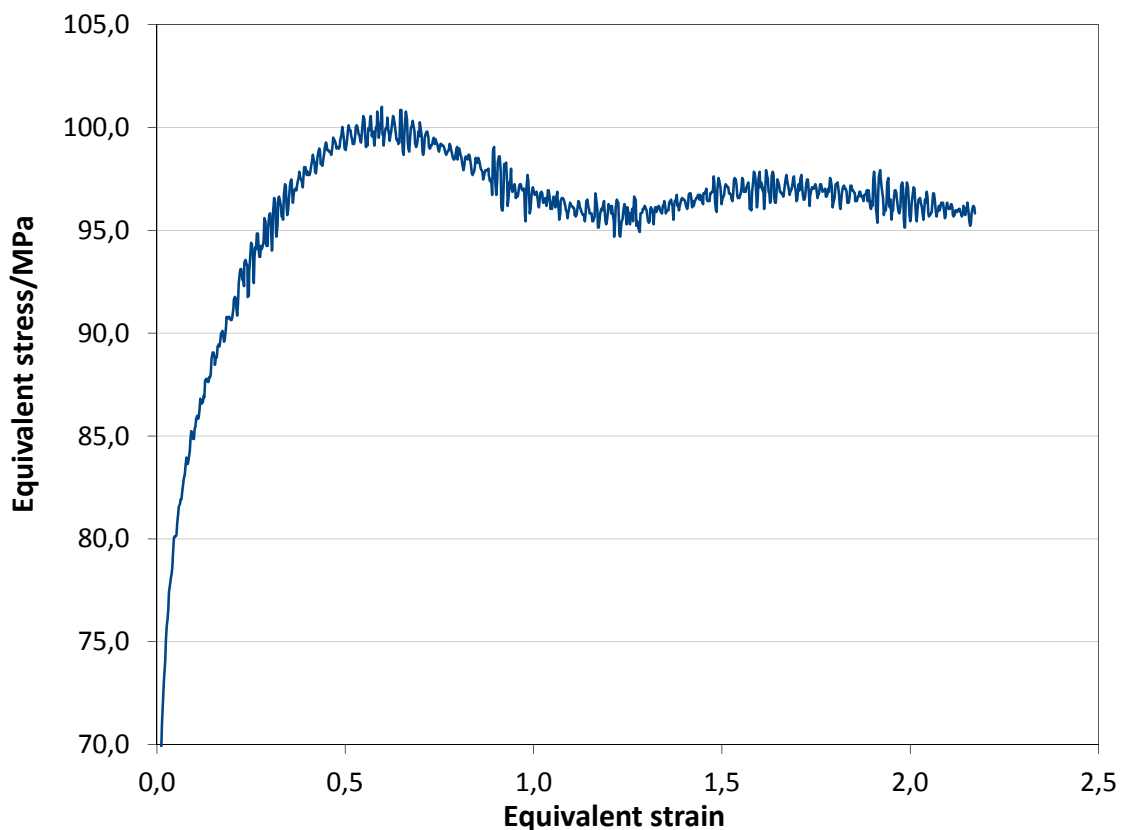

Figure 6.13: flow curve at 900 °C and 0.01 s^{-1} with noise

Therefore, it was necessary to filter the data relating to the different flow curves, before implementing them in ABAQUS. This is required, so as not to experience an early stop of the simulation. For this purpose, the "***smooth***" function in MATLAB was used.

This function, smooths the data in one column vector "y" using a moving average filter. The result after the filtering is show in Figure 6.14.
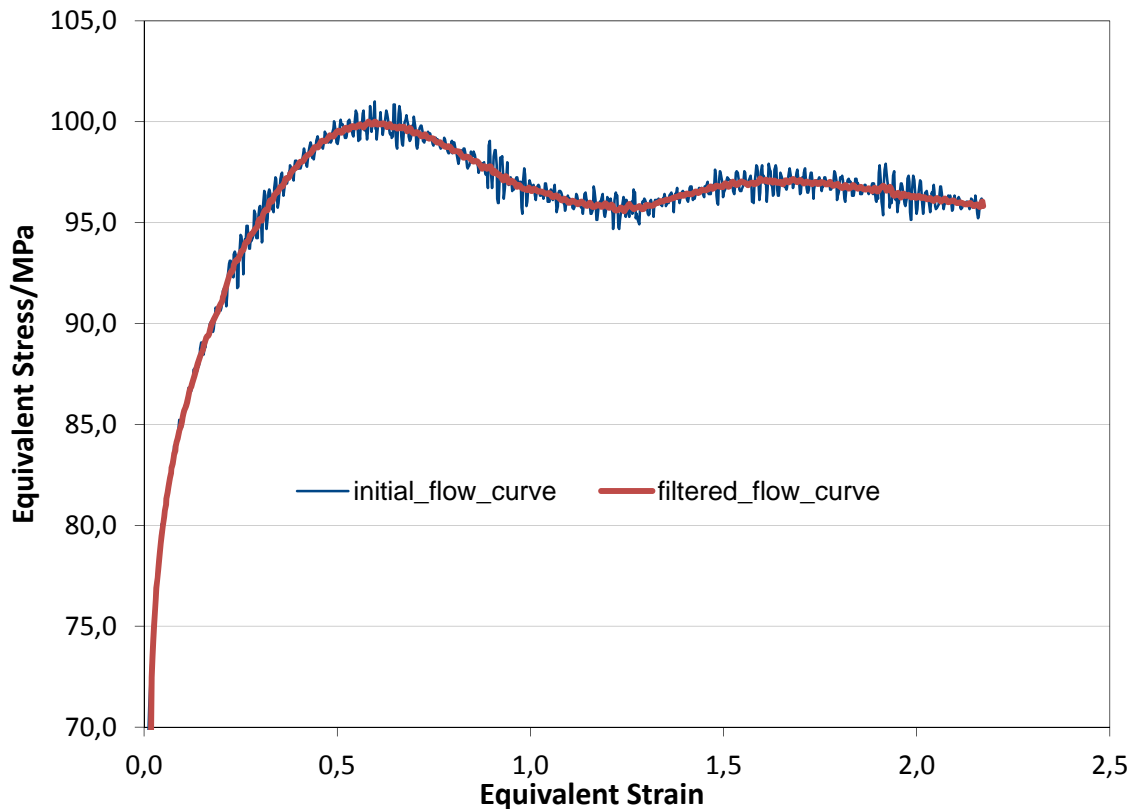
Figure 6.14: flow curve after the filtering

The red curve in Figure 6.14 is the smoothed one, and as it can see the noise is much lower than the previous case. After the filtering of all flow curves, it proceeded to their implementation in ABAQUS and it was possible run the simulations.

Since there are three different flow curves, three optimizations were carried out with different starting points. Also in this case for the evaluation of goodness of fit the coefficient of determination R_c was calculated. The information regarding the value of coefficient of determination for the three flow curves are added in the follow table

	Flow curve 900°C $0.01\ s^{-1}$	*Flow curve* 900°C $0.1\ s^{-1}$	*Flow curve* 900°C $1\ s^{-1}$
R_c	0.976	0.954	0.999

Table 6.6: information on the coefficient of determination of the three flow curves

As it can be seen from Table 6.6 the coefficient of determination is very close to 1, this is to confirm the fact that the Hasel-Spittel model is particularly suitable to describe the behavior of materials under hot working processes. The information regarding the starting points and the parameters after the optimization are stated in Table 6.7 and Table 6.8.

Starting points	Flow curve 900°C 0.01 s^{-1}
A	0.9224
m_1	0.000980
m_2	0.957600
m_3	-0.84490
m_4	-0.10140

Table 6.7: starting point of the optimization of the flow curve at a strain rate of 0.01 s^{-1}

Optimized parameters	Flow curve 900°C 0.01 s^{-1}
A	0.936
m_1	0.000998
m_2	0.0886
m_3	-0.8878
m_4	-0.107340
$Error$	1.46

Table 6.8: information about material parameters of the flow curve at a strain rate of 0.01 s^{-1}

The results of the optimization of the flow curve 0.01 s^{-1} are shown in

Figure 6.15: optimization of flow curve at a strain rate of 0.01 s^{-1}

As in the case of cold deformation the blue curve is the torque-twisted angle curve from the experiment at 900°C, the red one is the torque-twisted angle from the simulation of the optimized Hansel-Spittel model and the yellow one is the starting point. In the Figure 6.16 comparison between the flow curve obtained with the optimization of Hansel-Spittel model and the initial flow curve is shown.

Figure 6.16: optimized flow curve at a strain rate of 0.01 s^{-1}

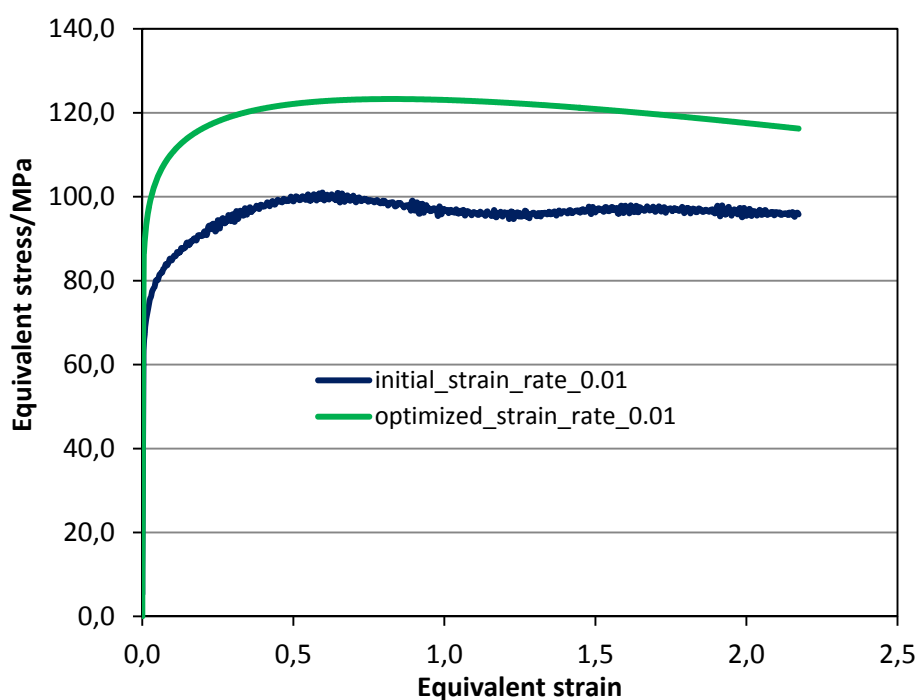As it can be seen from Figure 6.15 the difference between the two torque-twisted angle curves, is very low so this is a good result. However, the Hansel-Spittel model enables a universal flow stress prediction in the whole range of strains, but with omission of physical essence of the impact of dynamic recrystallization.

Therefore, this model is not able to reproduce the peak after the recrystallization, but only the steady-state behavior after the softening. The results of the flow curves 0.1 and 1 s^{-1} are show below. The information regarding the starting point of the optimization and the optimized parameters of the flow curves 0.1 and 1 s^{-1} are stated in Table 6.9, Table 6.10, Table 6.11 and Table 6.12 . The resulting torque vs twisted angle curves are shown in Figure 6.17 and Figure 6.19. The determined flow curves are shown in Figure 6.18 and Figure 6.20.

Starting points	*Flow curve* 900°C 0.1 s^{-1}
A	1.27200
m_1	0.001468
m_2	0.2291
m_3	-1.6150
m_4	-0.242500

Table 6.9: starting point of the optimization of the flow curve at a strain rate of 0.1 s^{-1}

Optimized parameters	Flow curve 900°C 0.1 s^{-1}
A	1.2822
m_1	0.001564
m_2	0.2241
m_3	-1.8006
m_4	-0.288510
Error	5.49

Table 6.10: information about material parameters of the flow curve at a strain rate of 0.1 s^{-1}
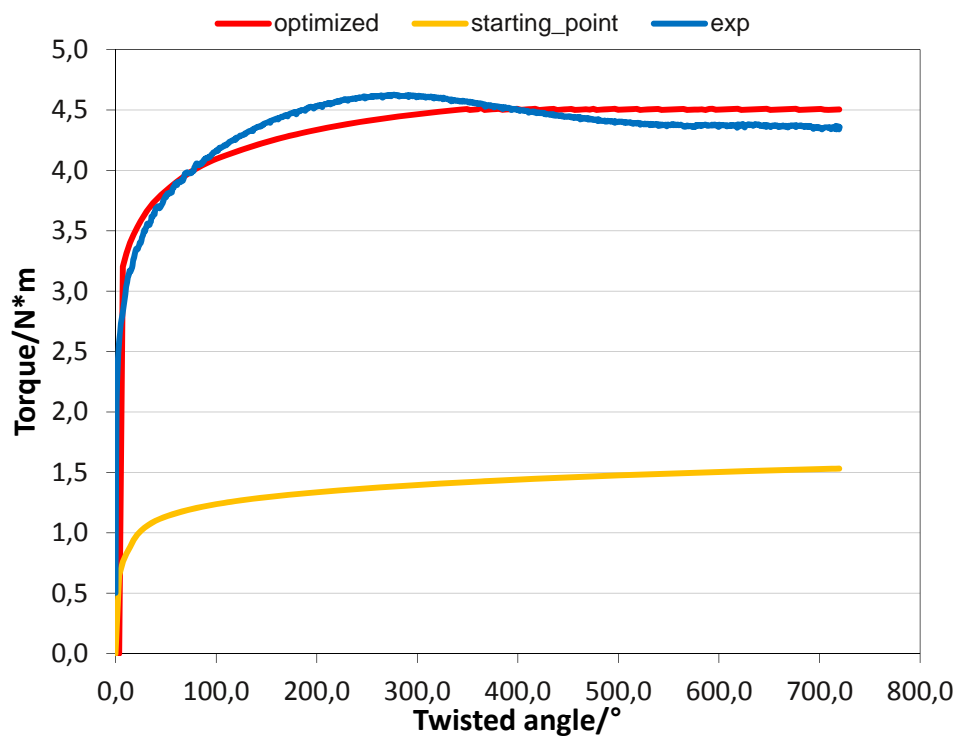
Figure 6.17: optimization of flow curve at a strain rate of 0.1 s^{-1}

Figure 6.18: optmized flow curve at strain rate of 0.1 s^{-1}

Starting points	Flow curve 900°C 1 s^{-1}
A	3.684
m_1	0.0047
m_2	0.239
m_3	0.097
m_4	-0.2164

Table 6.11: starting point of the optimization of the flow curve at a strain rate of 1 s^{-1}

Optimized parameters	Flow curve 900°C $1\ s^{-1}$
A	3.7107
m_1	0.004801
m_2	0.097715
m_3	0.097061
m_4	-0.175383
Error	43.07

**Table 6.12:** information about material parameters of the flow curve at a strain rate of $1\ s^{-1}$
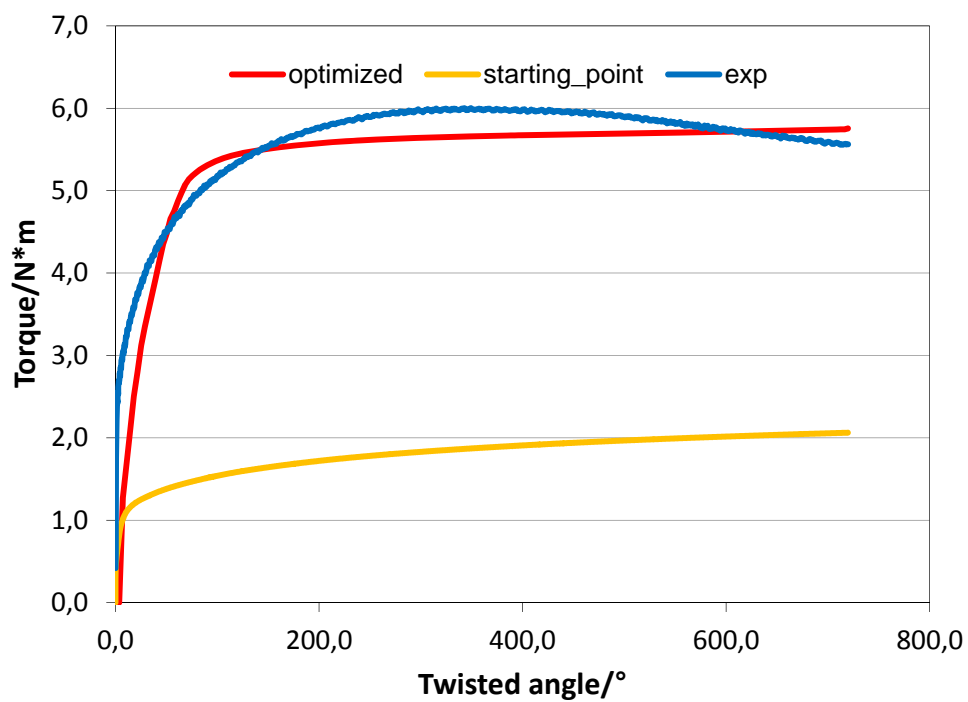
Figure 6.19: optimization of flow curve at a strain rate of $1\ s^{-1}$
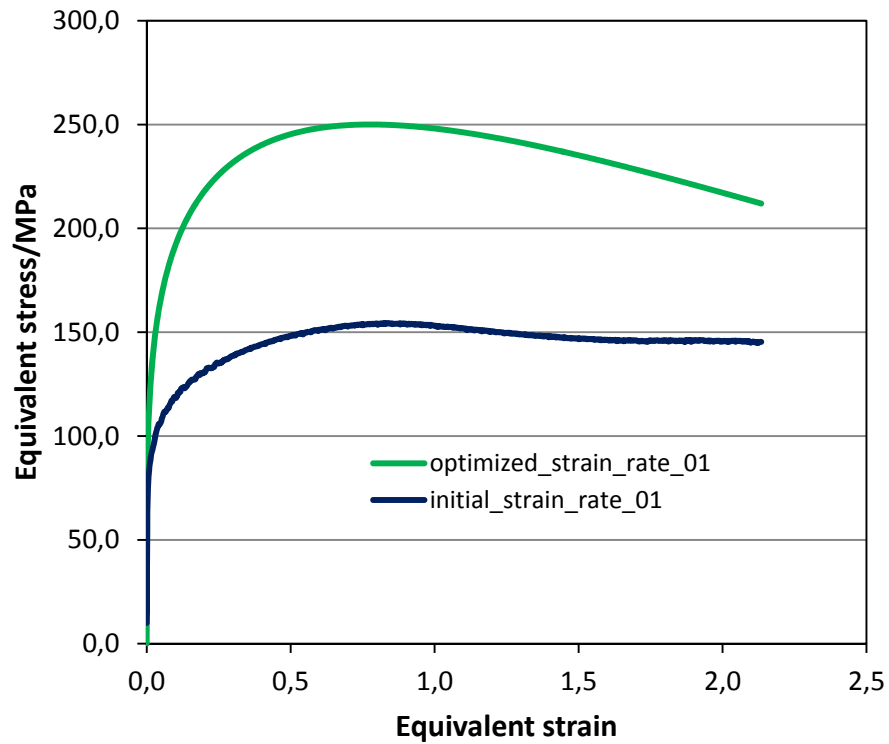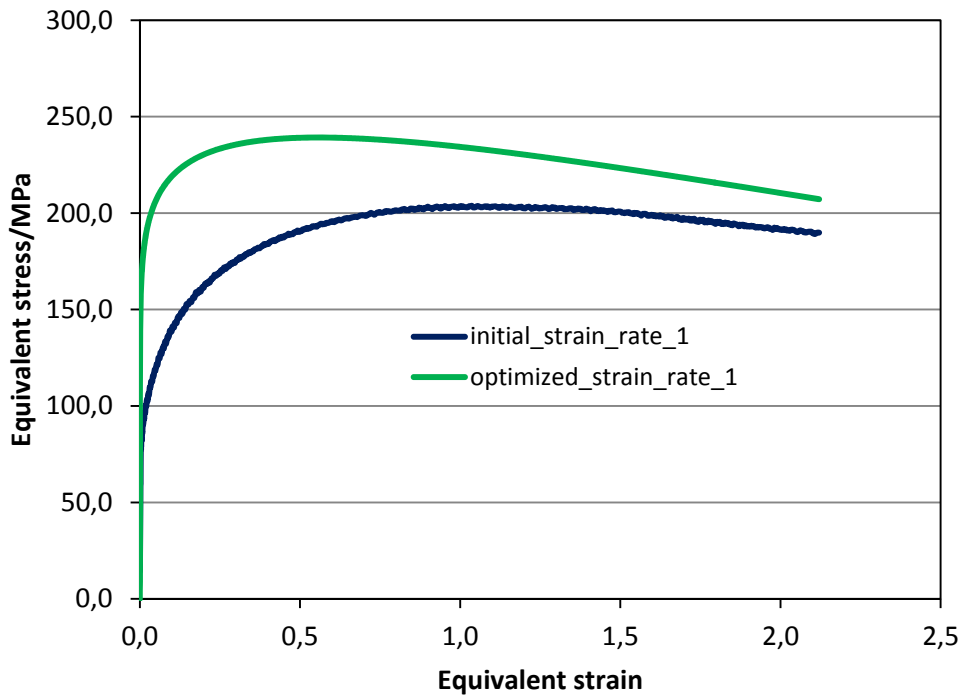
Figure 6.20: optimized flow curve at a strain rate of $1\ s^{-1}$

The deformation temperature is constant, so it is negligible for the purposes of the simulation. The only variable in the Hansel-Spittel was the strain rate.

One-way to see if this model is suitable to describe the flow behavior of the investigated material under hot working conditions, is to calculate the flow curves, using the optimized parameters belonging to one of three loops, changing only the strain rate. If the flow curves are the same, this means that the model is "perfect". The result is show in Figure 6.21.
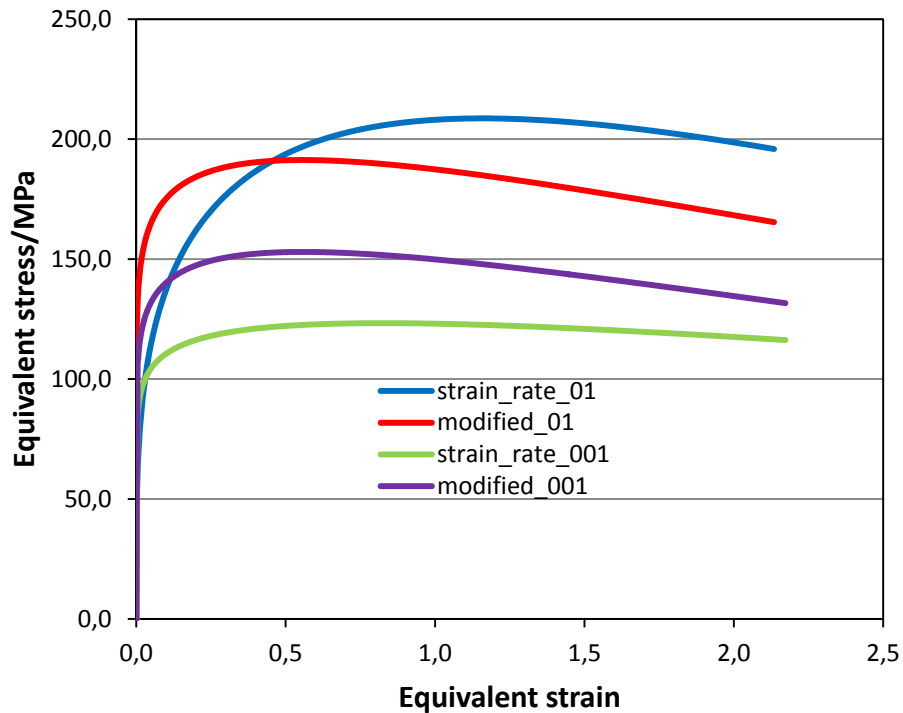
Figure 6.21: flow curve 0.1 and 0.01 s^{-1} obtained with the parameters of the flow curve 1 s^{-1}

In Figure 6.21 the blue curve is the flow curve 0.1 s^{-1} obtained with its material parameters of Hansel-Spittel, the red curve is the flow curve 0.1 s^{-1} obtained, instead, with the material parameters of the flow curve 1 s^{-1}. The same working principle was adopted for the flow curve 0.01 s^{-1}.

The inverse modelling approach using one fit parameters for strain rate of 1 s^{-1}, for example, results in a model which is only suitable for this strain rate. If a more complex optimization to fit parameters which describe flow behavior for the three different strain rates, is used, this may result in a better overall model.

7 Conclusion

The goal of this thesis was to determine flow stress of a case hardening steel in torsion test. In this context at first different analytical evaluation methods of torsion test for calculate the flow curve were investigated through a literature survey. In this latter, flow models able to reproduce the flow behavior of the investigated material, were determined. The study done on the traditional evaluation methods showed that the analytical treatments used to calculate the flow curves, are including simplifications to compensate the non-uniform deformation characteristic of the torsion test. Therefore, flow curves were determined from torsion tests data by using inverse modelling. At first, a FEM model of torsion test for inverse modelling was developed. During the simulations, an excessive distortion of the mesh has occurred. To fix this problem some kind of pre-deformed mesh mechanism was developed. In particular It was used an algorithm that was able to give a sort of pre-deformation to the mesh and after which, set the rotational moment in the opposite direction in order to compensate the excessive distortion.

Inverse modelling was performed by comparing torque as a function of rotation angle measured in experiments and calculated by the FE-model. For this purpose, an algorithm able to estimate optimized parameters of flow models was developed. The focus is on minimizing the differences between modelled and measured torque. To simplify the inverse problem, modelling was done first for cold deformation and then for hot deformation.

For cold deformation two flow models were used to determine the flow curves from the measured data. The Ludwick's model is the most used model to describe the materials behavior under cold working conditions, so was expecting a good agreement between torque-twisted angle curve from the simulation with this flow model and experimental one. The result indicates a good agreement between torque-twisted angle curves using this flow model, but with marked difference in some areas. The Voce model assumes the flow curve as a transient of the flow stress from an initial value to the saturation value. The torque-twisted angle curve obtained with this flow model, show a very low discrepancy with the experimental curve, revealing itself more suitable than the previous model, to describe the flow behavior of the investigated material under cold working conditions.

For hot deformation, the torsion test was conducted at 900°C with three different strain rate level: 0.01, 0.1, and 1 s^{-1}. The deformation temperature was constant; therefore, it was negligible for the purposes of the simulation. For each value of strain rate, instead, it was necessary, set the time period per step in ABAQUS, equal to the time required to

carry the torsion in the real experimental tests. This corresponds an increment of computational time, but it was necessary for reach the convergence in the simulation. The flow model used to describe the material behavior at high temperature was Hansel-Spittel. The results show a great agreement between the torque-twisted angle curves. This model enables a universal flow stress prediction in the whole range of strains, but with omission of physical essence of the impact of dynamic recrystallization. In other words is not able to reproduce the peak after the recrystallization, but only the steady-state behavior after the softening.
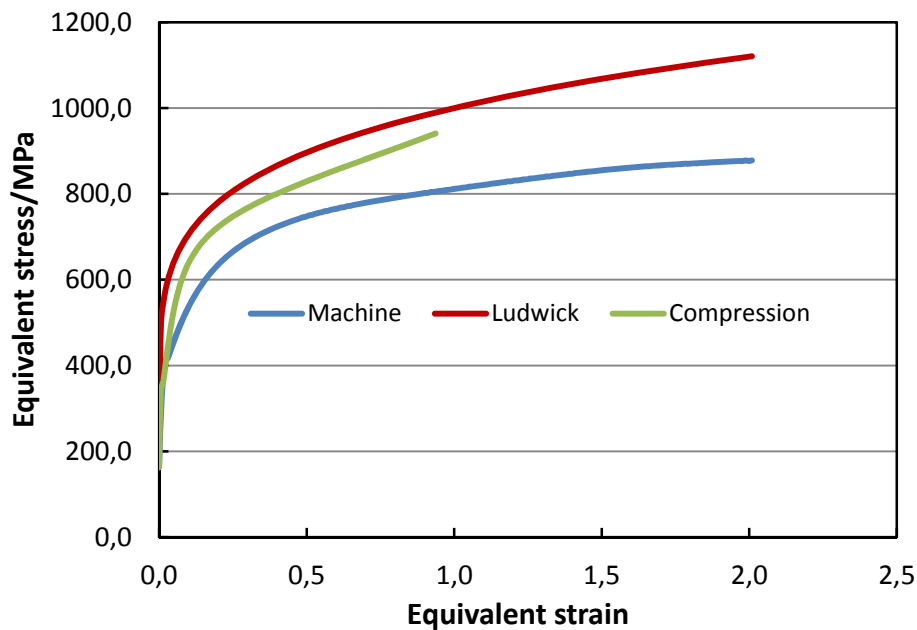
Figure 7.1: comparison between different flow curve determination approach

In Figure 7.1 the comparison between the flow curve obtained with the compression test, the flow curve obtained with the torsion machine build-in software and the flow curve obtained with the optimized Ludwick's model, is shown. Looking at this figure, there are some difference between the three flow curves, so it is hard to say what is the "correct" flow curve, maybe the difference lies in the fact that the flow curves obtained with the compression test and torsion machine use, analytical evaluation suitable for homogeneous deformation. But the torsion test is characterized by a non-uniform deformation, therefore it is possible that the flow curve obtained by inverse modelling is the "correct" one.

In summary, the Voce model provides accurate evaluation of stress-strain curve for cold torsion test. In case of hot torsion test, the flow stress in the steady state determined by

Hansel-Spittel model is accurate, but information regarding the onset of dynamic recrystallization is not accurate.

8 Future work

Further work is needed in a number of areas to improve the performance of simulation. One of the major problems of the software used for simulations, in this thesis, is the re-meshing. When the mesh is too distorted, it causes an increase of the computational time, and also errors in the simulation. So in the future, develop a re-meshing tool, could reduce these problems; in other words the elements must be refined locally in the zones where the strain is higher. This it can be achieved by prescribing a local size of the elements and imposing that the mesh is rebuilt accordingly.

Another factor to take into account in computations are the main sources of the uncertainties that there are in the simulations. Uncertainties have many origins: changes of material data, background noise, approximate modeling of interface, material behavior, boundary conditions, etc. The challenge consists in identifying, modeling and quantifying these uncertainties and then in considering them during process simulation and optimization. In this regard, it could use the Monte-Carlo approach, which are a broad class of computational algorithm that rely on repeated random sampling to obtain numerical results [78].

Furthermore there are some variables which are not easily included in the simulations yet and are know to have an influence on formability in practice. Temperature and strain rate sensitivity are significant in many processes, especially in hot working conditions. It may an opportunity determine flow curves for hot deformation with another inverse modelling approach, using results at different temperature and strain rates to determine parameters for one overall model.

The major challenge is reducing computational time. New emerging techniques show quite efficient and effective: the Proper Orthogonal Decomposition (PGD) method is one of them. The PGD allows to diminish drastically the computation and storage cost. The main point of PGD consists in calculating shape functions and the solution itself simultaneously. This is a departure from the incremental or step-by-step methods used traditionally. Indeed, PGD is not based on the concept of an increment; instead, it uses an iterative approach, which at each iteration, produces an approximation of the displacements, strain and stresses everywhere in the structure over the entire time interval of interest [79]. In some other fields such as fluid mechanics or structural mechanics, this method allow reducing the computational time by several order of magnitude, so It sounds reasonable to try to extend this method to metal forming problems [80].

9 Acknowledgements

Firstly, I would like to express my sincere gratitude to my supervisor Prof. Stefania Bruschi, for her patience, motivation and immense knowledge. Without her help, I would this opportunity to work my thesis in Germany. Besides my supervisor, I would like to thank Prof. Dr.-Ing. Gerhard Hirt, who provided me an opportunity to join in the institute of metal forming, in the RWTH Aachen University, and who gave access to the laboratory and research facilities. Without his precious support it would not be possible to conduct this thesis.

My sincere thanks also goes to my tutors: M. Sc., Jens Dierdorf and M. Sc. Alexander Braun, for their insightful comments and encouragement, but also for the hard question which incented me to widen my thesis from various perspectives. Their guidance helped me in all the time of the project and writing this thesis. I could not have imagined having a better tutors and mentors for my master thesis.

A special thanks to my family. Words cannot express how greatful I am to my mother and my father for all the sacrifices that they've made on my behalf. My father has been a pillar in my studies, without which I would never be able to finish. I want to repay all his sacrifices, by dedicating this and all of my future successes. My mother is the best person and good heart that I know, she did menial jobs to afford me to study, and I love her for this. She has suffered a lot in her life, and the least I can do is to make proud of having a son graduate.

My sister was the person on whom I could always rely on, she has never backed down when there was to help me. My bond with her is very strong, so we shared, joys and sorrows, but we were always together, and ours is a bond that will never dissolve.

Another special thanks goes to my grandparents. My grandma and grandpa, welcomed me into their home when I was still a child. They did have me to be the man I am today, teaching me so much. All this would not have been possible without their help. My love for them is undisputed.

Another thanks goes to my aunties. They were like the second mother for me, giving me support when there was the need, including my cousins. My bond with them is very special, different from other aunt-nephew relationship and cousins one, and I'll never stop loving them.

A final thanks, but certainly not least important, go to my friends, who " endured me" in this study path. Thanks to my housemates in Padova, Luca and Riccardo, thanks to a dear

colleague of study, Emanuele and thanks especially to the adventure companion in this Erasmus period, Antonio, who is like a brother for me. Thanks you all.

II Formula symbols

Symbol	Unit	Description
a	mm	Tubular specimen radius
b	-	Burgers vector
c	-	Schmid factor
$C(\bar{p})$	-	Cost function
f	N*m	Modeled torque
J	-	Jacobian
G	Pa	Shear modulus
E	Pa	Young's modulus
ν	-	Poisson's ratio
p	-	Parameters vector
R	mm	Solid bar specimen gauge radius
k	-	Strain hardening
σ	MPa	Flow stress
ε	-	Strain
τ	MPa	Shear stress
$\dot{\Upsilon}$	-	Strain rate
Υ	-	Shear strain
M	MPa	Torque
$\dot{\theta}$	-	Angular speed
θ	-	Twist angle per unit length
L	mm	Gauge length
I	m^4	Polar moment of inertia
n	-	Strain hardening exponent
m^*	-	Strain rate sensitivity
R_c	-	Coeff. of determination

III Literature

[1]   G. E. Dieter, H. A. Kuhn e S. L. Semiatin, «Torsion Testing to Assess Bulk Workability,» in *Handbook of Workability and Process Design*, 2003, pp. 86-121.

[2]   G. Saul, A. T. Male e V. De Pierre, «A New Method for Determination of Material Flow Stress Value Under Metal Working Condition,» Wright-Patterson Air Force Base, Ohio 45433, 1970.

[3]   T. Altan, «Flow Stress of Metals and it's Application in Metal Forming Analyses,» in *Journal of Testing and Evaluation for Industry*, 1973, pp. 1009-1019.

[4]   G. E. Dieter, Mechanical Metallurgy, McGraw-Hill Book Company, 1988.

[5]   «Total Materia,» Marzo 2001. [Online]. Available: www.totalmateria.com/page.aspx?ID=CheckArticle&site=kts&NM=43. [Consultato il giorno 19/01/2016 Gennaio 2016].

[6]   G. Gottstein, Physical Foundations of Materials Science, Berlin, 2004.

[7]   E. P. Degarmo, J. Black e R. A. Kohser, Materials and Processes in Manufacturing, Wiley, 2003.

[8]   M. Ashby, H. Shercliff e D. Cebon, Materials: Engineering, Science, Processing and Design, Butterworth-Heinemann, 2007.

[9]   J. E. Shackelford, Introduction to Materials Science for Engineers, 6th ed., Prentice Hall, 2004.

[10]   H. McQueen e J. Jonas, «Hot Workability Testing Techniques,» *Metal Formin: Interrelation Between Theory and Practice,* pp. 93-428, 1971.

[11]   W. Precht e J. Pickens, «A Study of the Hot Working Behavior of Al-Mg Alloy 5052 by Hot Torsion Testing,» 1987, pp. 1603-1611.

[12]   M. Cockcroft e D. Latham, «Ductility and the Workability of Metals,» 1993, pp. 33-39.

[13]   M. Mataya, «Simulating Microstructural Evolution during the Hot Working of Alloy 718,» JOM, 1999, pp. 18-26.

[14]   D. Zhao, «Testing of Deformation Modeling,» in *Mechanical Testing and Evaluation*, 2000, pp. 798-810.

[15]   W. Callister, Materials Science and Engineering: An Introduction, Wiley, 2006.

[16]   J. Shackelford, Introduction to Materials Science for Engineers, Prentice Hall, 2004.

[17]   R. Kopp e H. Wiegels, Einführung in die Umformtechnik, 1999.

[18]   T. Courtney, Mechanical Behavior of Materials, Waveland Press, 2005.

[19]   «ASM Handbook, Vol.8,» *Mechanical Testing and Evaluation,* vol. 8, 2000.

[20]   F. Cardelli, Materials Handbook: A Coincise Desk Reference, Springer, 2008.

[21]   B. Perret, in *Mechanical Testing of Materials*, Melbourne, Austalasia Ltd., 1994, pp. 41-44.

[22]   P. Han, Tensile Testing, ASM International, 1992.

[23]   W. F. Smith e J. Hashemi, Scienza e tecnologia dei materiali, Mc-Graw Hill, 2012.

[24]   G. Dieter, H. Kuhn e S. Semiatin, «Bulk Workability Testing,» 2003, pp. 47-56.

[25]   J. Jonas, R. Holt e C. Coleman, «Plastic Stability in Tension and Compression,» *Acta Metall.,* vol. 24, p. 911, 1976.

[26]   R. Plaut e C. Sellars, «Analysis of Hot Tension Test Data to Obtain Stress-Strain Curves to High Strains,» *J. Test Eval.,* vol. 13, pp. 39-45, 1985.

[27]   G. T. Rooyen e W. Backofen, «A Study of Interface Friction in Plastic Compression,» *International Journal of Mechanical Sciences,* vol. 1, pp. 1-27, 1960.

[28]   G. Pearsall e W. Backofen, «Frictional Boundary Conditions in Plastic Compression,» *Journal of Engineering for Industry ,* vol. 85/1, pp. 68-75, 1963.

[29]   P. Dadras, «Stress-Strain Behavior in Bending,» *Mechanical Testing and Evaluation,* vol. 8, pp. 109-114, 2000.

[30]   C. Clark e J. Russ, *Trans. AIME,* vol. 167, pp. 736-748, 1946.

[31]   K. Tajima e K. Kugai, «Tetsu-to-Hagané,» *J. Iron Steel Inst. Jpn.,* vol. 42, pp. 980-985, 1956.

[32]   W. Precht e J. Pickens, *Metall. Trans. A,* vol. 18A, pp. 1603-1607, 1987.

[33]   M. Clode, *Alum. Ind.,* vol. 11, pp. 34-39, 1992.

[34]   S. Semiatin, G. Lahoti e J. Jonas, «Application of the Torsion Test to Determine Workability,» *Metals Handbook,* vol. 8, pp. 154-184, 1985.

[35]   T. Maccagno, S. Yue, J. Jonas e K. Dyck, «Simulated Hot Working, Cold Working, and Annealing of Al-Containing Steels,» *Metallurgical Transactions A,* vol. 24, n. 7, pp. 1589-1596, 1993.

[36]   C. Clark e J. Russ, «A Laboratory Evaluation of the Hot-Working Characteristics of Metals,» *Transactions of the AIME,* vol. 167, pp. 736-748, 1946.

[37]   P. Regnet e H. Stuwe, «Zur Enstehung von Oberflaschentexturen Beim Walzen Kubischflashenzentrierter Metalle,» *Zeitschritf fur Metallkunde,* vol. 54, p. 275, 1963.

[38]   S. Semiatin e G. Lahoti, «Deformation and Unstable Flow in Hot Forging of Ti-6Ai-2Sn-4Zr-2Mo-0.1Si,» *Metallurgical Transactions A,* vol. 12, n. 10, pp. 1705-1717, 1981.

[39]   D. Hardwick e M. Tegart, *Mem. Sci. Rev. Met.,* vol. 58, pp. 869-880, 1961.

[40]   J. Robbins, O. Shepard e O. Sherby, *Trans. ASM,* vol. 60, pp. 205-216, 1967.

[41]   Y. Fridman, «Mechanical Testing of Material by The Torsion Method,» *Metallurgia,* vol. 37, p. 53, 1947.

[42]   H. Larson e E. Klier, «Strain Hardening of Mild Steel in the Torsion Test as a Function of Temperature,» *Transaction of ASM,* vol. 43, p. 1033, 1951.

[43]   A. Nadai, Theory of Flow and Fracture, McGraw-Hill, 1950.

[44]   D. Fields e W. Backofen, «Determination of Strain-Hardening Characteristics by Torsion Testing,» *Journal ASTM,* vol. 57, pp. 1259-1272, 1957.

[45]   S. Khoddam e P. Hodgson, «Post Processing of the Hot Torsion Test Result Using a Multi-Dimensional Modelling Approach,» *Material and Design,* vol. 31, pp. 2578-2584, 2010.

[46]   S. Khoddam e P. Hodgson, «A Heuristic Model Selection Scheme for Representing Hot Flow Data Using the Hot Torsion Test Results,» *Material and Design,* vol. 31, pp. 2011-2017, 2010.

[47]   W. Peiyang, *Comparison of Different Evaluation Methods of Torsion Test for the Determination of Flow Curves,* Aachen, 2016.

[48]   S. Cooreman, D. Lecompte, H. Sol, J. Vantomme e D. Debruyne, «Identification of Mechanical Material Behavior Through Inverse Modelling and DIC,» *Experimental Mechanics,* vol. 48, pp. 421-433, 2008.

[49] W. Menke, Geophysical Data Analysis: Dicrete Inverse Theory, Palisades, New York, 2012.

[50] A. Tarantola, Inverse Problem Theory, Elsevier Scientific Publishing Company, 1987.

[51] Z. Gronostajski, «The Constitutive Equations for FEM Analysis,» *Journal of Materials Processing Technology,* vol. 106, pp. 40-44, 2000.

[52] I. Gresovnik, *A General Purpose Computational Shell for Solving Inverse and Optimisation Problems,* PhD Thesis, University of Wales, 2000.

[53] B. Hochholdinger, H. Grass, A. Lipp e P. Hora, «Determination of Flow Curves by Stack Compression Tests and Inverse Analysis for the Simulation of Hot Forming,» Munich, 2009.

[54] «Wikipedia,» [Online]. Available: https://en.wikipedia.org/wiki/Simplex. [Consultato il giorno 26 January 2016].

[55] M. Wright, «Direct Search Methods: Once Scorned, Now Respectable,» in *Proceedings of the 1995 Dundee Biennial Conference in Numerical Analysis*, Harlow, UK, 1996.

[56] J. Lagarias, J. Reeds, M. Wright e P. Wright, «Convergence Properties of the Nelder-Mead Simplex Method in Low Dimensions,» *SIAM J. Optim.,* vol. 9, pp. 112-147, 1998.

[57] «What-When-How,» [Online]. Available: www.what-when-how.com/artificial-intelligence/nelder-mead-evolutionary-hybrid-algorithms-artificial-intelligence/. [Consultato il giorno 12 February 2016].

[58] K. Levenberg, «A Method for the Solution of Certain Non-Linear Problems in Least Squares,» *Quarterly of Applied Mathematics,* vol. 2, pp. 164-168, 1944.

[59] D. Marquardt, «An Algorithm for the Least-Squares Estimation of Nonlinear Parameters,» *SIAM Journal of Applied Mathematics,* vol. 2, n. 11, pp. 431-441, 1963.

[60] J. Moré, «The Levenberg-Marquardt Algorithm: Implementation and Theory,» 1970.

[61] G. Golub e C. Van Loan, Matrix Computations, Johns Hopkins University Press, 1996.

[62] D. Morrison, «Methods for Nonlinear Least Squares Problems and Convergence Proofs,» in *Proceedings of the Jet Propulsion Laboratory Seminar on Tracking Programs and Orbit Determination*, 1960.

[63] D. Samantaray, S. Mandal e A. Bhaduri, «A Comparative Study on Johnson Cook, Modified Zerilli-Armstrong and Arrhenius-type Contitutive Models to Predict Elevated Temperature Flow Behaviour in Modified 9Cr-1Mo Steel,» *Computational Material*

Science, vol. 47, pp. 568-576, 2009.

[64]   E. Niţu, M. Iordache, L. Marincei, I. Charpentier, G. Le Coz, G. Ferron e I. Ungureanu, «FE-Modeling of Cold Rolling by In-Feed Method of Circular Grooves,» *Journal of Mechanical Engineering,* vol. 9, n. 57, pp. 667-673, 2011.

[65]   W. Song, J. Ning, X. Mao e H. Tang, «A Modified Johnson-Cook Model for Titanium Matrix Composites Reinforced with Titanium Carbide Particles at Elevated Temperatures,» *Materials Science & Engineering A,* vol. A, n. 576, pp. 280-289, 2013.

[66]   B. Banerjee e A. Bhawalkar, «An Extended Mechanical Threshold Stress Plasticity Model. Modeling 6061-T6 Aluminum Alloy».

[67]   B. Banerjee, «The Mechanical Threshold Stress Model for Various Tempers of AISI 4340 steel,» *International Journal of Solids and Structures,* vol. 44, n. 3-4, pp. 834-859, 2006.

[68]   Z. Cyganek e M. Tkocz, «The Effect of AZ31 Alloy Flow Stress Description on the Accuracy of Forward Extrusion FE Simulation Results,» *Archives of Metallyrgy and Materials,* vol. 57, 2012.

[69]   B. G. Sainath, J. Choudhary, E. I. S. Christopher e M. Mathew, «Applicability of Voce Equation for Tensile Flow and Work Hardening Behaviour of P92 Ferritic Steel,» *International Journal of Pressure Vessels and Piping,* pp. 1-9, 2015.

[70]   G. Paolucci, Appunti dalle lezioni di Metallurgia per la laurea in Ingegneria Meccanica vol. 2, Padova: Edizioni Libreria Progetto Padova, 2013.

[71]   D. E. 10084, *DIN Deutsches Institut für Normung: Case Hardening Steels- Technical Delivery Conditions,* Berilin: Beuth Verlag GmbH, 2008.

[72]   T. Instruments, *Guidelines for Initial Setup STD812,* 2014.

[73]   O. Zienkiewicz, The Finite Element Method, New York: McGraw-Hill, 1977.

[74]   K. Bathe, Finite Element Procedures, Prentice Hill, 1996.

[75]   I. ABAQUS, Adaptive Meshing and Distortion Control.

[76]   T. L., S. Stahel e P. Hora, «Modeling for the FE-Simulation of Warm Metal Forming Processes,» Institute of Virtual Manufacturing, Swiss Federal Institute of Technology, Zurich.

[77]   C. Lawson e R. Hanson, Solving Least Squares Problems, Prentice-Hall, 1974.

[78]   M. Strano, «Technique for FEM Optimization Under Uncertainty of Time-dependent

Process Variables in Sheet Metal Forming,» *Int. J. Mater. Form. ,* vol. 1, pp. 13-20, 2008.

[79] F. Chinesta e E. Cueto, «Introduction,» in *PGD-Based Modeling of Materials*, Springer International Publishing, 2014, pp. 1-24.

[80] D. Ryckelynck, «Hyper-reduction of Mechanical Models Involving Internal Variables,» *Int. J. Numer. Meth. Engng,* vol. 77, n. 1, pp. 75-89, 2009.